Analysis of Hybrid Free Space Optics and Radio Frequency Cooperative Relaying Systems

A Dissertation

Presented in Partial Fulfillment of the Requirements for the

Degree of Master of Science

with a

Major in Electrical Engineering

in the

College of Graduate Studies

University of Idaho

by

Elyes Balti

Major Professor: Brian K. Johnson, Ph.D.

Committee: Zouheir Rezki, Ph.D.; Herbert Hess, Ph.D.

Department Administrator: Larry Stauffer, Ph.D., P.E.

May 2018

Authorization to Submit Thesis

This thesis of Elyes Balti, submitted for the degree of Master of Science with a Major in Electrical Engineering and titled "Analysis of Hybrid Free Space Optics and Radio Frequency Cooperative Relaying Systems," has been reviewed in final form. Permission, as indicated by the signatures and dates below is now granted to submit final copies for the College of Graduate Studies for approval.

Major Professor:	Brian K. Johnson, Ph.D.	Date
Committee:	Zouheir Rezki, Ph.D.	Date
	Herbert Hess, Ph.D.	Date
Department Chair:	Larry Stauffer, Ph.D., P.E.	Date

Abstract

The exponential increase in the number of mobile users, coupled with the strong demand for high-speed data services results in a significant growth in the required cellular backhaul capacity. Optimizing the cost efficiency while increasing the capacity is becoming a key challenge to the cellular backhaul. It refers to connections between base stations and mobile switching nodes over a variety of transport technologies such as copper, optical fibers, and radio links. These traditional transmission technologies are either expensive, or cannot provide high data rates. This work is focused on the opportunities of free-space-optical (FSO) technology in next generation cellular backhaul. FSO is a cost effective and wide bandwidth solution as compared with the traditional radio-frequency (RF) transmission. Moreover, due to its ease of deployment, license-free operation, high transmission security, and insensitivity to interference, FSO links are becoming an attractive solution for next generation cellular networks. However, the widespread deployment of FSO links is hampered by the atmospheric turbulence-induced fading, weather conditions, and pointing errors. Increasing the reliability of presented systems, while still exploiting their high data rate communications, is a key requirement in the deployment of an FSO-based backhaul. Therefore, the aim of my research topic is to provide different approaches to address these technical challenges. Moreover, performance analysis of asymmetric mmWave RF/FSO dual-hop systems is analyzed. In such system models, multiple RF users can be multiplexed and sent over the FSO link. More specifically, the end-to-end performance metrics are presented in closed-form. This also has increased the interest to study the performance of dual-hop mixed FSO/RF systems, where the FSO link is used as a multicast channel that serves different RF users. Having such interesting results motivates further the analysis of dual-hop FSO fixed-gain relaying communication systems, and exact closed-form performance metrics are presented in terms of the bivariate H-Fox function. This model is further enhanced through the deployment of a multihop FSO relaying system as an efficient technique to mitigate the turbulence-induced

fading as well as pointing errors. Furthermore, unlike similar works in the literature, I assumed that the relays are succeptible to hardware impairments that are harmful to the system performance. In fact, for a low rate system, the approximation of neglecting the hardware impairments is still valid. However, the effect of the imperfections become more pronounced for high rate systems particularly for the mmWave RF/FSO systems since they are operating at high rate. Capitalizing on this, I provide a global framework analysis for the impact of the impairments on the relaying systems. I mainly studied the impacts of High Power Amplifier (HPA) non-linearities and I considered the Soft Envelope Limiter (SEL), Traveling Wave Tube Amplifier (TWTA) and Solid State Power Amplifier (SSPA). Finally, performance metrics such as the end-to-end outage probability, the bit error probability, the ergodic capacity are derived in terms of the Meijer-G function, along with univariate, bivariate and trivariate Fox-H functions. Since the mathematical derivations include very complex functions, the asymptotical high signal-to-noise ratio are derived in terms of elementary functions to get engineering insights about the system gains such as the diversity and the array gains.

Acknowledgements

I would like to sincerely thank my advisor, Prof. Brian K. Johnson, for giving me the opportunity to be part of his research group and for providing me with an amazing research environment.

I would also like to thank Dr. Zouheir Rezki for his availability, support and advices during my experience in the University of Idaho. I am greatly indebted to him for his continuous guidance and encouragement throughout the course of this work.

I am also grateful to Prof. Herbert Hess for his support and time dedicated to my thesis.

Last, but definitely not least, I am forever grateful to my family for their unconditional support and constant encouragement. I dedicate everything that I have accomplished to them. Words fail me in expressing my love to them .

Dedicated to my parents, and my brother

Monia, Mahmoud, and Oussama.

Table of Contents

List of Figures

List of Tables

List of Acronyms

RF Radio Frequency
FSO Free Space Optics
AF Amplify-and-Forward
DF Decode-and-Forward
QF Quantize-and-Forward
QE Quantize-and-Encode
PRS Partial Relay Selection
ORS Opportunistic Relay Selection
CSI Channel State Information
ORS Opportunistic Relay Selection
CDF Cumulative Distribution Function
PDF Probability Density Function
MGF Moment Generating Function
IM/DD Intensity Modulation and Direct Detection
LOS Line Of Sight
OP Outage Probability
BEP Bit Error Probability
SEP Symbol Error Probability
EC Ergodic Capacity
SSPA Solid State Power Amplifier
SEL Soft Envelope Limiter
TWTA Traveling Wave Tube Amplifier
HPA High Power Amplifier
IBO Input Back-Off
ILR Image Leakage Ratio
IQ In Phase and In Quadrature
OF Optical Fiber
SNR Signal-to-Noise Ratio
SNDR Signal-to-Noise-plus-Distortion Ratio
SINR Signal-to-Interference-plus-Noise Ratio
AWGN Additive White Gaussian Noise
PAM Pulse Amplitude Modulation

PSK Phase Shift Keying
CBPSK Coherent Binary Phase Shift Keying
CBFSK Coherent Binary Frequency Shift Keying
NBFSK Non-Coherent Binary Frequency Shift Keying
DBPSK Differential Binary Phase Shift Keying
QAM Quadrature Amplitude Modulation
mmWave Millimeter Wave
MIMO Multiple Input Multiple Output

List of Symbols

$P_{\text{out}}(\cdot)$	Outage Probability
$\overline{P_{\text{e}}}$	Bit Error Probability
$\overline{C}$	Ergodic Capacity
f_d	Doppler Frequency
T_d	Delay Time
G_d	Diversity Gain
G_c	Coding Gain
ξ	Pointing Error Coefficient
σ	Atmospheric Path Loss
γ_{th}	Outage Threshold
γ_e	Euler-Mascheroni Constant
ρ	Correlation Coefficient
$\mathcal{M}$	Málaga Distribution
$\mathcal{CN}$	Complex Circular Gaussian Distribution
$F_a(\cdot)$	Amplitude to Amplitude Characteristic
$F_p(\cdot)$	Amplitude to Phase Characteristic
$\Gamma(\cdot)$	Gamma Function
$\text{erf}(\cdot)$	Error Function
$\text{erfc}(\cdot)$	Complementary Error Function
$\text{Ei}(\cdot)$	Exponential Integral Function
$\mathbb{E}[\cdot]$	Expectation Operator
$\Pr(\cdot)$	Probability Measure
$J_\nu(\cdot)$	The ν-th Order Bessel Function of the First Kind
$K_\nu(\cdot)$	The ν-th Order Bessel Function of the Second Kind
$\mathcal{Q}(\cdot)$	Gaussian-Q Function
$W_{p,q}(\cdot)$	Whittaker Function
${}_pF_q(\cdot)$	Hypergeometric Function
$G_{p,q}^{m,n}(\cdot)$	Meijer G-Function
$H_{p,q}^{m,n}(\cdot)$	Fox H-Function
$H_{p_1,q_1:p_2,q_2:p_3,q_3}^{m_1,n_1:m_2,n_2:m_3,n_3}(\cdot)$	Bivariate Fox H-Function
$\Psi(\cdot:\cdot\,;\,\cdot)$	Tricomi Confluent Hypergeometric Function

Chapter 1: Introduction

With the extremely high demand for the bandwidth, Radio Frequency (RF) technology, which is the second most used technology for the backhaul networking after the copper lines and represents 6% of the total used transport media in the US [70], becomes unable to support the big data flows of the large number of users since the spectrum is limited and the access license is very costly. Moreover, shared utilization of the bandwith between the primary and secondary user based systems reaches their bottlenecks since the last ones still suffer from the spectrum scarcity. Therefore, current RF systems cannot support the high performance requirements of the fifth generation (5G) standards and future mobile broadband networks such as 3GPP LTE-advanced, IEEE 802.16m, and IEEE 802.16j. To overtake this critical situation, recent research attempts have proposed the use of the optical fibers (OF) as a way to reduce the congestion of the backhaul networks. Unlike microwave and mmWave (from 6 to 300 GHz) channels, OF provides not only high rate communications over long distance, e.g., 155.52 Mbit/s for STM-1, 622 Mbit/s for STM-4, 2.4 Gbit/s for STM-16, and 9.9 Gbit/s for STM-64, but it is also immune against the interference problems and low coverage. However, since they are very expensive to install and need important investment [37], the total usage of OF for backhauling in the US is below 4%. The main drawback of OF is that they cannot be deployed in some restricted areas and applications. In this case, OF cannot be reliable for ultra dense networks wherein a considerable deployment of OF is required to serve the enormous demand of microcell, picocell, and femtocell, etc.

To address this shortcoming, Free Space Optical (FSO) communications were recently proposed as an alternative or complement to RF and OF solutions due its flexibility, free spectrum access license, immunity to interference, high security level, power efficiency, cost effectiveness, lack of installation restrictions and most importantly as a way to densify the cellular networks [9, 39, 3, 36, 71, 59, 69]. These features make the FSO links' capacities 25 fold more efficient than RF technology and essentially they are a cost-efficient solution compared to OF [35]. Because of these advantages, FSO becomes a promising solution for the last mile problem to bridge the bandwidth gap between the end-users and the OF backbone network. Based on the aforementioned points, FSO has been used both in academia and industry for applications such as enterprise/campus connectivities, video surveillance, redundant links, disaster recovery, security, and broadcasting [36].

1.1 Motivation

FSO technology becomes a reliable and promising technique which has recently gained enormous interests especially in mixed RF/FSO systems. Previous work have proposed various channel models for the optical fading. In fact, Log-normal distribution is widely employed to statistically model the optical irradiance [24] since it provides a good fit to the experimental data for weak turbulence. However, the Log-normal model largely deviates from the experimental data as atmospheric turbulence becomes more severe. To overcome this shortcoming, recent work have proposed the so-called Gamma-Gamma (G^2) [14] as a model for the FSO fading since it provides a good fit to the experimental data for a wider range of the atmospheric turbulence compared to the Log-normal distribution. However, G^2 fails to provide a good fit with the experimental data especially at the tails. Since the calculation of the fade and the detection probability are essentially based on the tail of the probability density function (PDF), underestimation or overestimation of the tail region affects the performance analysis accuracy and certainly leads to erroneous results. To address this problem, Kashani *et. al* [34] introduced a new efficient optical fading model called Double Generalized Gamma which not only reflects a wide range of the atmospheric turbulences but also provides a good fit to the experimental data, particularly at the tail region.

As the optical signal propagates in free-space, it is susceptible not only to the atmospheric turbulence but also to the path loss and the pointing error as well. The path loss basically depends on the link distance and the atmospheric attenuation which describe the weather conditions going from clear air to hazy, rainy and foggy. The works in [24, 45] provide some typical values of the atmospheric attenuations describing the corresponding weather conditions. Moreover, the optical signal is also subject to the pointing error which can be described as the misalignment between the laser-emitting relay and the receiver photodetector. In fact, this misalignment is mainly caused by building sway and seismic activities resulting in pointing error that may arise severely when the relays and the receiver are located on tall buildings. The pointing error can be interpreted as an additional FSO fading that requires an accurate model to quantify its impact on the FSO signal. Uysal *et. al* [48] have proposed various models for the radial displacement of the pointing error assuming a Gaussian laser beam. The most general model proposed is called the Beckmann pointing error model and there are various special cases derived from it. Previous work have assumed that the radial displacement can be modeled as Rician [75], Hoyt [25], Non Zero-Mean and Zero-Mean Single-Sided Gaussian, [23] but the most prevalent one is

Rayleigh [21, 63] for simplicity.

Furthemore, the optical signal could be detected following different schemes and the most widely used are the heterodyne and intensity-modulation and direct detection (IM/DD) [26]. Although previous work have shown that the heterodyne configuration outperforms IM/DD, it is still hard to be implement in the system. IM/DD with on-off keying (OOK) is a widely employed technique in commercial FSO systems. Although IM/DD with OOK is cost effective and easy to be implemented, the main flaw of OOK is the requirement for adaptive threshold setting for demodulation [26]. As alternative to IM/DD with OOK, subcarrier intensity modulation (SIM) technique has been proposed to improve the performance of FSO systems. Applying the SIM implies that the RF subcarrier signal is premodulated by the information data sequence, before it is used for modulation of the laser source intensity [49, 79]. Besides SIM, the FSO systems with coherent detection have been intensively studied, referring to systems where optical wave, generated by local oscillator, is added to the received optical signal.

It is true that while the FSO contributes in densifying the number of users, the cellular networks still suffer from low signal coverage in some areas, mainly located in forests and mountains where the optical signal cannot travel for such long distances and it is also heavily absorbed by the intermediate objects due to its high frequency. In an attempt to increase the coverage and the scalability of the network, one way is to implement relays between the source (S) and the destination (D). Because of this advantage, cooperative relaying-assisted communication is considered as one of the key technologies for the next generation wireless communications because it plays an important role in improving the Quality of Service (QoS), reliability and coverage [30]. The majority of the research attempts investigated mixed RF/FSO system considering various relaying schemes. The most prominent ones are Amplify-and-Forward (AF) [12, 13], Decode-and-Forward (DF) [60], Quantize-and-Encode (QE) [5], and Quantize-and-Forward (QF) [38]. Moreover, many research attempts have assumed systems employing either single or multiple relays. For the single relay system, there is only one way to forward the signal to the destination through the relay. However, for multiple relay systems, there are two possible options, either sending parallel transmissions when simultaneously activating all of the relays or selecting one relay among the total set. In fact, there are many relay selection protocols such as opportunistic relay selection, partial relay selection [10], distributed switch and stay, max-select protocol and all active relaying [62].

1.2 Literature

Although many contributions of the mixed RF/FSO system are presented and validated, these attempts considered ideal hardware without impairments. In fact, these impairments can be neglected for low rate systems but cannot be omitted in the case of high rate systems, especially when we introduce optics in order to improve the transfer rate. In practice, hardware always suffers from impairments, e.g., High Power Amplifier (HPA) non-linearities [11], phase noise [44] and I/Q imbalance [41]. Given that the relays have low-cost, they are certainly of low quality and hence their tranceivers are more prone to impairments. Qi *et. al* [55] concluded that the impairments have deleterious effects on the system by limiting its performance in terms of outage probability, symbol error rate and channel capacity, especially in the high Signal-to-Noise Ratio (SNR) regime. In fact, previous work [16] demonstrated that the impaired systems have a finite capacity limit at high SNR while there are floors for both the outage probability and the symbol error rate [46]. Regarding the HPA non-linearities, this impairment is originated by the non-linear relaying amplification, and as a result a non linear distortion is created which substantially affects the quality of the signal. In practice, the output power delivered by a given amplifier is finite and upperbounded by a saturation level that is basically amplifier-dependent and varies to some limited extent. But regardless of the amplifier model, this ceiling level is always bounded. In a case when the power amplifier becomes unable to produce such power level, a signal distortion over the peak may arise and such phenomena is called clipping (clipping factor) of the power amplifier. In addition, the HPA model can be classified into two categories which are memoryless HPA and HPA with memory. The HPA is considered memoryless or frequency-independent if its frequency response characteristics are flat over the operating frequency range and in this case, the HPA is fully characterized by the two characteristics AM/AM (amplitude to amplitude conversion) and AM/PM (amplitude to phase conversion). On the other hand, the HPA is said to be with memory if its frequency responce characteristics are totally dependent on the frequency components or to the thermal phenomena [42]. Such model can be classified as a Hammerstein system that can be modeled by a series of a memoryless HPA and a linear filter. There are many types of this impairment that have been already covered in the literature but the most widely used are Soft Envelope Limiter (SEL), Traveling Wave Tube Amplifier (TWTA) and Solid State Power Amplifier (SSPA) or also called the Rapp model [44, 58, 61]. The SEL is typically used to model a HPA with a perfect predistortion system while the TWTA has been primarily considered to model the non-linearities

effect in OFDM system. However, the SSPA is characterized by a smoothness factor to control the switching between the saturation and the linear ranges. This model effectively discusses a linear characteristic for low magnitudes of the input signal and then it is limited by a definite constant saturated output. As the smoothness factor grows largely to infinity, this HPA model becomes the SEL impairments model.

The existing work of mixed RF/FSO systems cover various permutations of the system parameters. The authors in [4, 78] consider a dual-hop hybrid RF/FSO system employing AF with fixed gain (FG). Particularly, Zedini *et. al* in [78] derive the outage probability, the bit error rate (BER) and the ergodic capacity assuming that the RF and FSO follow Nakagami-m and unified G^2, respectively. Besides, Al-Quwaiee *et. al* in [4] present the same performance as the aforementioned work but they assume that the RF and FSO channels experience Rayleigh and Double Generalized Gamma fading, respectively. On the other side, [6, 76] develop asymmetric dual-hop mixed RF/FSO systems with variable gain (VG). Ansari *et. al* in [6] derive novel closed-forms of the outage probability, BER and the average capacity where the RF and FSO links experience Rayleigh and unified G^2, while Yang *et. al* in [76] derive the same performance achieved by [6] but they assume transmit diversity at the source and selection combining at the receiver. In addition the RF links are subject to Nakagami-m while the FSO fading is modeled by Málaga distribution. Further work [14, 15] assume mixed RF/FSO multiple relays systems with outdated CSI and they extend their work compared to the previous attempts by considering non-ideal hardware suffering from an aggregate model of hardware impairments. Although, the aforementioned work have considered many permutations of the system parameters, they did not consider more realistic and practical RF/FSO systems including both the spatial diversity brought by the multiple relays and a particular model of the HPA non-linearities rather than assuming a general model of impairments. The contribution of this work is the objective of the next subsection.

1.3 Contribution

In this thesis, we will study the impacts of various hardware impairments models as well as the co-channel interference on the reliability of the dual-hop relaying system with multiple relays.

In the second chapter, we introduce three models of HPA non-linearities at the relays, which are SEL, TWTA, and SSPA to a full RF dual-hop relaying systems. Then we will study the effect of the relay saturation on the outage probability, the average BER and the ergodic capacity under different relaying schemes. These relaying modes are fixed

gain (FG), variable gain (VG) version I (VGI) and version II (VGII). Note that the first version of the variable gain scheme is based on calculating the amplification gain of the instantaneous CSI feedbacks between S, relays and D. The signal amplification will be based on this outdated CSI. For the second version of (VG), the relays are supposed to have an updated version of the CSI information to compute the amplification gain. To the best of our knowledge, this is the first work elaborating on a global framework analysis of multiple relays under the effect of various models of HPA non-linear distortion. We will show that both the outage and the error performances are saturated by inevitable floors while the system capacity is limited by a finite ceiling. For some special cases, we will show that the system can operate in acceptable conditions with the presence of the hardware impairments.
This chapter makes the following contributions:

- Present a detailed description of the system model and the relay selection protocol.
- Provide an analytical framework of the impairments and how to convert the non-linear distortion into a linear impact on the system using the Bussgang linearization theory.
- Present the statistics of the channels in terms of the high order moment, the probability density function (PDF) and the cumulative distribution function (CDF).
- Once obtaining the signal-to-noise-plus-distortion-ratio (SNDR), which is a measure of the degradation of the signal by unwanted or extraneous signals including noise and distortion, we will derive the closed-forms of the outage probability, BER and the ergodic capacity for FG, VGI and VGII.
- Finally, to obtain further insights on the proposed system, we derive asymptotic expressions of the outage probability and BER at high signal-to-noise-ratio (SNR) regime. Capitalizing on these asymptotes, we derive the diversity gain of the proposed system.

In the third chapter, we introduce two impairment models, SEL and TWTA, to the relays over a dual-hop mixed RF/FSO system with multiple relays. As a strategy to select the best candidate relay, we adopt the partial relay selection protocol with outdated channel state information (CSI) based on the partial knowledge of the first hop. In fact, the channels are generally time-varying and due to the slow feedback delay from the relays to the source, the CSI used for the relay selection is outdated and so the selected relay

is not necessarily the best choice. Moreover, we consider AF for both Fixed Gain (FG) and Variable Gain (VG) relaying and we assume that the optical signal can be detected following either heterodyne or IM/DD while a subcarrier signal is used to modulate the intensity of an optical carrier (representing SIM technique). We also consider different types of modulation to get accurate insights into the study of the bit error probability under the conditions of the impairments. To the best of our knowledge, this is the first work presenting a global analytical framework of mixed RF/FSO system with multiple relays suffering from various types of impairments. The contribution of this work are as follows:

- Present a detailed description of the system architecture and the different models of impairments, we then take into account a macroscopic analysis and study the impact of the hardware impairments on the system performance.
- Specify the statistics of the RF and the optical channels in terms of the probability density function (PDF), the cumulative distribution function (CDF) and the high order moments.
- After calculating the end-to-end Signal-to-Noise-plus-Distortion Ratio (SNDR) for both FG and VG relaying, we present the analytical formulations of the outage probability, the bit error probability, the ergodic capacity, the upper bounds and the asymptotic high SNR for SEL and TWTA and for various system parameters permutations such as the time correlation of the CSI, the atmospheric turbulence condition, the number of the relays, the rank of the selected relays, the path loss and the pointing error. Once the impacts of these parameters are quantified on the system performance, we can derive quantitative summaries and valuable engineering insights to draw meaningful conclusions and observations of the proposed system.

In the fourth chapter, our contribution is to consider the Málaga fading as a model for the optical channels which, is more accurate than the most common used Log-Normal and Gamma-Gamma distributions. We assume DF and AF with fixed gain relaying due to its low complexity/cost systems, where the low latency originating from the signal processing is of high importance. Moreover, the PRS protocol with outdated CSI is considered in our system to reduce the power consumption dedicated to the relay selection. Furthermore, the most important issue in this work is to introduce an aggregate model of the hardware impairments to the source and the relays. In addition, Subcarrier Intensity Modulation (SIM) is implemented into the relays to modulate the intensity of the FSO carriers.

Various binary modulation schemes are assumed to validate the error performance of the proposed system. To the best of our knowledge, we are the first group to propose a general model of hardware impairments to a mixed RF/FSO system with multiple relays and assuming the unified Málaga $\mathcal{M}$-distribution to model the optical channels. The analysis in this chapter follows these steps:

- Present a detailed analyis of the system and channels' models.
- Provide the Cumulative Distribution Function (CDF) and the PDF of the RF and FSO channels.
- Derive the expressions of the end-to-end Signal-to-Noise-plus-Distortion Ratio (SNDR), which is a measure of the degradation of the signal by unwanted or extraneous signals including noise and distortion, for AF and DF relaying protocols.
- Based on the aforementioned expressions, novel closed-forms, upper bounds as well as high SNR asymptotes of the outage probability (OP), the symbol error probability (SEP) and the ergodic capacity (EC) are derived.
- Capitalizing on the high SNR asymptotes, engineering insights into the system performance such as the diversity and the coding gains are derived.

In the fifth chapter, we propose a mixed RF/FSO system with multiple relays employing Fixed Gain (FG) relaying. PRS based on the CSI of the first hop is assumed with outdated CSI for relay selection and both the relays and the destination are respectively affected by non-linear power amplification (NLPA) and IQ imbalance. We will quantify the impacts of NLPA and IQ imbalance on the performance metrics of the proposed system. Analytical expressions of the outage probability and the ergodic capacity will be derived as well as the upper bounds. Since the derivation of closed-form expression of the bit error probability is not tractable, numerical integration is adopted to evaluate the bit error performance.

In the sixth chapter, we propose a mixed RF/FSO systems with multiple relays where the source and the relays are affected by a general model of impairment. The RF channels are modelled by correlated Rayleigh fading while the FSO channels are subject to the Double-Weibull fading. Moreover, the signal is received either by heterodyne or IM/DD detection methods. Mathematical expressions of the outage probability and the ergodic capacity are derived as well as the analytical upperbounds expressions.

The seventh chapter discusses a dual-hop mixed RF/FSO system with multiple relays where RF channels experience Nakagami-m fading and FSO links are subject to the double generalized gamma fading encompassing the turbulence-induced fading, atmospheric path loss, and pointing error. We also consider the co-channel interference, which is detrimental to RF links. Besides, the relays employ AF with CSI-assisted relaying and we consider partial relay selection with outdated CSI based on the RF channels information. Furthermore, the photodetector can detect the signal following either the coherent/heterodyne mode or the Intensity Modulation and Direct Detection (IM/DD). In addition, Subcarrier Intensity Modulation (SIM) is implemented into the relays to modulate the intensity of the FSO carriers. Various binary modulation schemes are assumed to validate the error performance of the proposed system. The analysis of this chapter follows these steps:

- Present a detailed analysis of the system and channels' models.
- Provide the Cumulative Distribution Function (CDF) and the Probability Density Function (PDF) of the RF and FSO channels.
- Derive the statistics of the end-to-end Signal-to-Interference-plus-Noise Ratio (SINR) such as the CDF, PDF, high order moment, amount of fading, and the Moment Generating Function (MGF).
- Based on the aforementioned statistics, novel closed-forms as well as high SNR asymptotes of the outage probability, the bit error probability, the ergodic capacity, and the outage rate are derived.
- Capitalizing on the asymptotic high SNR, engineering insight into the system gains such as the diversity gain is derived.

Chapter 2: Impact of Non-Linear High Power Amplifiers on Cooperative Relaying Systems

"Impact of Non-Linear High-Power Amplifiers on Cooperative Relaying Systems," in *IEEE Transactions on Communications*, vol. 65, no. 10, pp. 4163-4175, Oct. 2017.

2.1 Introduction

In this chapter, we quantify the impacts of three models of high-power amplifier (HPA) non-linear distortion (NLD), which are SEL, TWTA, and SSPA, on a given relaying network. This system consists of multiple relays between the source (S) and the destination (D) and employs three modes of the amplify-and-forward (AF) protocol. The transmission is done through one relay that should be selected following the opportunistic relay selection protocol based on imperfect channel state information (CSI). In this context, we will introduce the HPA non-linearity to a more complex relaying system configuration characterized by multiple relays, imperfect CSI and opportunistic relay selection. Given that, the non-linear distortion has deleterious impact on the system, a sophisticated selection protocol is highly required to reduce this negative effect and to overcome the fading impact as well. Closed-forms, analytical upper bounds and high SNR approximation of the outage probability (OP), the average bit error rate (BER) and the ergodic capacity (EC) are derived. Finally, analytical expressions are validated by Monte Carlo simulation.

2.2 System Model

The system is composed of a source S, destination D and N parallel relays $R_n, n = 1, .., N$ wirelessly connected to S and D as shown in Fig. 2.1. The channels of the first and the second hops are symmetric, independent and indentically distributed following the Rayleigh distribution.

2.2 CSI Model

As mentioned earlier, we assumed an outdated CSI instead of a perfect one. In this case, the relay selection protocol is achieved based on a delayed version of the CSI and not on the current one due to the feedback delay. In this way, the outdated and the current channels' gains are denoted by $\widetilde{h}_1$ and h_1, respectively. Hence, the outdated CSI between

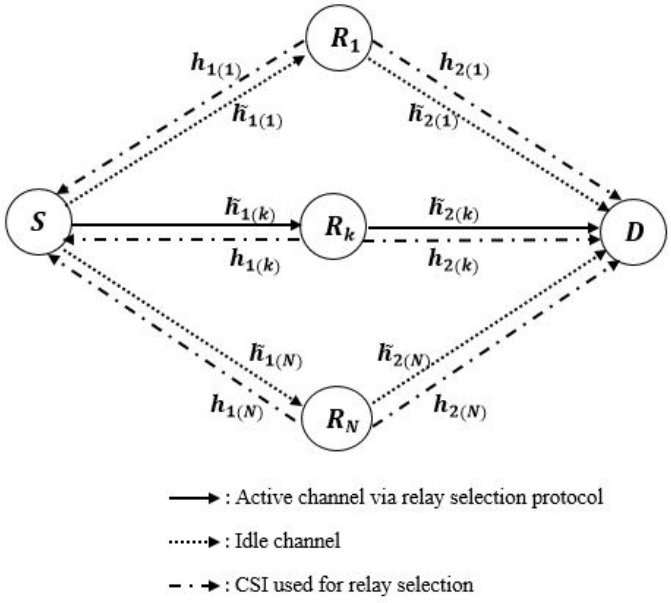

Figure 2.1: Dual-hop Cooperative Relaying System

S - kth relay and kth relay - D are respectively modeled as follows

$$\widetilde{h}_{1(k)} = \sqrt{\rho_1} h_{1(k)} + \sqrt{1-\rho_1} w_{1(k)}, \tag{2.1}$$

and

$$\widetilde{h}_{2(k)} = \sqrt{\rho_2} h_{2(k)} + \sqrt{1-\rho_2} w_{2(k)}, \tag{2.2}$$

where $w_{1(k)}$ and $w_{2(k)}$ are two random variables that, respectively, follow the circularly symmetric complex Gaussian distribution with the same variances of the channels' gains $h_{1(k)}$ and $h_{2(k)}$. The time correlation coefficients ρ_1 and ρ_2 are between the channels $h_1 - \widetilde{h}_1$ and $h_2 - \widetilde{h}_2$, respectively. The coefficients ρ_1 and ρ_2 are given by the Jakes' autocorrelation model as follows [31]

$$\rho_i = J_0(2\pi f_{d,i} T_d), \ i = \{1, \ 2\}, \tag{2.3}$$

where $J_0(\cdot)$ is the zeroth order Bessel function of the first kind [27, Eq. (8.411)], T_d is the time delay between the current CSI and the delayed version and f_d is the maximum Doppler frequency of the channels.

2.2 Opportunistic Relay Selection

This protocol states that each relay should quantify its appropriateness as an active relay, using a function describing the link quality of the two hops. The first step is to select the minimum channel gains between two hops for each relay. Based on the first step, the relay of rank k characterized by the strongest bottleneck is the one with the best overall path between S and D.

$$\gamma_i = \min(\gamma_{1(i)}, \gamma_{2(i)}), \tag{2.4}$$

Then

$$k = \arg\max_i(\gamma_i), \tag{2.5}$$

where $\gamma_{1(i)}, \gamma_{2(i)}$ are the instantaneous SNRs of the ith channel of the first and second hops, respectively.
Since the relays operate in a half-duplex mode, they cannot send and receive simultaneously. Consequently, the best relay may not be always available to receive the data from the source, and hence, the control unit will select the next best available relay.

2.2 HPA non-linearities Model

We assume that the relays are subject to HPA non-linearities. For a given transmission, the selected relay receives the signal $y_{1(k)}$ from S and then amplifies it by the factor gain G. This amplification takes place in two time slots. In the first phase, the gain G is applied to the received signal as follows

$$\phi_k = G y_{1(k)}, \tag{2.6}$$

In the second phase, the output signal ϕ_k passes through a non-linear circuit as follows

$$\psi_k = f(\phi_k), \tag{2.7}$$

where $f(\cdot)$ is the function of amplitude and phase of the non-linear circuit. In addition, we assume that the relays power amplifiers are memoryless. A given memoryless power amplifier is characterized by both AM/AM and AM/PM. The signal at the output of the non-linear circuit is given by [54]

$$\psi_k = F_a(\phi_k)\ \exp(j(\arg(\phi_k) + F_p(\phi_k))), \tag{2.8}$$

where $\arg(\phi_k)$ is the phase of the complex signal ϕ_k and $F_a(\cdot),\ F_p(\cdot)$ are the characteristic functions AM/AM, AM/PM, respectively.

2.2.3.1 SEL

This type of impairment is suitable to model a HPA with perfect predistortion system. The characteristic functions of SEL are expressed as follows [58]

$$F_a(\phi_k) = \begin{cases} |\phi_k|, & |\phi_k| \leq A_{sat} \\ A_{sat}, & \text{otherwise} \end{cases}, \tag{2.9}$$

$$F_p(\phi_k) = 0, \tag{2.10}$$

where A_{sat} is the HPA input saturation amplitude.

2.2.3.2 SSPA

This impairment model, also called the Rapp model, was detailed in [56] and presents only the amplitude characteristic AM/AM. The functions are given by

$$F_a(\phi_k) = |\phi_k| \left[1 + \left(\frac{|\phi_k|}{A_{sat}} \right)^{2\nu} \right]^{-\frac{1}{2\nu}}, \tag{2.11}$$

$$F_p(\phi_k) = 0, \tag{2.12}$$

where ν is the smoothness factor that controls the transition from linear to saturation domain. As ν converges to infinity, SSPA effectively converges to the SEL model.

2.2.3.3 TWTA

This impairment is used to model the impact of non-linearities in OFDM systems [61], [77]. The characteristic functions of this model are given by

$$F_a(\phi_k) = A_{sat}^2 \frac{|\phi_k|}{|\phi_k|^2 + A_{sat}^2}, \tag{2.13}$$

$$F_p(\phi_k) = \Phi_0 \frac{|\phi_k|^2}{|\phi_k|^2 + A_{sat}^2}, \tag{2.14}$$

where Φ_0 controls the maximum phase distortion.
In practice, to mitigate the impacts of the non-linear distortion, the HPA operates at an input back-off (IBO) from a given saturation level. In the literature, there have been many definitions of the IBO, but in this work, we will adopt the following definition

$$\text{IBO} = 10\log_{10}\left(\frac{A_{sat}^2}{\sigma^2}\right), \tag{2.15}$$

where σ^2 is the mean power of the signal at the output of the gain block. Fig. 2.2 presents the variations of the AM/AM with respect to the normalized input modulus for SEL, TWTA, and SSPA.

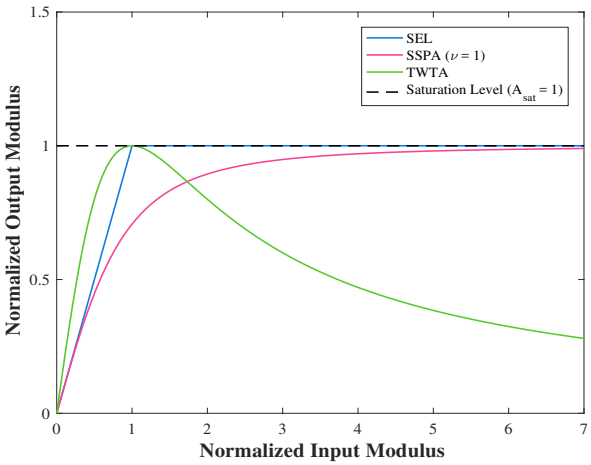

Figure 2.2: AM/AM characteristics of SEL, SSPA and TWTA

2.2 Bussgang Linearization Theory

This theory states that the output of the non-linear power amplifier circuit can be expressed in terms of a linear scale parameter δ of the input signal and a non-linear distortion τ, which is uncorrelated with the input signal and distributed following the complex circular Gaussian random variable $\tau \backsim \mathcal{CN}(0,\ \sigma_\tau^2)$. In this case, the characteristic function of the amplitude is given by

$$\psi_k = \delta\phi_k + \tau, \tag{2.16}$$

We can derive the expressions of δ and σ_τ^2 following the two corollaries.

Corollary 1. *The linear scale δ can be derived as follows*

$$\delta = \frac{\mathbb{E}\left[\phi_k^* \psi_k\right]}{\mathbb{E}\left[|\phi_k|^2\right]}, \tag{2.17}$$

Corollary 2. *The variance of the non-linear distortion is given by*

$$\sigma_\tau^2 = \mathbb{E}\left[|\psi_k|^2\right] - \delta \mathbb{E}\left[\phi_k \psi_k^*\right], \tag{2.18}$$

For the SEL model, δ and σ_τ^2 can be expressed as follows [44, Eq. (10)]

$$\delta = 1 - \exp\left(-\frac{A_{sat}^2}{\sigma^2}\right) + \frac{\sqrt{\pi} A_{sat}}{2\sigma} \text{erfc}\left(-\frac{A_{sat}}{\sigma}\right), \tag{2.19}$$

$$\sigma_\tau^2 = \sigma^2 \left[1 - \exp\left(-\frac{A_{sat}^2}{\sigma^2}\right) - \delta^2\right], \tag{2.20}$$

where $\text{erfc}(\cdot)$ is the complementary error function.
To simplify the calculation for the case of SSPA, we first assume that the smoothness factor ($\nu = 1$) and then we refer to [1] to derive the parameters as follows

$$\delta = \frac{A_{sat}}{2\sigma} \left[\frac{2A_{sat}}{\sigma} - \sqrt{\pi} \text{erfc}\left(\frac{A_{sat}}{\sigma}\right) \exp\left(\frac{A_{sat}^2}{\sigma^2}\right) \left(\frac{2A_{sat}^2}{\sigma^2} - 1\right)\right], \tag{2.21}$$

$$\sigma_\tau^2 = \sigma^2 \left[\frac{A_{sat}^2}{\sigma^2} \left(1 + \frac{A_{sat}^2}{\sigma^2} \exp\left(\frac{A_{sat}^2}{\sigma^2}\right) \text{Ei}\left(-\frac{A_{sat}^2}{\sigma^2}\right)\right) - \delta^2\right], \tag{2.22}$$

where $\text{Ei}(\cdot)$ is the exponential integral function.
If the phase characteristic AM/PM is negligeable (i.e., $\Phi_0 \approx 0$), the impairment parameters δ and σ^2 for TWTA can be obtained by [44, Eq. (11)]

$$\delta = \frac{A_{sat}^2}{\sigma^2} \left[1 + \frac{A_{sat}^2}{\sigma^2} \exp\left(\frac{A_{sat}^2}{\sigma^2}\right) \text{Ei}\left(-\frac{A_{sat}^2}{\sigma^2}\right)\right], \tag{2.23}$$

$$\sigma_\tau^2 = -\frac{A_{sat}^4}{\sigma^2} \left[\left(1 + \frac{A_{sat}^2}{\sigma^2}\right) \exp\left(\frac{A_{sat}^2}{\sigma^2}\right) \text{Ei}\left(-\frac{A_{sat}^2}{\sigma^2}\right) + 1\right] - \sigma^2 \delta^2, \tag{2.24}$$

2.2 Statistics of the channels

Since the channels of the first hop experience Rayleigh fading with outdated CSI and the system employs the opportunistic relay selection protocol, the PDF of the SNR of the

first hop of the kth channel is given by [66, Eq. (21)]

$$f_{\widetilde{\gamma}_{1(k)}}(x) = \frac{k}{\overline{\gamma}_1}\binom{N}{k}\sum_{n=0}^{k-1}\sum_{j=1}^{2} P_n Q_{n,j} \exp\left(-\frac{R_{n,j}x}{\overline{\gamma}_2}\right), \tag{2.25}$$

Due to the symmetry of the channels fading, the CDF of the second hop at the kth channel can be expressed as follows

$$F_{\widetilde{\gamma}_{2(k)}}(x) = 1 - k\binom{N}{k}\sum_{m=0}^{k-1}\sum_{i=1}^{2} S_m T_{m,i} \exp\left(-\frac{U_{m,i}x}{\overline{\gamma}_1}\right), \tag{2.26}$$

where $P_n, S_m, Q_{n,j}, R_{n,j}, T_{m,i}, U_{m,i}$, and $\overline{\gamma}$ are defined by:

$$P_n = \frac{(-1)^n\binom{k-1}{n}}{1+\frac{\overline{\gamma}_2}{\overline{\gamma}}(N-k+n)}, \tag{2.27}$$

$$S_m = \frac{(-1)^m\binom{k-1}{m}}{1+\frac{\overline{\gamma}_1}{\overline{\gamma}}(N-k+m)}, \tag{2.28}$$

$$Q_{n,1} = 1, \tag{2.29}$$

$$Q_{n,2} = \frac{(N-k+n)\overline{\gamma}_2}{\rho_1\overline{\gamma}+(1-\rho_1)(N-k+n+1)\overline{\gamma}_1}, \tag{2.30}$$

$$R_{n,1} = 1, \tag{2.31}$$

$$R_{n,2} = \frac{(N-k+n+1)\overline{\gamma}_1}{\rho_1\overline{\gamma}+(1-\rho_1)(N-k+n+1)\overline{\gamma}_1}, \tag{2.32}$$

$$T_{m,1} = 1, \tag{2.33}$$

$$T_{m,2} = \frac{(N-k+m)\overline{\gamma}_1}{(N-k+m+1)\overline{\gamma}_2}, \tag{2.34}$$

$$U_{m,1} = \frac{\overline{\gamma}_1}{\overline{\gamma}_2}, \tag{2.35}$$

$$U_{m,2} = \frac{(N-k+m+1)\overline{\gamma}_2}{\rho_2\overline{\gamma}+(1-\rho_2)(N-k+m+1)\overline{\gamma}_2}, \tag{2.36}$$

$$\overline{\gamma} = \frac{\overline{\gamma}_1\overline{\gamma}_2}{\overline{\gamma}_1+\overline{\gamma}_2}, \tag{2.37}$$

The nth moment can be derived using [27, Eq. (3.326.2)]

$$\begin{aligned}\mathbb{E}\left[\widetilde{\gamma}_{1(k)}^{n}\right] =& \frac{k}{\overline{\gamma}_1}\binom{N}{k}\sum_{m=0}^{k-1}\frac{\binom{k-1}{m}(-1)^m n!}{1+\frac{\overline{\gamma}_2}{\overline{\gamma}}(N-k+m)} \\ &\times \left[\overline{\gamma}_1^{n+1} + \overline{\gamma}_2\left(\frac{\rho_1\overline{\gamma}+(1-\rho_1)(N-k+m+1)\overline{\gamma}_1}{N-k+m+1}\right)^n\right],\end{aligned} \tag{2.38}$$

2.2 End-to-End SNDR: Fixed Gain Relaying

The relaying gain of the FG scheme is given by

$$G \triangleq \sqrt{\frac{\sigma^2}{\mathbb{E}\left[|\widetilde{h}_{1(k)}(t)|^2\right]P_1+\sigma_0^2}}, \tag{2.39}$$

where P_1 is the average transmitted power from S and σ_0^2 is the noise variance. The end-to-end SNDR of the FG relaying can be expressed as follows

$$\gamma_{\text{ni}}^{\text{FG}} = \frac{\widetilde{\gamma}_{1(k)}\widetilde{\gamma}_{2(k)}}{\zeta\widetilde{\gamma}_{2(k)}+\mathbb{E}\left[\widetilde{\gamma}_{1(k)}\right]+\zeta}, \tag{2.40}$$

where ζ is defined by

$$\zeta = 1+\frac{\sigma_\tau^2}{\delta^2 G^2\sigma_0^2}, \tag{2.41}$$

For ideal relays ($\zeta = 1$), the end-to-end SNR can be written as follows

$$\gamma_{\text{id}}^{\text{FG}} = \frac{\widetilde{\gamma}_{1(k)}\widetilde{\gamma}_{2(k)}}{\widetilde{\gamma}_{2(k)}+\mathbb{E}\left[\widetilde{\gamma}_{1(k)}\right]+1}, \tag{2.42}$$

2.2 End-to-End SNDR: Variable Gain Relaying I

In this relaying scheme, the relays compute the gain using the CSI of the channel S-R_k. The relays already know the CSI information since it was measured during the relay selection. However, this CSI information is not updated and it will be used to calculate the signal amplification gain which can be written as follows

$$G \triangleq \sqrt{\frac{\sigma^2}{|\widetilde{h}_{1(k)}(t-T_d)|^2P_1+\sigma_0^2}}, \tag{2.43}$$

The end-to-end SNDR is given by

$$\gamma_{\text{ni}}^{\text{VGI}} = \frac{\widetilde{\gamma}_{1(k)}\widetilde{\gamma}_{2(k)}}{\zeta\widetilde{\gamma}_{2(k)} + \gamma_{1(k)} + \zeta}, \tag{2.44}$$

2.2 End-to-End SNDR: Variable Gain Relaying II

This relaying scheme states that unlike the VGI, the relays computes the amplification gain using the current estimated CSI rather than the outdated one. Although this scheme appears to be more realistic and sophisticated, it is very complex for implementation compared to the first version of VG since the two CSIs h and $\widetilde{h}$ are required to be estimated by the control unit. The estimation of the CSI $\widetilde{h}$ is achieved by the superimposed pilots used during the feedback exchange between the various nodes of the system.
The amplification gain can be obtained by

$$G \triangleq \sqrt{\frac{\sigma^2}{|\widetilde{h}_{1(k)}(t)|^2 P_1 + \sigma_0^2}}, \tag{2.45}$$

In this case, the end-to-end SNDR can be derived as follows

$$\gamma_{\text{ni}}^{\text{VGII}} = \frac{\widetilde{\gamma}_{1(k)}\widetilde{\gamma}_{2(k)}}{\zeta\widetilde{\gamma}_{2(k)} + \widetilde{\gamma}_{1(k)} + \zeta}, \tag{2.46}$$

2.3 Outage Probability Analysis

The outage probability is the probability that the overall SNDR falls below a given threshold γ_{th} of acceptable transmission quality. It can be defined as

$$P_{\text{out}}(\gamma_{\text{th}}) \triangleq \Pr[\gamma < \gamma_{\text{th}}], \tag{2.47}$$

where γ is the effective overall SNDR and $\Pr(\cdot)$ is the probability measure.

2.3 Fixed Gain Relaying

After substituting the expression of the effective SNDR (2.40) in Eq. (2.47) and applying the following identity [27, Eq. (3.324.1)], the outage expression is given by

$$\begin{aligned} P_{\text{out}}(\gamma_{\text{th}}) =& 1 - \frac{2k^2}{\overline{\gamma}_1}\binom{N}{k}^2 \sum_{m=0}^{k-1}\sum_{n=0}^{k-1}\sum_{i=1}^{2}\sum_{j=1}^{2} S_m P_n T_{m,i} Q_{n,j} \exp\left(-\frac{R_{n,j}\zeta\gamma_{\text{th}}}{\overline{\gamma}_1}\right)\sqrt{\frac{U_{m,i}c\gamma_{\text{th}}}{R_{n,j}}} \\ & \times \; K_1\left(\frac{2}{\overline{\gamma}_1}\sqrt{U_{m,i}R_{n,j}c\gamma_{\text{th}}}\right), \end{aligned} \tag{2.48}$$

where $K_\nu(\cdot)$ is the modified Bessel function of the second kind of order ν and the parameter $c = \mathbb{E}\left[\widetilde{\gamma}_{1(k)}\right] + \zeta$.

To get a more accurate insight on the system, we derive an analytical expression of the outage probability at high SNR regime which is given by Eq. (2.49).

$$\begin{aligned} P^{\infty}_{\text{out}}(\gamma_{\text{th}}) \underset{\overline{\gamma}_1,\overline{\gamma}_2\gg 1}{\cong} & \frac{k^2\gamma_{\text{th}}}{\overline{\gamma}_1}\binom{N}{k}^2 \sum_{m=0}^{k-1}\sum_{n=0}^{k-1}\sum_{i=1}^{2}\sum_{j=1}^{2} S_m P_n T_{m,i} Q_{n,j} \\ & \times \; \left[\frac{T_{m,i}c}{\overline{\gamma}_1}\,\log\left(\frac{\overline{\gamma}_1}{R_{n,j}}\right) + \exp\left(-\frac{U_{m,i}c}{\overline{\gamma}_1}\right) + \frac{U_{m,i}c}{\overline{\gamma}_1}\right. \\ & \times \; \left.\left\{1 - \gamma_e + \text{Ei}\left(-\frac{U_{m,i}c}{\overline{\gamma}_1}\right) - \log\left(\frac{U_{m,i}c}{\overline{\gamma}_1}\right)\right\}\right], \end{aligned} \tag{2.49}$$

where γ_e is the Euler-Mascheroni constant.

2.3 Variable Gain Relaying I

In this case, we should substitute the expression of the effective SNDR (2.44) in Eq. (2.47). Since the derivation of a closed-form of the outage performance for VGI

is very complex, an approximation is provided by Eq. (2.50).

$$\begin{aligned} P_{\text{out}}(\gamma_{\text{th}}) \cong & 1 - k^2 \binom{N}{k}^2 \sum_{m=0}^{k-1} \sum_{n=0}^{k-1} \sum_{i=1}^{2} \sum_{j=1}^{2} S_m P_n T_{m,i} Q_{n,j} \\ & \times \quad \exp\left[-\frac{\gamma_{\text{th}}}{(1-\rho_1)\overline{\gamma}_1} \left(\frac{\rho_1 (U_{m,i} - R_{n,j}\zeta)}{(1-\rho_1) R_{n,j}^2} + \zeta \right) \right] \\ & \times \quad \left[\left(R_{n,j} \left(1 - \frac{\rho_1}{(1-\rho_1) R_{n,j}} \right) \right)^{-1} + \frac{\gamma_{\text{th}} U_{m,i}}{(1-\rho_1)\overline{\gamma}_1 R_{n,j}^2} \right. \\ & + \quad \left. \log\left(\frac{1}{(1-\rho_1)\overline{\gamma}_1} - \frac{\rho_1}{(1-\rho_1)^2 \overline{\gamma}_1 R_{n,j}} \right) \right], \end{aligned} \tag{2.50}$$

2.3 Variable Gain Relaying II

After replacing the end-to-end SNDR (2.46) in Eq. (2.47) and after applying the identity [27, Eq. (3.324.1)], the outage probability can be finally expressed as follows

$$\begin{aligned} P_{\text{out}}(\gamma_{\text{th}}) = 1 - \frac{2k^2}{\overline{\gamma}_1} \binom{N}{k}^2 \sum_{m=0}^{k-1} \sum_{n=0}^{k-1} \sum_{i=1}^{2} \sum_{j=1}^{2} S_m P_n T_{m,i} Q_{n,j} \exp\left[-\frac{\gamma_{\text{th}}}{\overline{\gamma}_1} (U_{m,i} + \zeta R_{n,j}) \right] \\ \times \quad \sqrt{\frac{U_{m,i}\zeta\gamma_{\text{th}}(1+\gamma_{\text{th}})}{R_{n,j}}} K_1\left(\frac{2}{\overline{\gamma}_1} \sqrt{U_{m,i} R_{n,j} \zeta \gamma_{\text{th}} (1+\gamma_{\text{th}})} \right), \end{aligned} \tag{2.51}$$

For every value of x very close to zero, we get $K_1(x) \approx \frac{1}{x}$, and $e^x \approx 1 + x$. Based on these asymptotic expressions, a simpler approximation of the outage expression for VGII at high-SNR regime is given by

$$P_{\text{out}}^{\infty}(\gamma_{\text{th}}) \underset{\overline{\gamma}_1, \overline{\gamma}_2 \gg 1}{\cong} \frac{k^2 \gamma_{\text{th}}}{\overline{\gamma}_1} \binom{N}{k}^2 \sum_{m=0}^{k-1} \sum_{n=0}^{k-1} \sum_{i=1}^{2} \sum_{j=1}^{2} S_m P_n T_{m,i} Q_{n,j} \left(\zeta + \frac{U_{m,i}}{R_{n,j}} \right), \tag{2.52}$$

For ideal or linear relaying, the diversity gain can be derived from Eqs. (2.49, 2.50, 2.52). It can be expressed as follows

$$G_d = \begin{cases} N, & \rho_1 = \rho_2 = 1 \\ 1, & \rho_1, \rho_2 < 1 \end{cases} \tag{2.53}$$

If the relays are impaired, the outage performance saturates by the impairments floor and so the diversity gain in this case is equal to zero ($G_d = 0$).

2.4 Average Bit Error Rate Analysis

In this section we address the error performance of the system for different modulation schemes and considering the three relaying modes. The average BER for various modulation formats such as BPSK, M-PAM, M-PSK and M-QAM is defined by

$$\overline{P_e} = \alpha \mathbb{E}\left[Q(\sqrt{2\beta\gamma})\right], \tag{2.54}$$

where $Q(x) = \frac{1}{\sqrt{2\pi}} \int_x^\infty e^{-\frac{t^2}{2}} dt$ is the Gaussian Q-function and α, β are the modulation parameters. Using integration by parts, Eq. (2.54) can be expressed as follows

$$\overline{P_e} = \frac{\alpha\sqrt{\beta}}{2\sqrt{\pi}} \int_0^\infty \frac{e^{-\beta\gamma}}{\sqrt{\gamma}} F_\gamma(\gamma) d\gamma, \tag{2.55}$$

2.4 Fixed Gain Relaying

To derive a closed-form of the average BER for the FG relaying scheme, we should substitute the expression of the outage probability (2.48) into Eq. (2.55). Then we must apply the identity [2, Eq. (4.17.37)] to get the expression as follows

$$\begin{aligned}\overline{P_e} =& \frac{\alpha}{2} - \frac{\alpha k^2}{2}\sqrt{\frac{\beta\overline{\gamma}_1}{\pi}}\Gamma\left(\frac{1}{2}\right)\Gamma\left(\frac{3}{2}\right)\binom{N}{k}^2 \sum_{m=0}^{k-1}\sum_{n=0}^{k-1}\sum_{i=1}^{2}\sum_{j=1}^{2} \frac{S_m P_n T_{m,i} Q_{n,j}}{R_{n,j}\sqrt{2R_{n,j}\zeta + \beta\overline{\gamma}_1}} \\ &\times \exp\left(\frac{U_{m,i} R_{n,j} c}{\overline{\gamma}_1(\beta\overline{\gamma}_1 + 2\zeta R_{n,j})}\right) W_{-\frac{1}{2},\frac{1}{2}}\left(\frac{2U_{m,i}R_{n,j}}{\overline{\gamma}_1(\beta\overline{\gamma}_1 + 2\zeta R_{n,j})}\right),\end{aligned} \tag{2.56}$$

where $W_{p,q}(\cdot)$ is the Whittaker function.
Now, we should substitute Eq. (2.49) in (2.55). After applying the identity [52, Eq. (2.3.3.1)], the high SNR approximation of the average BER of FG relaying can be expressed as fol-

lows:

$$\overline{P}_e^{\infty} \underset{\overline{\gamma}_1,\overline{\gamma}_2\gg 1}{\cong} \frac{\alpha k^2}{2\overline{\gamma}_1}\binom{N}{k}^2 \sum_{m=0}^{k-1}\sum_{n=0}^{k-1}\sum_{i=1}^{2}\sum_{j=1}^{2} S_m P_n T_{m,i} Q_{n,j} \left[\frac{U_{m,i}c}{\overline{\gamma}_1}\ \log\left(\frac{\overline{\gamma}_1}{R_{n,j}}\right)\right.$$
$$\left. +\ \ \exp\left(-\frac{U_{m,i}c}{\overline{\gamma}_1}\right) + \frac{U_{m,i}c}{\overline{\gamma}_1}\left\{1-\gamma_e+\mathrm{Ei}\left(-\frac{U_{m,i}c}{\overline{\gamma}_1}\right) - \log\left(\frac{U_{m,i}c}{\overline{\gamma}_1}\right)\right\}\right], \tag{2.57}$$

2.4 Variable Gain Relaying I

After substituting the expression (2.50) in Eq. (2.55) and applying the identity [52, Eq. (2.3.3.1)], the approximation of the average BER can be derived as follows

$$\overline{P_e} \cong \frac{\alpha}{2} - \frac{\alpha k^2}{2}\binom{N}{k}^2 \sum_{n=0}^{k-1}\sum_{i=1}^{2}\sum_{j=1}^{2} S_m P_n T_{m,i} Q_{n,j} \sqrt{\frac{\beta}{2\mu+\beta}}\left[\eta + \frac{\nu}{2\mu+\beta}\right], \tag{2.58}$$

where η, μ, and ν are given by

$$\eta = \frac{1}{R_{n,j} - \dfrac{\rho_1}{1-\rho_1}}, \tag{2.59}$$

$$\mu = \frac{1}{(1-\rho_1)\overline{\gamma}_1}\left(\frac{\rho_1(U_{m,i}-R_{n,j}\zeta)}{(1-\rho_1)R_{n,j}^2} + \zeta\right), \tag{2.60}$$

$$\nu = \frac{U_{m,i}}{(1-\rho_1)\overline{\gamma}_1 R_{n,j}^2}\log\left(\frac{1}{(1-\rho_1)^2} - \frac{\rho_1}{(1-\rho_1)^2\overline{\gamma}_1 R_{n,j}}\right), \tag{2.61}$$

2.4 Variable Gain Relaying II

Since the derivation of a closed-form of the average BER is complex, we should consider a simpler form. After some mathematical manipulation, the analytical approximation is given by Eq. (2.62).

$$\overline{P_e} = \frac{\alpha}{2} - \frac{\alpha k^2\sqrt{2}}{\beta\overline{\gamma}_1}\Gamma\left(\frac{1}{2}\right)\Gamma\left(\frac{5}{2}\right)\binom{N}{k}^2 \sum_{m=0}^{k-1}\sum_{n=0}^{k-1}\sum_{i=1}^{2}\sum_{j=1}^{2} S_m P_n T_{m,i} Q_{n,j}\sqrt{\frac{\zeta U_{m,i}}{R_{n,j}}}\frac{\varrho}{(\omega+\varrho)^{\frac{5}{2}}}$$
$$\times\ {}_2F_1\left(\frac{5}{2},\frac{3}{2},2,\frac{\omega-\varrho}{\omega+\varrho}\right), \tag{2.62}$$

where ${}_pF_q$(a,b,z) is the hypergeometric function.
After substituting the expression (2.52) in Eq. (2.55) and applying the identity [52, Eq. (2.3.3.1)], the asymptotic high SNR of the BER is given by

$$\overline{P_e^{\infty}} \underset{\overline{\gamma}_1,\overline{\gamma}_2 \gg 1}{\cong} \frac{\alpha k^2}{2\beta\overline{\gamma}_1}\binom{N}{k}^2 \sum_{m=0}^{k-1}\sum_{n=0}^{k-1}\sum_{i=1}^{2}\sum_{j=1}^{2} S_m P_n T_{m,i} Q_{n,j}\left(\zeta + \frac{U_{m,i}}{R_{n,j}}\right), \tag{2.63}$$

2.5 Ergodic Capacity Analysis

The channel capacity, expressed in (bit/s/Hz), is defined as the maximum error-free data rate transmitted by the system. It can be written as follows:

$$\overline{C} = \frac{1}{2}\mathbb{E}\left[\log_2(1+\gamma)\right], \tag{2.64}$$

Since the transmission is achieved in two steps, the system capacity is multiplied by the factor $\frac{1}{2}$. After some mathematical manipulation, the egodic capacity can be expressed as follows:

$$\overline{C} = \frac{1}{2\log(2)}\int_0^{\infty}\frac{\overline{F}_{\gamma}(\gamma)}{\gamma+1}d\gamma, \tag{2.65}$$

where γ is the end-to-end SNDR and $\overline{F}_{\gamma}$ is the complementary cumulative distribution function (CCDF) of γ.
Since the non-linear distortion deteriorates the system performance, an indesirable ceiling is created by the impairments which limits the achievable rate of the system. The ceiling expression is given by [44, Eq. (37)]

$$\overline{C}^{*} = \frac{1}{2}\log_2\left(1 + \frac{1}{\frac{\varepsilon}{\delta^2}-1}\right), \tag{2.66}$$

where ε is the clipping factor of the hardware impairments.

2.5 Fixed Gain Relaying

After replacing the CCDF of the SNDR (2.40) in (2.65) and applying some mathematical manipulation, the closed-form of the ergodic capacity is derived in term of bivariate

Meijer G-function as follows:

$$\begin{aligned}\overline{C} =&\frac{k^2\binom{N}{k}^2}{2\log(2)\overline{\gamma}_1}\sum_{m=0}^{k-1}\sum_{n=0}^{k-1}\sum_{i=1}^{2}\sum_{j=1}^{2}S_mP_nT_{m,i}Q_{n,j}\sqrt{\frac{U_{m,i}c}{R_{n,j}}}\\ &\times\ G_{1,1:0:1:0,2}^{1,1:1,0:2,0}\left(\begin{array}{c|c|c|c} -\frac{1}{2} & - & - & \\ -\frac{1}{2} & 0 & \frac{1}{2},-\frac{1}{2} & \frac{R_{n,j}\zeta}{\overline{\gamma}_1},\frac{U_{m,i}R_{n,j}c}{\overline{\gamma}_1^2}\end{array}\right),\end{aligned} \tag{2.67}$$

2.5 Variable Gain Relaying I

In this case, we should replace the expression of the CCDF of (2.44) in Eq. (2.65). After referring to the identity [27, Eq. (3.353.5)], the approximation of the capacity is derived as follows:

$$\overline{C}^{\text{ub}} \cong \frac{k^2}{2\log(2)}\binom{N}{k}^2\sum_{m=0}^{k-1}\sum_{n=0}^{k-1}\sum_{i=1}^{2}\sum_{j=1}^{2}S_mP_nT_{m,i}Q_{n,j}\left[\frac{\nu}{\mu}+e^{\mu}\text{Ei}(-\mu)(\nu-\eta)\right], \tag{2.68}$$

2.5 Variable Gain Relaying II

Since the integral (2.65) is not solvable for the case of VGII, we derive a very tight upper bound in term of bivariate Fox H-function.

$$\begin{aligned}\overline{C}^{\text{ub}} \cong&\frac{k^2\overline{\gamma}_1\binom{N}{k}^2}{4\log(2)}\sum_{m=0}^{k-1}\sum_{n=0}^{k-1}\sum_{i=1}^{2}\sum_{j=1}^{2}\frac{S_mP_nT_{m,i}Q_{n,j}}{(U_{m,i}+\zeta R_{n,j})^2}\sqrt{\frac{U_{m,i}\zeta}{R_{n,j}}}\\ &\times\ H_{1,0:1:1:0,2}^{0,1:1,1:2,0}\left(\begin{array}{c|c|c|c} (\text{-}1;1,1) & (0,1) & \text{-} & \\ \text{-} & (0,1) & (\frac{1}{2},\frac{1}{2}),(-\frac{1}{2},\frac{1}{2}) & \tau_1,\tau_2\end{array}\right),\end{aligned} \tag{2.69}$$

where τ_1, τ_2 are defined by

$$\tau_1 = \frac{\overline{\gamma}_1}{U_{m,i}+\zeta R_{n,j}}, \tag{2.70}$$

$$\tau_2 = \frac{\sqrt{\zeta U_{m,i}R_{n,j}}}{U_{m,i}+\zeta R_{n,j}}, \tag{2.71}$$

2.6 Numerical Results and Discussion

In this section, we present the analytical and simulation results illustrating the effects of the hardware impairments, the relaying schemes, the number of the relays, the rank of

the selected relay and the outdated CSI on the system. The performance metrics used to quantify the robustness and the resiliency of the system are the outage probability, the average bit error rate and the ergodic capacity. The analytical results are confirmed by Monte Carlo simulation considering 10^9 iterations.

Fig. 2.3 shows the variations of the outage probability of FG, VGI and VGII with respect

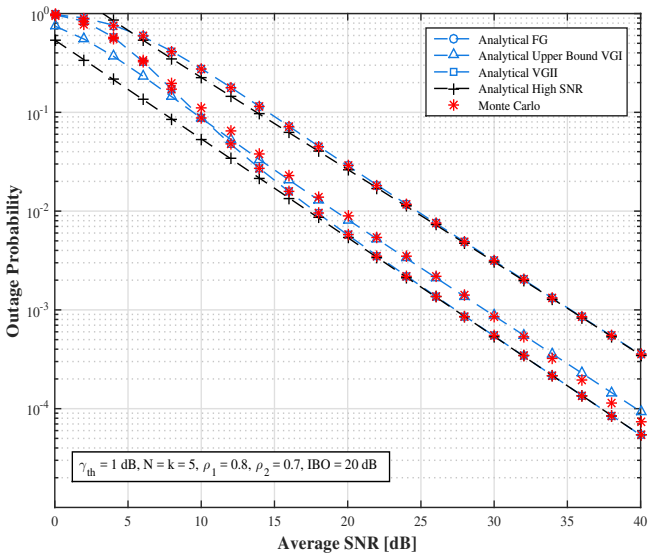

Figure 2.3: Outage probabilities of FG, VGI and VGII relaying under the SEL hardware impairment.

to the average SNR. As expected, it is clear that the variable gain relaying outperforms the FG scheme. Regarding the variable gain protocol, the system performs better when using the second version compared to the first one. In fact, the main difference between the two versions is the CSI used for the relaying amplification. Given that the second version employs the perfect CSI retrieved by the pilot training technique, the amplification in the first version is based on the outdated CSI. As a result, the CSI used for the amplification makes the second version of the variable gain relaying more efficient than the first one.

Fig. 2.4 presents the dependence of the outage performance of VGII relaying against the average SNR under the different models of impairment. For low SNR, the system response to the impairment is acceptable as the three impairments' models have the same impact. As the average SNR increases above 20 dB, the system responses to the various hardware impairments significantly differ from each other. We note that in the high SNR region, the impairment effect becomes more severe particularly for the TWTA and SSPA.

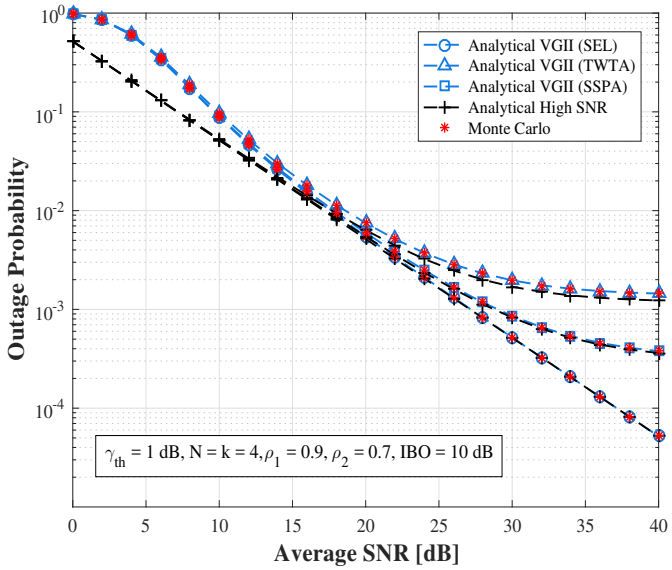

Figure 2.4: Outage probability of VGII relaying under the SEL, TWTA and SSPA impairments.

As the average SNR exceeds 25 dB, an irreducible outage floor is created which inhibits the performance from converging to zero. Graphically, we note that the system saturates at 0.002 and 0.0003 for TWTA and SSPA, respectively. Consequently, the TWTA has the most detrimental effect on the system. For the SEL impairment model, the system still operates in acceptable conditions and there is no significant impact on the system performance, especially the non-creation of the outage floor, unlike SSPA and TWTA, at least below 40 dB.

Fig. 2.5 shows the variations of the outage probability of FG relaying against the average SNR under the SSPA impairment and for various number of relays. For low SNR below 10 dB, the number of relays has no remarkable impact on the outage probability. However, as the SNR grows largely, the performance significantly deviates from each other. In fact, the system operates better as the number of relays increases. To achieve an outage probability equal to 10^{-3}, the system requires the following average SNRs 20 dB, 27 dB and 35 dB, respectively, for N = 10, 5 and 2 relays. Thereby, the main contribution of the number of relays is useful to reduce the power consumption of the system. This main advantage is explained by the fact that for a higher number of relays, there is a higher probability to select a better channel/relay. However, as the average SNR increases, the impairments effect becomes more severe as the outage probability saturates

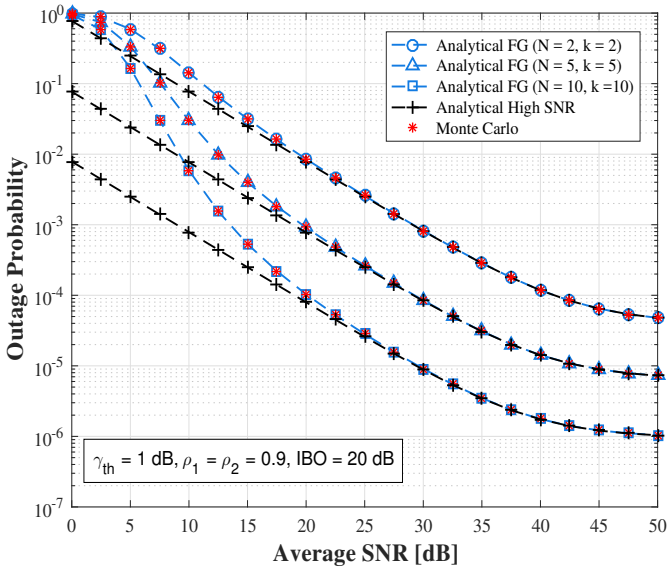

Figure 2.5: Outage probability of FG relaying for various number of relays.

by the irreducible floor created by the impairments. Even the number of relays play no significant role in this situation. Therefore, the number of relays introduces limited improvements at low SNR, however, it does not contribute in anyway as the impairments become severe at high SNR.

Fig. 2.6 illustrates the variations of the BER of VGII relaying under the SEL impairment and for different values of the IBO. For low SNR below 20 dB, the IBO factor has no observable impact on the system, i.e, the BER is the same regardless of the IBO values. However, when the average SNR overtakes 25 dB, the IBO factor gets more involved. In fact, as the IBO value increases, the system performs better. For lower value of IBO = 5 dB, the BER is limited by a floor created at higher value of the SNR. Considering a large value of IBO = 10 dB, the system performance improves and the BER floors are mitigated. Technically, increasing the IBO value comes directly from increasing the input saturation level A_{sat}. We already showed that the saturation's amplifier is relieved as the input saturation level increases. For a lower value of A_{sat}, i.e, lower value of IBO, the system becomes more saturated by the impairment's distortion. Consequently, the relation between the input saturation level and the IBO thoroughly explains the impact of higher values of IBO on the system performance.

Fig. 2.7 illustrates the variations of the average BER of FG relaying under the SSPA impairment and for different values of the correlation coefficients ρ_1 and ρ_2. We note

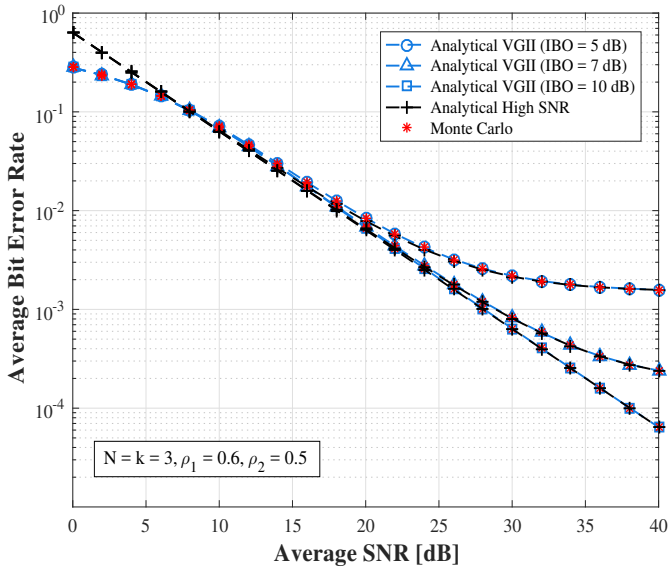

Figure 2.6: Average Bit Error Rate of VGII relaying for various IBO levels.

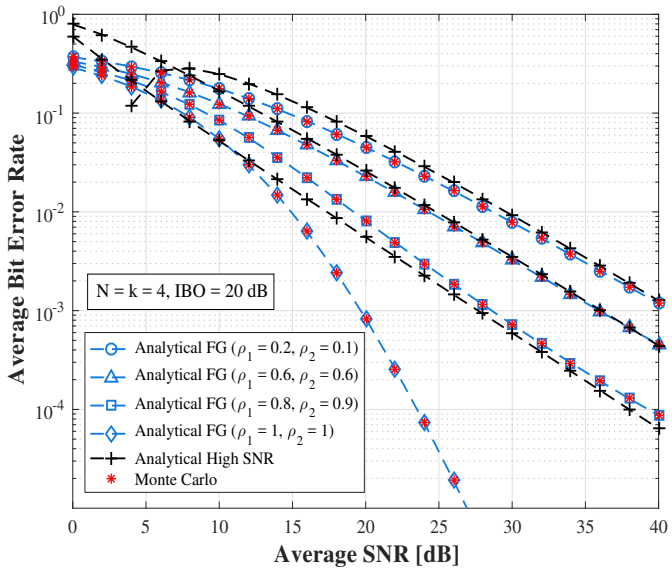

Figure 2.7: Average Bit Error Rate of FG relaying for various correlation values under the SSPA impairment.

that the system performs better as the correlation coefficients increase. In fact, both the arrangement and the selection of the relay are based on the CSI monitored by the control unit. As the correlation coefficients grow, the CSI estimation becomes more accurate and

so the relay selection will be based on error-free CSI estimation. Furthermore, when we achieve a full correlation between the CSIs ($\rho_1, \rho_2 \approx 1$), the performance improves further particularly when the relay of the last rank is selected. However, when the correlation coefficients decrease, i.e, the CSIs become more uncorrelated, the relay selection will be based on a completely outdated CSI. In this case, even when we select the relay of the last rank N, the performance gets worse since the selection of the best relay becomes uncertain and there is no relation between the received CSI and the rank of the selected relay.

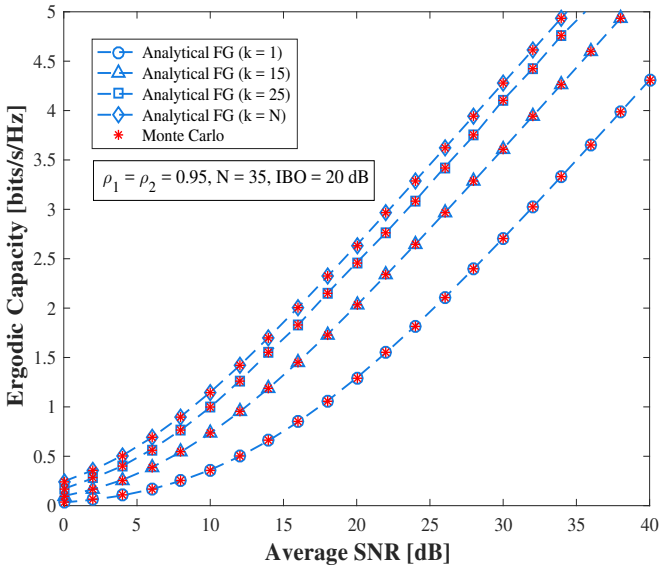

Figure 2.8: Ergodic capacity of FG relaying for various ranks of the selected relay and low correlation.

The same results given by Fig. 2.7 are confirmed by other approaches in figures 2.8 and 2.9 which present the variations of the channel capacity for different values of k and for high and low correlation coefficients, respectively. Unlike the configuration assumed in Fig. 2.7, the correlation coefficients (ρ_1, ρ_2) are fixed to a high value (0.95) and the rank k is varied. We note that the capacity performance significantly enhances when the rank k increases. Given that we assumed the opportunistic protocol for the relay selection, we stated that the control unit arranges the CSIs in an increasing order. Thereby, as the rank of the selected relay becomes closer to the rank of the best relay (rank = N), the system performs better. In this case, the efficiency of the channel/relay is related to the rank given that the correlation must be high. However, the results of Fig. 2.9 are absolutely

the opposite for the configuration adopted in Fig. 2.8. We clearly see that the system performs worse as the rank k becomes higher. In fact, this result is expected since the CSIs are completely uncorrelated (low correlation 0.009) and so the rank k has nothing to do with the channel/relay efficiency.

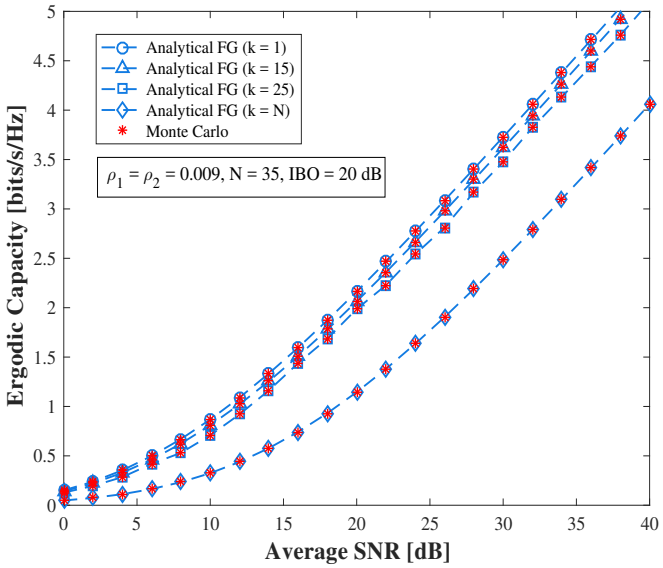

Figure 2.9: Ergodic capacity of FG relaying for various ranks of the selected relay and high correlation.

The effect of IBO is illustrated by Fig. 2.10 which presents the variations of the ergodic capacity for different values of IBO. As we concluded about the effect of IBO on the BER performance in Fig. 2.6, the impact of IBO is more notable on the capacity performance at high SNR. As the IBO decreases, the channel capacity saturates more especially for IBO = 4 dB and the maximum rate is around 2 bits/s/Hz. However, the level of saturation vanishes for a higher value of IBO equal to 20 dB. For low SNR, the effect of IBO is negligeable and the system operates efficiently. This result is graphically shown by the small difference between the capacities for different values of IBO, especially for an average SNR range less than 15 dB. As the average SNR increases, the IBO essentially contributes to improve the extent of the achievable rate.

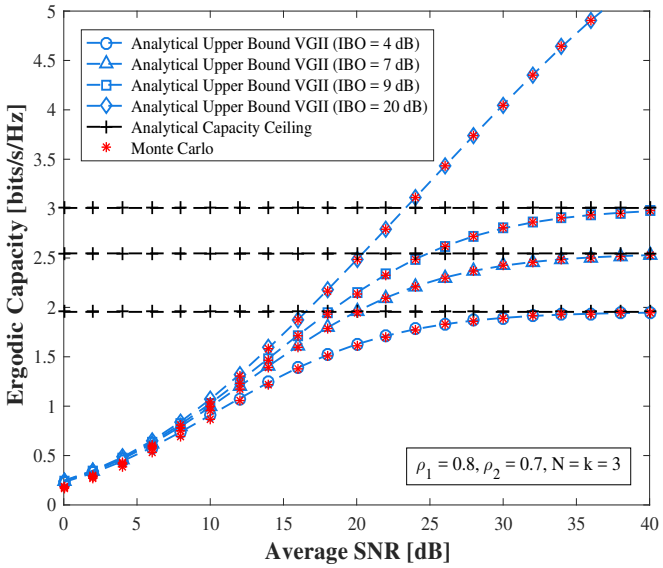

Figure 2.10: Ergodic capacity of VGII relaying for various IBO levels under the TWTA impairment.

2.7 Conclusion

In this work, we present a system with multiple relays operating at various relaying schemes FG, VGI and VGII. We assume the opportunistic relay selection to choose a single relay to forward the signal. Moreover, we introduce three models of the hardware impairments: SEL, TWTA and SSPA that affect the relays during the power amplification. We quantify the impacts of these imperfections on the system performance in terms of the outage probability, the average BER and the ergodic capacity. We also investigate the effects of the IBO, the number of relays, the rank of the selected relay and the correlation coefficients on the system. We conclude that the impairments have deleterious impacts on the system as the average SNR increases and particularly the TWTA impairment model has the most detrimental effects on the system compared to SSPA and SEL. We also demonstrate that as the number of relays increases, the performance substantially improves mainly the power consumption significantly decreases. Furthermore, we show that the system performs better when selecting the relay with the highest rank simultaneously coupled with higher values of the correlation coefficients. In addition, we prove that the capacity saturates quickly at high SNR when the IBO level is low and grows up infinitely as the IBO takes higher values.

Chapter 3: Hybrid RF/FSO Relaying With Transceiver Hardware Impairments

3.1 Introduction

In this chapter, we investigate the performance of a dual-hop multiple relays system consisting of mixed Radio-Frequency (RF)/Free Space Optical channels. The RF channels are subject to Rayleigh fading while the optical links experience the Double Generalized Gamma including atmospheric turbulence, path loss and the misalignment between the transmitter and the receiver aperture (also known as the pointing error). The FSO model also takes into account the receiver detection technique which could be either heterodyne or intensity modulation and direct detection. Partial Relay Selection with outdated Channel State Information is assumed based on the RF channels to select a relay and we also consider fixed and variable Amplify-and-Forward relaying schemes. In addition, we assume that the relays are affected by the high power amplifier non-linearities and herein we discuss two power amplifiers called Soft Envelope Limiter and Traveling Wave Tube Amplifier. Furthermore, novel closed-forms and tight upper bounds of the outage probability, the bit error probability, and the ergodic capacity are derived. Capitalizing on this performance, we derive the high SNR asymptotic to get engineering insights about the system gains such as the diversity and the coding gains. Finally, the mathematical expressions are validated using Monte Carlo simulation.

3.2 System and Channels Models

3.2 System Model

3.2.1.1 Relay Selection Protocol

Our system consists of S, D and N relays wirelessly linked to S and D shown by Fig. 3-1. As mentioned earlier, these relays amplify the incoming signal and then forward it to the destination. The amplification gain can be either FG or VG. FG relaying consists of amplifying the signal based on the average received SNR. However, VG relaying consists of amplifying the signal based on the received instantaneous SNR. To select the candidate relay of rank m, we refer to the Partial Relay Selection (PRS) with outdated CSI to pick the best one based on the local feedbacks of the RF channels. For a given communication, S receives local feedback ($\gamma_{1(i)}$ for $i = 1,\ldots N$) of the first hop obtained by the channel

estimation from the N relays and arranges them in an increasing order of amplitudes as follows: $\gamma_{1(1)} \leq \gamma_{1(2)} \leq \ldots \leq \gamma_{1(N)}$. The best scenario is to select the best relay *(m = N)*. However, the best relay is not always available, so S will pick the next best available relay. Thus PRS consists of selecting the m-th worst or *(N - m)*-th best relay $R_{(m)}$. Given that the local feedback coming from the relays to S are very slow and the channels are very time-varying, the CSI that is used for the relay selection is not the same as the CSI used for the transmission. In this case, an outdated CSI must be considered instead of a perfect CSI. As a result, the current and outdated CSI are correlated with the correlation coefficient ρ as follows

$$h_{1(m)} = \sqrt{\rho}\ \hat{h}_{1(m)} + \sqrt{1-\rho}\ \omega_m, \tag{3.1}$$

where ω_m is a random variable that follows the circularly complex Gaussian distribution with the same variance of the channel gain $h_{1(m)}$. The correlation coefficient ρ is given by the Jakes' autocorrelation model [31] as follows

$$\rho = J_0(2\pi f_d T_d), \tag{3.2}$$

where $J_0(\cdot)$ is the zeroth order Bessel function of the first kind, T_d is the time delay between the current and the delayed CSI versions and f_d is the maximum Doppler frequency of the channels.

3.2.1.2 High Power Amplifier Non-linearities Models

Since the distortion created by the HPA non-linearities is not linear, the analysis will be somewhat complex, we refer to the Bussgang linearization theory to linearize the distortion. This theory states that the output of the non-linear HPA circuit is a function of the linear scale parameter Ω of the input signal and a non-linear distortion ς uncorrelated with the input signal and modeled as a complex Gaussian random variable $\varsigma \backsim \mathcal{CN}(0,\ \sigma_\varsigma^2)$. According to [44, 17], the parameters Ω and σ_ς^2 for SEL are given by [11, Eq. (17)]

$$\Omega = 1 - \exp\left(-\frac{A_{\text{sat}}^2}{\sigma_{\text{r}}^2}\right) + \frac{\sqrt{\pi} A_{\text{sat}}}{2\sigma_{\text{r}}^2}\ \text{erfc}\left(\frac{A_{\text{sat}}}{\sigma_{\text{r}}}\right), \tag{3.3}$$

$$\sigma_\varsigma^2 = \sigma_{\text{r}}^2\ \left[1 - \exp\left(-\frac{A_{\text{sat}}^2}{\sigma_{\text{r}}^2}\right) - \Omega^2\right], \tag{3.4}$$

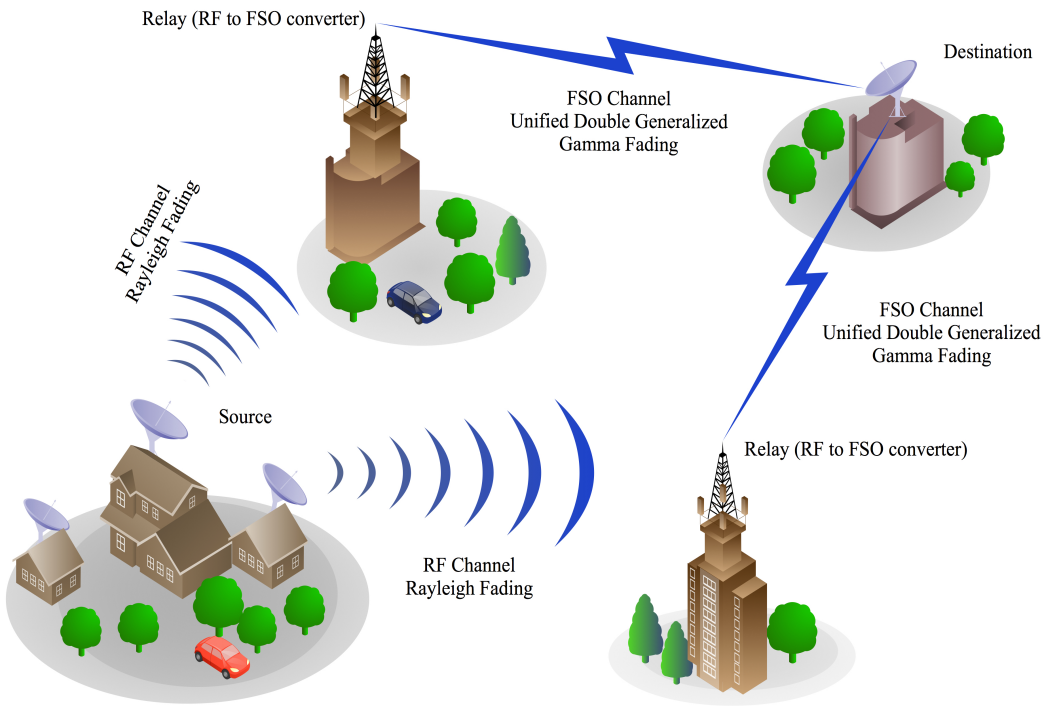

Figure 3.1: Outdoor Communications of Mixed RF/FSO Cooperative Relaying System

For TWTA, Ω and σ_ς^2 are given by [11, Eq. (18)]

$$\Omega = \frac{A_{\text{sat}}^2}{\sigma_{\text{r}}^2}\left[1 + \frac{A_{\text{sat}}^2}{\sigma_{\text{r}}^2} e^{\frac{A_{\text{sat}}^2}{\sigma_{\text{r}}^2}} + \text{Ei}\left(-\frac{A_{\text{sat}}^2}{\sigma_{\text{r}}^2}\right)\right], \tag{3.5}$$

$$\sigma_\varsigma^2 = -\frac{A_{sat}^4}{\sigma_{\text{r}}^2}\left[\left(1 + \frac{A_{\text{sat}}^2}{\sigma_{\text{r}}^2}\right) e^{\frac{A_{\text{sat}}^2}{\sigma_{\text{r}}^2}} \text{Ei}\left(-\frac{A_{\text{sat}}^2}{\sigma_{\text{r}}^2}\right) + 1\right] - \sigma_{\text{r}}^2\Omega^2, \tag{3.6}$$

where A_{sat}, σ_{r}^2, $\text{erfc}(\cdot)$ and $\text{Ei}(\cdot)$ are the input saturation amplitude of the power amplifier, the mean power of the signal at the output of the gain block, the complementary error function, and the exponential integral function, respectively.

We also provide the expressions of the clipping factor for SEL and TWTA [44, Eqs. (13), (14)] as follows

$$\eta_{\text{SEL}} = 1 - \exp\left(-\frac{A_{\text{sat}}^2}{\sigma_{\text{r}}^2}\right), \tag{3.7}$$

$$\eta_{\text{TWTA}} = -\frac{A_{sat}^4}{\sigma_{\text{r}}^4}\left[\left(1 + \frac{A_{\text{sat}}^2}{\sigma_{\text{r}}^2}\right) \exp\left(\frac{A_{\text{sat}}^2}{\sigma_{\text{r}}^2}\right) \text{Ei}\left(-\frac{A_{\text{sat}}^2}{\sigma_{\text{r}}^2}\right) + 1\right], \tag{3.8}$$

We also define the so-called the input back-off (IBO) given by IBO $= \frac{A_{\text{sat}}^2}{\sigma^2}$. Fig. 3-2 illustrates the amplitude to amplitude (AM/AM) characteristics of the SEL, TWTA, and Solid State Power Amplifier (SSPA) with respect to the normalized input modulus. Further details about of those characteristics are provided in our related work [11].

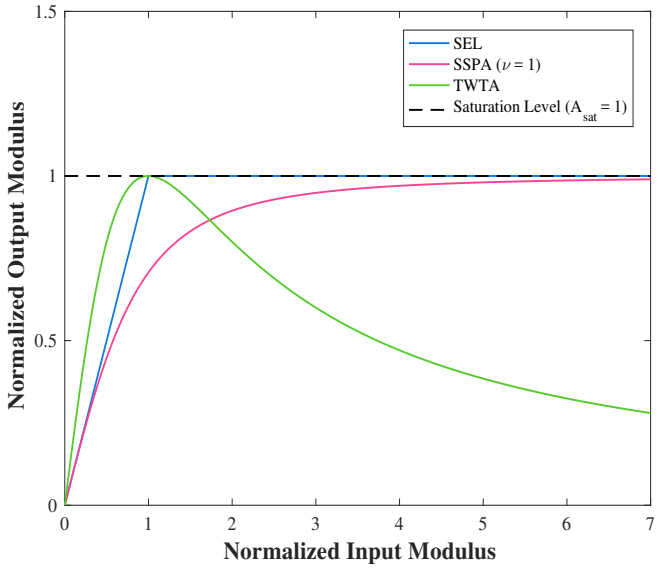

Figure 3.2: AM/AM characteristics of SEL, SSPA and TWTA

3.2 Channels Models

3.2.2.1 Statistics of RF channels

Since the RF channels experience Rayleigh fading, the PDF expression of the instantaneous SNR $\gamma_{1(m)}$ of the channel between S and $R_{(m)}$ taking into account the outdated CSIs and the CSIs sorting can be written as follows [51, Eq. (8)]

$$f_{\gamma_{1(m)}}(x) = m\binom{N}{m}\sum_{n=0}^{m-1}\frac{(-1)^n}{[(N-m+n)(1-\rho)+1]\overline{\gamma}_1}\binom{m-1}{n}e^{-\frac{(N-m+n+1)x}{[(N-m+n)(1-\rho)+1]\overline{\gamma}_1}}, \quad (3.9)$$

After integrating the above expression, the CDF of $\gamma_{1(m)}$ can be obtained as

$$F_{\gamma_{1(m)}}(x) = 1 - m\binom{N}{m}\sum_{n=0}^{m-1}\binom{m-1}{n}\frac{(-1)^n}{N-m+n+1}e^{-\frac{(N-m+n+1)x}{[(N-m+n)(1-\rho)+1]\overline{\gamma}_1}}, \quad (3.10)$$

Using the identity [27, Eq. (3.326.2)], the t-th moment of $\gamma_{1(m)}$ can be derived the as follows

$$\mathbb{E}\left[\gamma_{1(m)}^{t}\right] = m\binom{N}{m}\sum_{n=0}^{m-1}\binom{m-1}{n}\Gamma(t+1)\frac{(-1)^{n}([(N-m+n)(1-\rho)+1]\overline{\gamma}_{1})^{t}}{(N-m+n+1)^{t+1}}, \quad (3.11)$$

3.2.2.2 Statistics of FSO channels

The FSO part consists of three components I_a, I_l, and I_p which are turbulence-induced fading, the path loss and the pointing error fading, respectively. The channel gain I_m of the FSO between the relay $R_{(m)}$ and D can be expressed as follows

$$I_m = I_a \cdot I_l \cdot I_p, \quad (3.12)$$

The table below summarizes the parameters of the optical part.

Table 3.1: FSO Sub-System

Parameter	**Definition**
σ	Weather attenuation
σ_{s}^2	Jitter variance
σ_{R}^2	Rytov variance
k	Wave number
λ	Wavelength
ξ	Pointing error coefficient
ω_0	Beam waist at the relay
ω_z	Beam waist
$\omega_{z_{eq}}$	Equivalent beam waist
L	Length of the optical link
a	Radius of the receiver aperture
A_0	Fraction of the collected power at L = 0
F_0	Radius of curvature
C_n^2	Refractive index of the medium
R	Radial displacement of the beam at the receiver

Using the Beers-Lambert law, the path loss can be expressed as follows [21, Eq. (12)]

$$I_l = \exp(-\sigma L), \tag{3.13}$$

The pointing error I_p made by Jitter can be given as [24, Eq. (9)]

$$I_p = A_0 \exp\left(-\frac{2R^2}{\omega_{z_{eq}}^2}\right), \tag{3.14}$$

Assuming that the radial displacement of the beam at the detector follows the Rayleigh distribution, the PDF of the pointing error can be expressed as follows

$$f_{I_p}(I_p) = \frac{\xi^2}{A_0^{\xi^2}} I_p^{\xi^2-1}\ , \quad 0 \le I_p \le A_0, \tag{3.15}$$

The pointing error coefficient can be expressed in terms of the Jitter standard deviation and the equivalent beam waist as follows

$$\xi = \frac{\omega_{z_{eq}}}{2\sigma_{\mathrm{s}}}, \tag{3.16}$$

We can also relate $\omega_{z_{eq}}$ with the beam width ω_z of the Gaussian laser beam at the distance L as follows

$$\omega_{z_{eq}}^2 = \frac{\omega_{\mathrm{L}}^2 \sqrt{\pi}\mathrm{erf}(v)}{2v\exp(-v^2)}, \tag{3.17}$$

where $v = \frac{\sqrt{\pi}a}{\sqrt{2}\omega_{\mathrm{L}}}$, and $\mathrm{erf}(\cdot)$ is the error function. The fraction of the collected power A_0 at the relay is given by

$$A_0 = |\mathrm{erf}(v)|^2, \tag{3.18}$$

The Gaussian beam waist can be defined as

$$\omega_z = \omega_0 \sqrt{(\Theta_0 + \Lambda_0)(1 + 1.63\ \sigma_{\mathrm{R}}^{12/5}\Lambda_1)}, \tag{3.19}$$

where $\Theta_0 = 1 - \frac{L}{F_0}$, $\Lambda_0 = \frac{2L}{kw_0^2}$, $\Lambda_1 = \frac{\Lambda_0}{\Theta_0^2+\Lambda_0^2}$, and σ_{R}^2 is the Rytov variance given by [21, Eq. (15)]

$$\sigma_{\mathrm{R}}^2 = 1.23\ C_n^2 k^{7/6} L^{11/6}, \tag{3.20}$$

The turbulence-induced fading I_a is modeled by the Double Generalized Gamma and can be expressed as the product of two independent random variables I_x and I_y describing the

large-scale and small-scale fluctuations, respectively. I_x and I_y each follows the generalized gamma distribution $I_x \backsim GG(\alpha_1, m_1, \Omega_1)$ and $I_y \backsim GG(\alpha_2, m_2, \Omega_2)$, where m_1 and m_2 are the shaping parametes defining the atmospheric turbulence fading. Moreover, $\alpha_1, \alpha_2, \Omega_1$ and Ω_2 are defined using the variance of the small and large scale fluctuations from [34, Eqs. (8.a), (8.b), and (9)]. Thereby, the PDF of the turbulence-induced fading I_a can be given by [34, Eq. (4)]

$$\begin{aligned} f_{I_a}(I_a) =& \frac{\alpha_2 p^{m_2+\frac{1}{2}} q^{m_1-\frac{1}{2}} (2\pi)^{1-\frac{p+q}{2}}}{\Gamma(m_1)\Gamma(m_2) I_a} \\ & \times \; G_{p+q,0}^{0,p+q}\left[\left(\frac{1}{I_a}\right)^{\alpha_2 p} \frac{p^p q^q \Omega_1^q \Omega_2^p}{m_1^q m_2^p} \;\middle|\; \begin{matrix} \Delta(q{:}1-m_1), \Delta(p{:}1-m_2) \\ - \end{matrix} \right], \end{aligned} \tag{3.21}$$

where $G_{p,q}^{m,n}[\cdot]$ is the Meijer's-G function, p and q are positive integers satisfying $\frac{p}{q} = \frac{\alpha_1}{\alpha_2}$ and $\Delta(j\ ;\ x) \triangleq \frac{x}{j}, \ldots, \frac{x+j-1}{j}$. In case of the heterodyne detection, the average SNR μ_1 is given by $\mu_1 = \frac{\eta \mathbb{E}[I_m]}{\sigma_0^2}$. Regarding the IM/DD detection, the average electrical SNR μ_2 is given by $\mu_2 = \frac{(\eta \mathbb{E}[I_m])^2}{\sigma_0^2}$ while the instantaneous optical SNR is $\gamma_{2(m)} = \frac{(\eta I_m^2)}{\sigma_0^2}$. Unifying the two detection schemes and applying the transformation of the random variable $\gamma_{2(m)} = \frac{(\eta I_m)^r}{\sigma_0^2}$, the unified PDF of the instantaeous SNR $\gamma_{2(m)}$ can be expressed as follows

$$\begin{aligned} f_{\gamma_{2(m)}}(\gamma) =& \frac{\xi^2 p^{m_2-\frac{1}{2}} q^{m_1-\frac{1}{2}} (2\pi)^{1-\frac{p+q}{2}}}{r\Gamma(m_1)\Gamma(m_2)\gamma} \\ & \times \; G_{p+q+\alpha_2 p, \alpha_2 p}^{0, p+q+\alpha_2 p}\left[\left(\frac{p\Omega_1}{m_2}\right)^p \left(\frac{q\Omega_2}{m_1}\right)^q (A_0 I_l)^{\alpha_2 p} \left(\frac{\mu_r}{\gamma}\right)^{\frac{\alpha_2 p}{r}} \;\middle|\; \begin{matrix} \kappa_1 \\ \kappa_2 \end{matrix} \right], \end{aligned} \tag{3.22}$$

where σ_0^2, η are the channel noise and the electrical-to-optical conversion coefficient, respectively. The parameter r takes two values 1 and 2 standing for heterodyne and IM/DD, respectively. The vectors $\kappa_1 = \Delta(\alpha_2 p : 1-\xi^2),\ \Delta(q : 1-m_1),\ \Delta(p : 1-m_2)$, and $\kappa_2 = \Delta(\alpha_2 p : -\xi^2)$.

The average SNR $\overline{\gamma}_r$[1] can be expressed as

$$\overline{\gamma}_r = \frac{\mathbb{E}[I_m^r]}{\mathbb{E}[I_m]^r} \mu_r, \tag{3.23}$$

[1]The average SNR $\overline{\gamma}_r$ is defined as $\overline{\gamma}_r = \eta^r \mathbb{E}[I_m^r]/\sigma_0^2$, while the average electrical SNR μ_r is given by $\mu_r = \eta^r \mathbb{E}[I_m]^r/\sigma_0^2$. Therefore, the relation between the average SNR and the average electrical SNR is trivial given that $\frac{\mathbb{E}[I_m^2]}{\mathbb{E}[I_m]^2} = \sigma_{\text{si}}^2 + 1$, where σ_{si}^2 is the scintillation index [50].

where μ_r is the average electrical SNR given by

$$\mu_r = \frac{\eta^r \mathbb{E}\left[I_m\right]^r}{\sigma_0^2}, \tag{3.24}$$

After integrating Eq. (19), the CDF of the instantaneous SNR $\gamma_{2(m)}$ can be expressed as follows

$$\begin{aligned} F_{\gamma_{2(m)}}(\gamma) =& \frac{\xi^2 p^{m_2-\frac{3}{2}} q^{m_1-\frac{1}{2}} (2\pi)^{1-\frac{p+q}{2}}}{\alpha_2 \Gamma(m_1)\Gamma(m_2)\gamma} \\ & \times \; G_{p+q+2\alpha_2 p, 2\alpha_2 p}^{\alpha_2 p, p+q+\alpha_2 p}\left[\left(\frac{p\Omega_1}{m_2}\right)^p \left(\frac{q\Omega_2}{m_1}\right)^q (A_0 I_l)^{\alpha_2 p} \left(\frac{\mu_r}{\gamma}\right)^{\frac{\alpha_2 p}{r}} \;\middle|\; \begin{matrix} \kappa_3 \\ \kappa_4 \end{matrix} \right], \end{aligned} \tag{3.25}$$

The vectors $\kappa_3 = \Delta(\alpha_2 p : 1-\xi^2),\ \Delta(q : 1-m_1),\ \Delta(p : 1-m_2),\ [1]_{\alpha_2 p}$, and $\kappa_4[0]_{\alpha_2 p},\ \Delta(\alpha_2 p : -\xi^2)$. Also $[x]_j$ is defined as the vector of length j and its components are equal to x. After changing the variable of the integration ($x = \gamma^{-\frac{\alpha_2 p}{r}}$) and applying the following identity [53, Eq. (2.24.2.1)], the t-th moment of the optical SNR can be derived as follows

$$\begin{aligned} \mathbb{E}\left[\gamma_{2(m)}^t\right] =& \frac{\xi^2 p^{m_2-1} q^{m_1-\frac{1}{2}} (2\pi)^{1-\frac{p+q}{2}} \zeta^{t\left[\frac{r}{\alpha_2 p}-1\right]-1}}{\Gamma(m_1)\Gamma(m_2)\prod_{j=1}^{\alpha_2 p}\Gamma\left(t\left[\frac{r}{\alpha_2 p}-1\right]-\kappa_{2,j}\right)} \\ & \times \; \frac{\prod_{j=1}^{p+q+\alpha_2 p}\Gamma\left(t\left[\frac{r}{\alpha_2 p}-1\right]-\kappa_{1,j}\right)}{\prod_{j=p+q+\alpha_2 p+1}^{p+q+2\alpha_2 p}\Gamma\left(t\left[\frac{r}{\alpha_2 p}-1\right]-\kappa_{1,j}\right)}, \end{aligned} \tag{3.26}$$

where $\zeta = \left(\frac{p\Omega_1}{m_2}\right)^p \left(\frac{q\Omega_2}{m_1}\right)^q (A_0 I_l)^{\alpha_2 p} \mu_r^{\frac{\alpha_2 p}{r}}$.

3.3 Performance Analysis of Fixed Gain Relaying

This relaying scheme consists of amplifying the signal by a fixed gain based on the average received CSI. The gain factor can be expressed as follows

$$G = \sqrt{\frac{\sigma_{\mathrm{r}}^2}{\mathbb{E}\left[|h_{1(m)}|^2\right] P_1 + \sigma_0^2}}, \tag{3.27}$$

where P_1 is the average transmitted power from S. The end-to-end Signal-to-Noise-plus-Distortion-Ratio (SNDR) can be expressed as follows [44, Eq. (16)]

$$\gamma_{\text{e2e}} = \frac{\gamma_{1(m)}\gamma_{2(m)}}{\kappa\gamma_{2(m)} + \mathbb{E}\left[\gamma_{1(m)}\right] + \kappa}, \tag{3.28}$$

The HPA non-linearities factor κ can be given by [44, Eq. (17)]

$$\kappa = 1 + \frac{\sigma_\varsigma^2}{\Omega^2 G^2 \sigma_0^2}, \tag{3.29}$$

Note that for the case of linear relaying, the factor κ is reduced to one and so the end-to-end SNR (3.28) describes an ideal system.

3.3 Outage Probability Analysis

The outage probability (OP) is defined as the probability that the end-to-end SNDR falls below a given threshold γ_{th}. It can be generally written as

$$P_{\text{out}}(\gamma_{\text{th}}) \triangleq \Pr[\gamma_{\text{e2e}} < \gamma_{\text{th}}] = F_{\gamma_{\text{e2e}}}(\gamma_{\text{th}}), \tag{3.30}$$

where $F_{\gamma_{\text{e2e}}}(\cdot)$ is the CDF of the end-to-end SNDR. After substituting (3.28) in (3.30), the OP can be derived as follows

$$\begin{aligned} P_{\text{out}}(\gamma_{\text{th}}) =& 1 - \frac{m\xi^2 p^{m_2-1} q^{m_1-\frac{1}{2}} r^{\mu-1}}{\sqrt{\alpha_2}\,\Gamma(m_1)\Gamma(m_2)(2\pi)^{\frac{\alpha_2 p + r(p+q)-3}{2}}} \binom{N}{m} \sum_{n=0}^{m-1} \binom{m-1}{n} \frac{(-1)^n}{N-m+n+1} \\ &\times \exp(-\beta\kappa\gamma_{\text{th}})\; G_{r(p+q+\alpha_2 p)+\alpha_2 p,\, r\alpha_2 p}^{0,\, r(p+q+\alpha_2 p)+\alpha_2 p} \left(\left(\frac{\alpha_2 p}{\beta\gamma_{\text{th}} c} \right)^{\alpha_2 p} (\zeta r^{p+q})^r \;\middle|\; \begin{matrix} \kappa_5 \\ \kappa_6 \end{matrix} \right), \end{aligned} \tag{3.31}$$

where $\beta = \frac{N-m+n+1}{[(N-m+n)(1-\rho)+1]\overline{\gamma}_1}$, $\mu = \sum_{j=1}^{\alpha_2 p} \kappa_{2,j} - \sum_{j=1}^{p+q+\alpha_2 p} \kappa_{1,j} + \frac{p+q}{2} + 1$, $c = (\kappa+1)\mathbb{E}\left[\gamma_{1(m)}\right]$, $\kappa_5 = [1]_{\alpha_2 p}$, $\Delta(r : \alpha_2 p : 1-\xi^2)$, $\Delta(r : q : 1-m_1)$, $\Delta(r : p : 1-m_2)$, and $\kappa_6 = \Delta(r : \alpha_2 p : -\xi^2)$. The operator $\Delta(\cdot : \cdot : \cdot)$ is defined by $\Delta(r : j : x) \triangleq \Delta\left(r : \frac{x}{j}\right), \ldots, \Delta\left(r : \frac{x+j-1}{j}\right)$. We also derive the asymptotic high SNR using the expansion of the Meijer's-G function

for large values of the average electrical SNR μ_r as follows

$$\begin{aligned} P_{\text{out}}^{\infty}(\gamma_{\text{th}}) \underset{\mu_r \gg 1}{\cong} 1 - & \frac{m\xi^2 p^{m_2-1} q^{m_1-\frac{1}{2}} r^{\mu-1}}{\sqrt{\alpha_2}\,\Gamma(m_1)\Gamma(m_2)(2\pi)^{\frac{\alpha_2 p + r(p+q)-3}{2}}} \binom{N}{m} \sum_{n=0}^{m-1} \binom{m-1}{n} \frac{(-1)^n}{N-m+n+1} \\ & \times \exp(-\beta\kappa\gamma_{\text{th}}) \sum_{i=1}^{r(p+q+\alpha_2 p)+\alpha_2 p} \frac{\prod_{j=1,\ j\neq i}^{r(p+q+\alpha_2 p)+\alpha_2 p} \Gamma(\kappa_{5,i}-\kappa_{5,j})}{\prod_{j=1}^{r\alpha_2 p} \Gamma(\kappa_{5,i}-\kappa_{6,j})} \\ & \times \left[\left(\frac{\alpha_2 p}{\beta\gamma_{\text{th}} c} \right)^{\alpha_2 p} (\zeta r^{p+q})^r \right]^{\kappa_{5,i}-1}, \end{aligned} \tag{3.32}$$

3.3 Bit Error Probability Analysis

The bit error probability (BEP) for most binary modulation can be given by

$$\overline{P_e} = \frac{\delta^\tau}{2\Gamma(\tau)} \int_0^\infty \gamma^{\tau-1} e^{-\delta\gamma} F_{\gamma_{\text{e2e}}}(\gamma) d\gamma, \tag{3.33}$$

where τ and δ are the parameters of the modulation which can be summarized in Table 3.2. First, we should replace the expression of the CDF of the end-to-end SNDR (3.31) in

Table 3.2: Parameters of Binary Modulations

Modulation	δ	τ
Coherent Binary Frequency Shift Keying (CBFSK)	0.5	0.5
Non-Coherent Binary Frequency Shift Keying (NBFSK)	0.5	1
Coherent Binary Phase Shift Keying (CBPSK)	1	0.5
Differential Binary Phase Shift Keying (DBPSK)	1	1

(3.33) and then we change the variable of the integration ($x = \gamma^{-1}$). After transforming the exponential into Meijer's-G function [1, Eq. (07.34.03.0046.01)] and using the identity [53, Eq. (2.24.1)], the BEP is finally derived as follows

$$\begin{aligned} \overline{P_e} = & \frac{1}{2} - \frac{m\xi^2 p^{m_2-\frac{1}{2}} q^{m_1-\frac{1}{2}} r^{\mu-1}}{2(\alpha_2 p)^{1-\tau}(2\pi)^{\frac{2\alpha_2 p + r(p+q)-4}{2}} \Gamma(m_1)\Gamma(m_2)\Gamma(\tau)} \binom{N}{m} \sum_{n=0}^{m-1} \binom{m-1}{n} \\ & \times \frac{(-1)^n}{N-m+n+1} \left(\frac{\delta}{\delta+\beta\kappa} \right)^\tau \\ & \times G_{r(p+q+\alpha_2 p)+\alpha_2 p,(r+1)\alpha_2 p}^{\alpha_2 p, r(p+q+\alpha_2 p)+\alpha_2 p} \left(\left(\frac{\delta+\beta\kappa}{\beta c} \right)^{\alpha_2 p} (\zeta r^{p+q})^r \,\middle|\, \begin{matrix} \kappa_5 \\ \kappa_7 \end{matrix} \right), \end{aligned} \tag{3.34}$$

where the vector $\kappa_7 = \Delta(\alpha_2 p : \tau),\ \kappa_6$.
Applying the expansion of the Meijer's-G function, the asymptotic high SNR of BEP is given by Eq. (3.35).

$$\begin{aligned}\overline{P_e}^{\infty} \underset{\mu_r \gg 1}{\cong} & \frac{1}{2} - \frac{m\xi^2 p^{m_2-\frac{1}{2}} q^{m_1-\frac{1}{2}} r^{\mu-1}}{2(\alpha_2 p)^{1-\tau}(2\pi)^{\frac{2\alpha_2 p + r(p+q)-4}{2}}\Gamma(m_1)\Gamma(m_2)\Gamma(\tau)} \binom{N}{m} \sum_{n=0}^{m-1} \binom{m-1}{n} \\ \times & \frac{(-1)^n}{N-m+n+1} \sum_{i=1}^{r(p+q+\alpha_2 p)+\alpha_2 p} \frac{\prod_{j=1,\ j\neq i}^{r(p+q+\alpha_2 p)+\alpha_2 p} \Gamma(\kappa_{5,i}-\kappa_{5,j}) \prod_{j=1}^{\alpha_2 p} \Gamma(1-\kappa_{5,i}+\kappa_{7,j})}{\prod_{j=\alpha_2 p+1}^{(r+1)\alpha_2 p} \Gamma(\kappa_{5,i}-\kappa_{7,j})} \\ \times & \left[\left(\frac{\delta+\beta\kappa}{\beta c}\right)^{\alpha_2 p} (\zeta r^{p+q})^r\right]^{\kappa_{5,i}-1} \left(\frac{\delta}{\delta+\beta\kappa}\right)^{\tau},\end{aligned} \tag{3.35}$$

Eqs. (3.32) and (3.35) provide engineering insights about the achieved gain such as the diversity order G_d. Note that the system saturated at high SNR since the impact of the hardware impairments becomes more pronounced at high rate, and hence an outage floor is created. Consequently the system achieves no gain $G_d = 0$. In the absence of the hardware impairments, the system achieves a diversity gain equal to

$$G_d = \min\left(1,\ \frac{\alpha_1 m_1}{r},\ \frac{\alpha_2 m_2}{r}, \frac{\xi^2}{r}\right), \tag{3.36}$$

Note that in our previous work [11], the system employs the opportunistic relay selection protocol with outdated CSI. We proved that the diversity gain achieved is equal to $G_d = N$ for full correlation ($\rho = 1$) and $G_d = 1$ for outdated CSI ($\rho < 1$). Since this proposed system employs partial relay selection, however, the diversity gain for the RF sub-system is always $G_d = 1$ for either perfect or outdated CSI.

3.3 Ergodic Capacity Analysis

The system capacity, expressed in bps/Hz, is defined as the maximum error-free data rate transferred by the system channel. It can be expressed as follows

$$\overline{C} \triangleq \mathbb{E}\left[\log_2(1+\varpi\gamma)\right], \tag{3.37}$$

where ϖ can take the values 1 or $e/2\pi$ for heterodyne or IM/DD, respectively. After some mathematical manipulations, the ergodic capacity can be expressed in terms of the

complementary CDF $\overline{F}_{\gamma}$ as follows

$$\overline{C} = \frac{\varpi}{\ln(2)} \int_{0}^{\infty} (1+\varpi\gamma)^{-1} \overline{F}_{\gamma_{\mathrm{e2e}}}(\gamma)\, d\gamma, \tag{3.38}$$

After replacing the complementary CDF of (3.28) in Eq. (3.38), then we should transform $(1+\varpi\gamma)^{-1}$, the exponential and the Meijer's-G into the Fox-H function. Applying the following identity [47, Eq. (2.3)] and after some mathematical manipulations, the average ergodic capacity can be derived as follows

$$\overline{C} = \frac{m\xi^2 p^{m_2-\frac{1}{2}} q^{m_1-\frac{1}{2}} \varpi r^{\mu-1}}{(\alpha_2 p)^{\frac{3}{2}} (2\pi)^{\frac{\alpha_2 p + r(p+q)-3}{2}} \ln(2)\Gamma(m_1)\Gamma(m_2)\kappa} \binom{N}{m} \sum_{n=0}^{m-1} \binom{m-1}{n} \frac{(-1)^n}{(N-m+n+1)\beta}$$
$$H^{0,1:1,1:0,r(p+q+\alpha_2 p)+\alpha_2 p}_{1,0:1,1:r(p+q+\alpha_2 p)+\alpha_2 p, r\alpha_2 p} \left(\begin{matrix} (0;1,-1) \\ - \end{matrix} \middle| \begin{matrix} (0,1) \\ (0,1) \end{matrix} \middle| \begin{matrix} (\kappa_5, [\frac{1}{\alpha_2 p}]_{r(p+q+\alpha_2 p)+\alpha_2 p}) \\ (\kappa_6, [\frac{1}{\alpha_2 p}]_{r\alpha_2 p}) \end{matrix} \middle| \frac{\varpi}{\beta\kappa}, \frac{\alpha_2 p \kappa}{c} (\zeta r^{p+q})^{\frac{r}{\alpha_2 p}} \right), \tag{3.39}$$

where $H^{m_1,n_1:m_2,n_2:m_3,n_3}_{p_1,q_1:p_2,q_2:p_3,q_3}[\cdot,\cdot]$ is the bivariate Fox-H function. An efficient MATLAB implementation of this function is given in [64, Appendix(B)].
Since the relays are impaired, we can also derive a ceiling in terms of the impairment clipping factor that limits the capacity as the impairment becomes more severe. This ceiling is given by [44, Eq. (37)]

$$\overline{C_c} = \log_2 \left(1 + \frac{\varpi \Omega^2}{\eta_{\mathrm{SEL/TWTA}} - \Omega^2} \right), \tag{3.40}$$

3.4 performance Analysis of Variable Gain Relaying

This relaying scheme consists of amplifying the signal by a variable gain based on the instantaneous received CSI. The gain factor can be written as follows

$$G = \sqrt{\frac{\sigma_{\mathrm{r}}^2}{|h_{1(m)}|^2 P_1 + \sigma_0^2}}, \tag{3.41}$$

The end-to-end SNDR can be formulated as follows [16, Eq. (14)]

$$\gamma_{\mathrm{e2e}} = \frac{\gamma_{1(m)}\gamma_{2(m)}}{\kappa\gamma_{2(m)} + \gamma_{1(m)} + \kappa}, \tag{3.42}$$

The closed-form of the end-to-end SNDR statistics in (3.42) is mathematically intractable. Thereby, we consider an approximate expression of the end-to-end SNDR as follows

$$\gamma_{\mathrm{e2e}} \cong \min\left(\gamma_{1(m)},\ \frac{\gamma_{2(m)}}{(\kappa-1)\gamma_{2(m)}+1}\right), \tag{3.43}$$

3.4 Outage Probability Analysis

Since the derivation of the OP is intractable, we derive a tight upper bound based on (3.43) as follows

$$P_{\mathrm{out}}^{\mathrm{up}}(\gamma_{\mathrm{th}}) = F_{\gamma_{1(m)}}(\gamma_{\mathrm{th}}) + F_{\gamma_{2(m)}}\left(\frac{\gamma_{\mathrm{th}}}{(\kappa-1)\gamma_{\mathrm{th}}+1}\right) - F_{\gamma_{1(m)}}(\gamma_{\mathrm{th}})F_{\gamma_{2(m)}}\left(\frac{\gamma_{\mathrm{th}}}{(\kappa-1)\gamma_{\mathrm{th}}+1}\right), \tag{3.44}$$

To get a deep scope about the system behavior, we derive an asymptotic high SNR using the Meijer's-G expansion of the CDF of $\gamma_{2(m)}$ as follows

$$G_{p+q+2\alpha_2 p,2\alpha_2 p}^{\alpha_2 p,p+q+\alpha_2 p}\left[\zeta\left(\frac{1+(\kappa-1)\gamma_{\mathrm{th}}}{\gamma_{\mathrm{th}}}\right)^{\frac{\alpha_2 p}{r}} \;\middle|\; \begin{matrix}\kappa_3\\ \kappa_4\end{matrix}\right] \underset{\mu_r\gg 1}{\cong} \sum_{i=1}^{p+q+\alpha_2 p}\left[\zeta\left(\frac{1+(\kappa-1)\gamma_{\mathrm{th}}}{\gamma_{\mathrm{th}}}\right)^{\frac{\alpha_2 p}{r}}\right]^{\kappa_{3,i}-1}$$
$$\times\ \frac{\prod_{j=1,\ j\neq i}^{p+q+\alpha_2 p}\Gamma(\kappa_{3,i}-\kappa_{3,j})\prod_{j=1}^{\alpha_2 p}\Gamma(1-\kappa_{3,i}+\kappa_{4,j})}{\prod_{j=\alpha_2 p+1}^{2\alpha_2 p}\Gamma(\kappa_{3,i}-\kappa_{4,j})\prod_{j=p+q+\alpha_2 p+1}^{p+q+2\alpha_2 p}\Gamma(\kappa_{3,j}-\kappa_{3,i}+1)}, \tag{3.45}$$

3.4 Bit Error Probability Analysis

Since a closed-form of the BEP derived by introducing the upper bound (3.44) in (3.33) is not solvable due to the impairment factor, we only derive an asymptotic high SNR by introducing the high SNR approximation of the upper bound of OP (3.32) in (3.33) as follows

$$\overline{P_e}^{\infty} \underset{\mu_r\gg 1}{\cong} \mathcal{I}_1 + \mathcal{I}_2 - \mathcal{I}_3, \tag{3.46}$$

Using the identity [27, Eq. (3.351.3)], $\mathcal{I}_1$ can be derived as follows

$$\mathcal{I}_1 = \frac{1}{2} - \frac{m\delta^\tau}{2}\binom{N}{m}\sum_{n=0}^{m-1}\binom{m-1}{n}\frac{(-1)^n}{N-m+n+1}(\delta+\beta)^{-\tau}, \tag{3.47}$$

The expansion of the third term gives $\mathcal{I}_3 = \mathcal{I}_2 - \mathcal{I}_4$. There is no need to compute the term $\mathcal{I}_2$ in (3.46) since it is cancelled out by itself inside the expression of $\mathcal{I}_3$. After transforming the exponential into Meijer's-G function and using the identity [53, Eq. (2.24.2.4)], $\mathcal{I}_4$ can be derived as follows

$$\begin{aligned}\mathcal{I}_4 =& \frac{\delta^\tau \xi^2 p^{m_2-\frac{3}{2}} q^{m_1-\frac{1}{2}} (2\pi)^{1-\frac{p+q}{2}} m}{2\alpha_2(\kappa-1)^\tau \Gamma(m_1)\Gamma(m_2)\Gamma(\tau)}\binom{N}{m}\sum_{n=0}^{m-1}\binom{m-1}{n}\frac{(-1)^n}{N-m+n+1} \\ &\times \sum_{i=1}^{p+q+\alpha_2 p}\frac{\prod_{j=1,\ j\neq i}^{p+q+\alpha_2 p}\Gamma(\kappa_{3,i}-\kappa_{3,j})}{\prod_{j=\alpha_2 p+1}^{2\alpha_2 p}\Gamma(\kappa_{3,i}-\kappa_{4,j})}\, G_{1,2}^{2,1}\left(\frac{\delta+\beta}{\kappa-1}\,\middle|\, \begin{matrix} 1-\tau,\ \frac{\alpha_2 p(\kappa_{3,i}-1)}{r} \\ -\tau,\ 0\end{matrix}\right) \\ &\times \frac{\prod_{j=1}^{\alpha_2 p}\Gamma(1-\kappa_{3,i}+\kappa_{4,j})\ \zeta^{\kappa_{3,i}-1}}{\prod_{j=p+q+\alpha_2 p+1}^{p+q+2\alpha_2 p}\Gamma(\kappa_{3,j}-\kappa_{3,i}+1)\ \Gamma\left(\frac{\alpha_2 p}{r}(1-\kappa_{3,i})\right)},\end{aligned} \tag{3.48}$$

3.4 System Gains

For the most coherent linear modulation, the BEP can be reformulated as follows

$$\overline{P_e} = \mathbb{E}\left[\mathcal{Q}(\sqrt{c\gamma})\right], \tag{3.49}$$

where $\mathcal{Q}(\cdot)$ is the Gaussian-Q function, and c is a parameter related to the format of the modulation, e.g, $c = 2$ stands for BPSK modulation. After applying an integration by parts on Eq. (50), BEP can be written as

$$\overline{P_e} = \sqrt{\frac{c}{8\pi}}\int_0^\infty \frac{e^{-\frac{c}{2}\gamma}}{\sqrt{\gamma}}F_\gamma(\gamma)d\gamma, \tag{3.50}$$

The derivation of the closed-form of the BEP is mathematically not tractable due to the presence of the terms related to the hardware impairments. Thereby, a numerical integration is needed. As we mentioned earlier, the hardware impairments introduces indesirable effects on the reliability of the system and this effects become more significant for high SNR range. As a result, an irreducuble floor is created and degrades the error performance as the transmitted power increases. Therefore, the diversity gain G_d is equal

to zero. Now, considering an ideal system and since the CDF of the instantaneous SNR consists of complex functions such as the Meijer-G function, such function did not unpack engineering insights about the system gains. Consequently, it is more meaningful to derive the BEP at high SNR range as follows

$$\overline{P_e} \approx (G_c \overline{\gamma})^{-G_d}, \tag{3.51}$$

where G_d and G_c are the diversity and the coding gains, respectively. To get this form of the BEP, we refer to the technique proposed by [80, 73, 57, 72] to approximate the PDF of the overall SNR as follows:

$$f_\gamma(\gamma) = a\gamma^b + o(\gamma), \tag{3.52}$$

From the above approximation, the asymptotical high SNR expression of the BEP can be written as

$$\overline{P_e} \approx \frac{\prod_{i=1}^{b+1}(2i-1)}{2(b+1)!\, c^{b+1}} \frac{\partial^b f_\gamma}{\partial \gamma^b}(0) = \frac{2^b a \Gamma(b+3/2)}{\sqrt{\pi}(b+1)} (c\overline{\gamma})^{-(b+1)}, \tag{3.53}$$

where a is a constant and b must be a natural number for the first equation in (54) and not necessarily an integer for the second equation. Consequently, we derive the approximate expression of the PDF to find the diversity gain $G_d = b+1$ and the coding gain G_c. Given that the CDF of the overall SNR for the ideal case, it can be approximated at high SNR region as

$$F_\gamma(\gamma) \approx F_{\gamma_{1(m)}}(\gamma) + F_{\gamma_{2(m)}}(\gamma), \tag{3.54}$$

Deriving (55) gives the approximate PDF of the end-to-end SNR as

$$f_\gamma(\gamma) \approx f_{\gamma_{1(m)}}(\gamma) + f_{\gamma_{2(m)}}(\gamma), \tag{3.55}$$

Since $\gamma_{1(m)}$ is exponentially distributed under the assumption of PRS with outdated CSI, b is equal to zero. On the other side, the high SNR approximation of $f_{\gamma_{2(m)}}$ can be derived by using the expansion of the Meijer-G function given by Eq. (46). Note that for Eq. (46), we must substitute $\kappa = 1$ to consider the ideal case.
Consequently, the PDF of $\gamma_{2(m)}$ can be written as

$$f_{\gamma_{2(m)}}(\gamma) \approx D\gamma^{\min\left(\frac{\xi^2}{r},\ \frac{\alpha_1 m_1}{r},\ \frac{\alpha_2 m_2}{r}\right)}, \tag{3.56}$$

where D is a constant parameter. After combining the PDF approximations of $\gamma_{1(m)}$ and $\gamma_{2(m)}$, the PDF of the overall SNR can be derived as follows

$$f_\gamma(\gamma) \approx a\gamma^{\min\left(1,\ \min\left(\frac{\xi^2}{r},\ \frac{\alpha_1 m_1}{r},\ \frac{\alpha_2 m_2}{r}\right)\right)}, \tag{3.57}$$

Finally, the diversity gain G_d can be given by

$$G_d = \min\left(1,\ \min\left(\frac{\xi^2}{r},\ \frac{\alpha_1 m_1}{r},\ \frac{\alpha_2 m_2}{r}\right)\right), \tag{3.58}$$

While the coding gain G_c can be derived as follows

$$G_c = c\left(\frac{2^b a\Gamma(a+3/2)}{\sqrt{\pi}(b+1)}\right)^{-\frac{1}{b+1}}, \tag{3.59}$$

3.4 Ergodic Capacity Analysis

The closed-form can be computed by numerical integration using the PDF of the end-to-end SNDR. However, deriving a closed-form of the channel capacity in our case is very complex if not impossible. To overcome this problem, we should refer to the approximation given by [16, Eq. (35)]

$$\mathbb{E}\left[\log_2\left(1+\frac{\varphi}{\psi}\right)\right] \cong \log_2\left(1+\frac{\mathbb{E}\left[\varphi\right]}{\mathbb{E}\left[\psi\right]}\right), \tag{3.60}$$

Given that the RF and FSO channels are independent and using (44), we can derive an approximate expression of the ergodic capacity.
To characterize the ergodic capacity of our system, we derive an upper bound using the following theorem:

Theorem 1. *For asymmetric (Rayleigh/Double Generalized Gamma) fading channels, the ergodic capacity $\overline{C}$ in (bps/Hz) with AF and non-linear relaying has an upper bound using the Jensen's inequality as follows*

$$\overline{C} \leq \log_2\left(1+\varpi\mathcal{J}\right), \tag{3.61}$$

The term $\mathcal{J}$ is given by Eq. (3.62). The capacity ceiling $\overline{C}_c$ is the same as the FG relaying scheme (3.40).

$$\mathcal{J} = \frac{m\xi^2 p^{m_2-1} q^{m_1-\frac{1}{2}} (2\pi)^{1-\frac{p+q}{2}}}{\alpha_2 \kappa \Gamma(m_1)\Gamma(m_2)} \binom{N}{m} \sum_{n=0}^{m-1} \binom{m-1}{n} \frac{(-1)^{n+1}}{[(N-m+n)(1-\rho)+1]\overline{\gamma}_1 \beta^2}$$
$$\times H^{0,1:2,0:0,p+q+\alpha_2 p}_{1,0:0,2:p+q+\alpha_2 p,\alpha_2 p} \left(\begin{matrix} (-1;1,1) \\ - \end{matrix} \middle| \begin{matrix} (1,1) \\ (-1,1),\ (0,1) \end{matrix} \middle| \begin{matrix} (\kappa_1, [-\frac{r}{\alpha_2 p}]_{p+q+\alpha_2 p}) \\ (\kappa_2, [-\frac{r}{\alpha_2 p}]_{\alpha_2 p}) \end{matrix} \middle| -1,\ -\frac{\zeta^{-\frac{r}{\alpha_2 p}}}{\beta\kappa} \right), \tag{3.62}$$

3.5 Numerical Results and Discussion

In this section, we verify the analylical expressions with the numerical results using the Monte Carlo simulation [1]. Temporally correlated Rayleigh channel coefficients are generated using (3.1). The atmospheric turbulence I_a is generated using the expression $I_a = I_{aX} \times I_{aY}$, where the two independent random variables I_{aX} and I_{aY} follow the Generalized Gamma distribution using [32]. In addition, the pointing error is simulated by generating the radial displacement R following the Rayleigh distribution with scale equal to the jitter standard deviation (σ_s) and then we generate the samples using (3.14). Since the path loss is deterministic, it can be generated using the relation (3.13). Table 3.3 summarizes the main simulation parameters.

Table 3.3: Main Simulation Parameters

Parameter	Value
L	1 km
λ	1550 nm
F_0	-10 m
a	5 cm
ω_0	5 mm
σ_s	3.75 cm

Fig. 3.3 shows the dependence of the OP of FG relaying with respect to the average SNR considering various values of the outage threshold γ_{th} and the time correlation coefficient ρ. In addition, the relays are supposed to be impaired by SEL impairments and the receiver employs the IM/DD as a method of detection. For both correlation values,

[1] For all cases, 10^9 realizations of the random variables were generated to perform the Monte Carlo simulation in MATLAB.

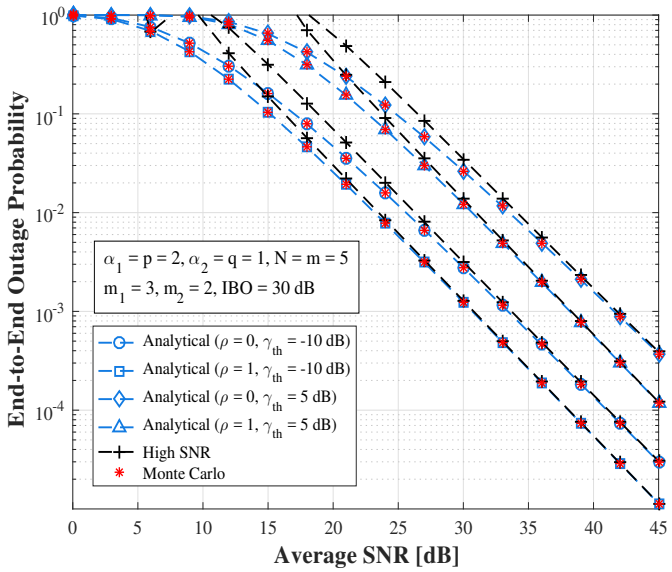

Figure 3.3: FG relaying, SEL, and IM/DD.

we observe that the performance deteriorates as the γ_{th} becomes higher and this result is certainly expected since for a given SNDR, the probability that the SNDR falls below a higher outage threshold becomes higher. For a given threshold, the system works better when the best relay of the last rank ($m = N$) is selected according to PRS protocol. We observe that the performance improves as the correlation coefficient increases. For a perfect CSI estimation ($\rho = 1$), there are full correlation between the two CSIs and the selection of the best relay is certainly achieved based on the feedback or the outdated CSI. However, for a completely outdated CSI ($\rho = 0$) the two CSIs are completely uncorrelated and hence the selection of the best relay is uncertain since the selection is based on a completely outdated CSI. As a result, the performance deteriorates substantially. Fig. 3.4 illustrates the variations of the OP of VG relaying versus the average SNR for moderate and strong atmospheric turbulences considering both the heterodyne and IM/DD as a detection scheme at the receiver. For moderate turblence (higher values of α_1, α_2), the system works better for the heterodyne mode compared to IM/DD. As the turbulence-induced fading becomes severe (lower values of α_1, α_2), the system performs worse compared to the first case. We also observe that the system works better for IM/DD under moderate turbulence than the heterodyne mode for severe turbulences even though the heterodyne mode outperforms the IM/DD. It turned out that the system depends to a large extent on the state of the optical channel.

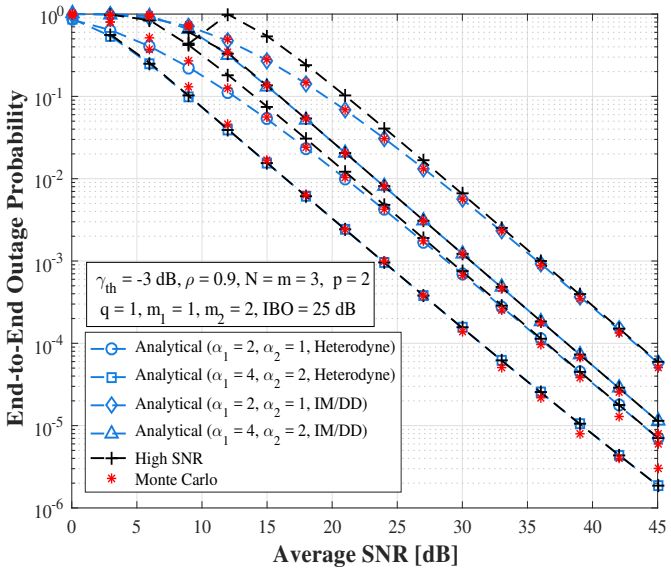

Figure 3.4: VG relaying, and TWTA.

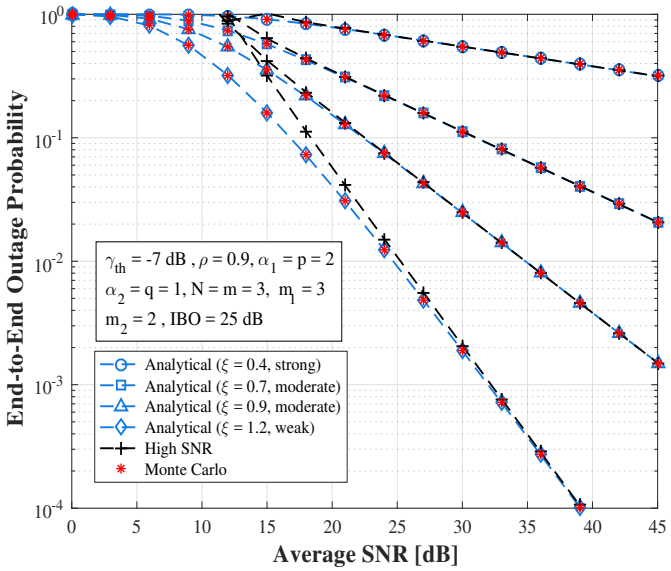

Figure 3.5: VG relaying, IM/DD, and TWTA.

Fig. 3.5 provides the variations of the OP for FG relaying against the average SNR for different values of the pointing error coefficients. In addition, the relays suffer from TWTA impairments and the receiver detects the incoming signal using IM/DD method.

We observe that the system works better as the pointing error coefficient decreases. In fact, as this coefficient ξ decreases, the pointing error fading becomes more severe. For a given average SNR of 30 dB, the system achieves roughly the following outage values $2\ 10^{-3}$, $2.5\ 10^{-2}$, 0.1 and 0.5 for the pointing error coefficients equal to 0.4, 0.7, 0.9 and 1.2, respectively. It turned out that the outage performance gets better as the pointing error coefficient becomes higher and thereby we prove again that the system depends substantially on the state of the optical channel. Fig. 3.6 presents the dependence of

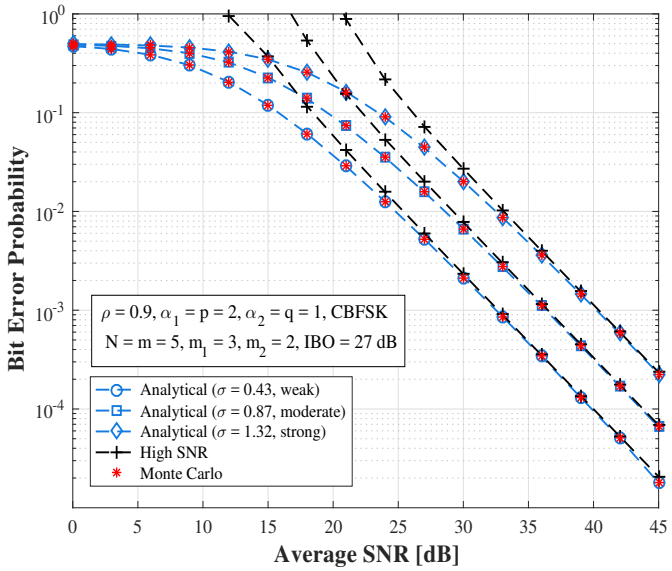

Figure 3.6: FG relaying, IM/DD, and SEL.

the BEP of FG relaying versus the average SNR for various weather condition assuming CBFSK modulation. The system is also assumed to suffer from the SEL impairments while the IM/DD is adopted as the detection technique. We observe that for lower weather attenuation, the system works better. However, as the path loss becomes more severe, the performance gets worse. Thereby, the system proves its high dependence on the third component of the optical fading which is the atmospheric path loss.

Fig. 3.7 illustrates the variations of the BEP of VG relaying with respect to the average SNR for various modulation schemes given in Table 3.2. The relays are impaired by the SEL imperfection and the receiver uses the heterodyne mode to detect the incoming FSO signal. We observe the accuracy of the asymptotic high SNR since it matches the exact Monte Carlo simulation for higher values of the average SNR. Thereby, this graph confirms the correctness of the asymptotic high SNR derivation. We also note that

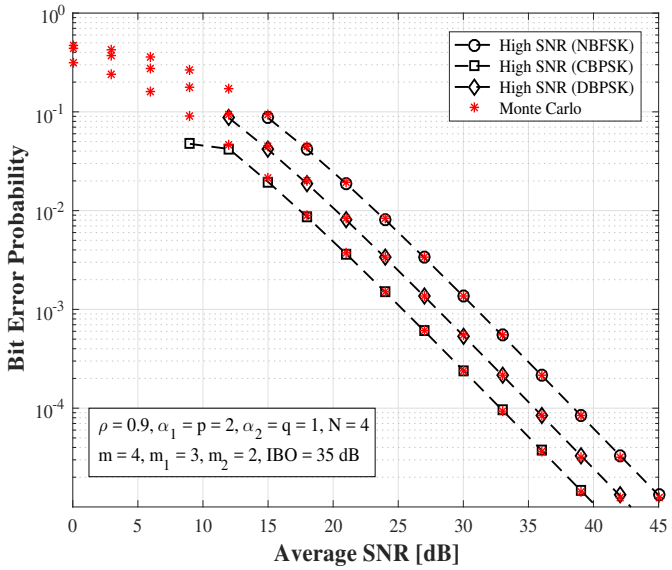

Figure 3.7: VG relaying, heterodyne, and SEL.

the system works better for CBPSK, however, the performance gets worse for NBFSK modulation. Fig. 3.8 presents the dependence of the ergodic capacity of FG relaying

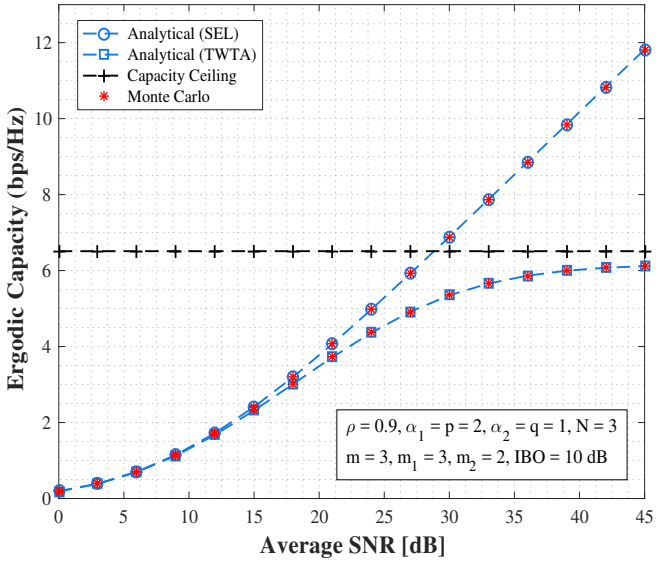

Figure 3.8: FG relaying, TWTA, and SEL.

against the average SNR provided that the system suffers from either SEL or TWTA

HPA impairment. For low average SNR, the system response to both SEL and TWTA is still acceptable as the impacts of the two HPA impairments are the same and also negligeable. Hence, in this SNR range, we can neglect the impacts of the SEL and TWTA and consider the system operating under linear relaying. However, as the average SNR increases and for a given IBO value equal to 10 dB, the impact of TWTA becomes more severe than SEL and this can be shown by the saturation of the capacity by an irreducible ceiling which is roughly 6.2 bps/Hz. Although, the relays's amplifiers for both SEL and TWTA are characterized by having the same IBO value, the system performance degrades substantially under the TWTA impairments. We also note that even for high SNR, the SEL impact is still acceptable on the system performance since the capacity is not limited by a ceiling or a floor at least in this SNR range (below 45 dB). It turned out that the system operates better in acceptable conditions under the SEL impairments than the TWTA for a given IBO level. Fig. 3.9 shows the variations of the ergodic capacity of VG

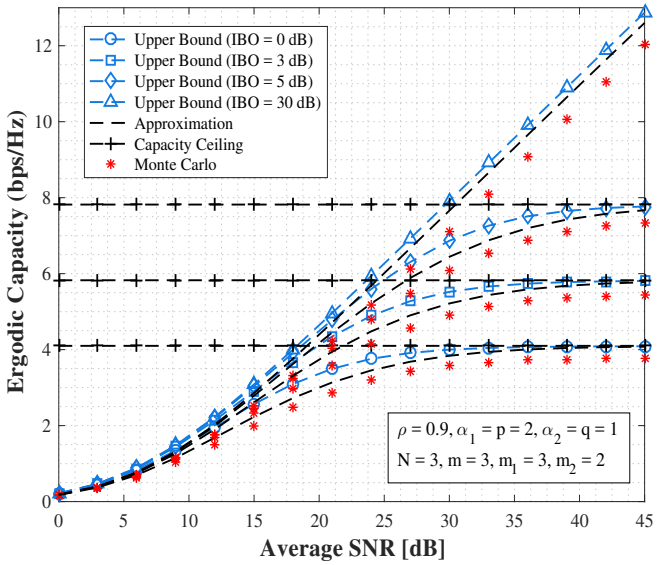

Figure 3.9: VG relaying, heterodyne, and SEL.

relaying versus the average SNR for different values of IBO. The relays suffer from the SEL impairments and the receiver detects the signal following IM/DD. Clearly, the three characteristics of the ergodic capacity, which are the exact Monte Carlo, approximate and upper bound, deviate from each other for low SNR but they overlap asymptotically at high SNR. Although the approximation given by (3.60) has no theoretical foundations, it is more tighter to the exact capacity compared to the upper bound derived from the

Jensen's inequality. Graphically, we observe that the ergodic capacity saturates by the hardware ceilings created by the HPA non-linearities as shown by Fig. 3.9. In addition, these ceilings disappear for an IBO = 30 dB but the performance is limited for the case of lower values of IBO. For the following values of IBO equal to 0, 3 and 5 dB, the system capacity is saturated by the following ceiling values 4, 5.9 and 7.9 bps/Hz, respectively. Note that these ceilings are inversely proportional to the values of the IBO. In fact, as the IBO increases, the saturation amplitude of the relay amplifier increases and thereby the distortion effect is reduced. However, as the IBO decreases, i.e, the relay amplifier level becomes lower, the nonlinear distortion impact becomes more severe and the channel capacity substantially saturates. Note that the capacity ceiling depends only on the hardware impairment parameters like the clipping factor and the scale of the input signal and not on the system parameters as the number of the relays and the channel parameters. Hence, it is straightforward that for any system suffering from the hardware impairments, the channel capacity is always limited by the impairment ceiling regardless of the system configuration such as the channels nature (RF/FSO) and the number of the relays, etc. Fig. 3.10 illustrates the variations of the outage probability with respect to

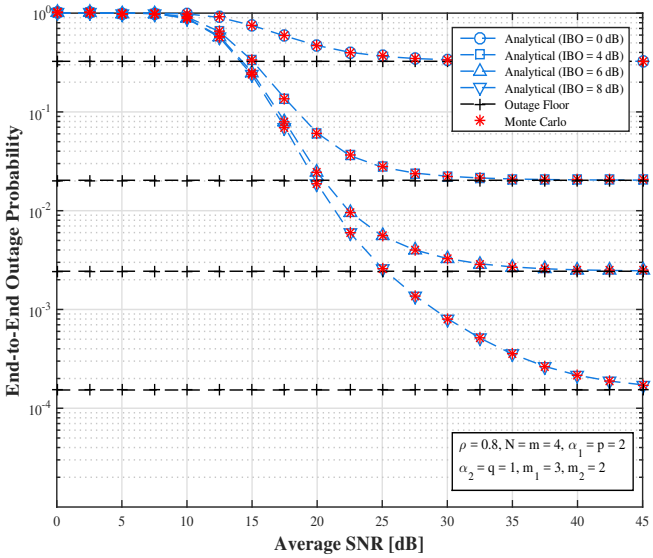

Figure 3.10: FG relaying, TWTA, and SEL.

the IBO. Clearly, we observe the distortion impact on the performance by the creation of the outage floor. This floor essentially saturates the system since the relay amplifier is not able to provide the required power and as a result a clipping and a distortion both affect

the signal. As the IBO increases, i.e, the saturation level of the relay enhances and the amplifier can provide higher amount of power. Consequently, the impacts of the distortion and the clipping on the signal are mitigated. This case is importantly manifested for IBO = 8 dB, although, the inevitable outage floor is created, the system is still working better than for the case of lower IBO values.

3.6 Conclusion

In this paper, we investigate a mixed RF/FSO systems with multiple relays where the RF and FSO links are modeled by Rayleigh and unified Double Generalized Gamma distributions, respectively. PRS with outdated CSI is assumed to select one relay among the set since the channels are time-varying and hence the selection is primarily based on the outdated CSI due to the propagation delay. We also consider FG and VG relaying schemes for the global performance analysis and we introduce the SEL and TWTA HPA non-linearities to the relays that occur during the amplification. We derive new closed-forms of the OP, BEP and ergodic capacity and we also evaluate the asymptotic performance of the system at high SNR regime. We show that the system works better for weak optical fading such as the turbulence-induced fading, the atmospheric path loss and the pointing error fading, howerver, as the FSO fading becomes severe, the performance gets worse even for better system configuration. We also prove that a better correlation of the CSIs yields a lower outage performance. Additionally, the analysis of the ergodic capacity shows that for a given IBO, the effect of the HPA non-linearities can be neglected and the system can be considered operating under linear relaying regime. However, as the average SNR increases, the system performance becomes very sensitive to the TWTA and the capacity saturates quickly around 30 dB than for the SEL impairments. Practically, the SEL amplifier is shown to be more efficient than TWT amplifier since it allows the system to operate in acceptable condition for the same amount of IBO. Furthermore, further investigation of the ergodic capacity for CSI-assisted relaying prove that the system rate substantially improves as the IBO increases since the constraint on the peak power during the amplification allow the amplifier to provide higher power to the signal without clipping the signal peaks.

Chapter 4: Aggregate Hardware Impairments Over Mixed RF/FSO Relaying Systems With Outdated CSI

"Aggregate Hardware Impairments Over Mixed RF/FSO Relaying Systems With Outdated CSI," in *IEEE Transactions on Communications*, vol. 66, no. 3, pp. 1110-1123, March 2018.

4.1 Introduction

In this chapter, we propose a dual-hop RF (Radio-Frequency)/FSO (Free-Space Optical) system with multiple relays employing the Decode-and-Forward (DF) and Amplify-and-Forward (AF) with a Fixed Gain (FG) relaying scheme. The RF channels are subject to a Rayleigh distribution while the optical links experience a unified fading model emcopassing the atmospheric turbulence that follows the Málaga distribution (or also called the $\mathcal{M}$-distribution), the atmospheric path loss and the pointing error. Partial relay selection (PRS) with outdated channel state information (CSI) is proposed to select the candidate relay to forward the signal to the destination. At the reception, the detection of the signal can be achieved following either heterodyne or Intensity Modulation and Direct Detection (IM/DD). Many previous attempts neglected the impact of the hardware impairments and assumed ideal hardware. This assumption makes sense for low data rate systems but it would no longer be valid for high data rate systems. In this work, we propose a general model of hardware impairment to get insight into quantifying its effects on the system performance. We will demonstrate that the hardware impairments have small impact on the system performance for low signal-to-noise ratio (SNR), but they can be destructive at high SNR values. Furthermore analytical expressions and upper bounds are derived for the outage probability and ergodic capacity while the symbol error probability is obtained through the numerical integration method. Capitalizing on these metrics, we also derive the high SNR asymptotes to get valuable insight into the system gains such as the diversity and the coding gains. Finally, analytical and numerical results are presented and validated by Monte Carlo simulation.

4.2 System Model

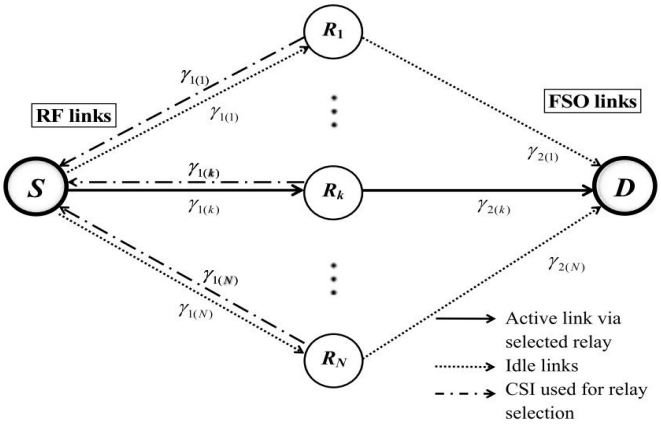

Figure 4.1: Mixed RF/FSO system with PRS

Our system consists of a source (S), a destination (D) and M parallel relays wirelessly connected to (S) and (D) as shown in Fig. 4.1. To select the relay of rank m, we refer to the PRS with outdated CSI to select the best one primarily on the feedback of the CSI coming from the relays. For a given transmission, (S) receives the feedbacks about the CSI of the RF channels from the M relays ($\tilde{\gamma}_{1(l)}$ for $l = 1,\ldots M$) and arranges them in an increasing order of amplitudes as follows $\tilde{\gamma}_{1(1)} \leq \tilde{\gamma}_{1(2)} \leq \ldots \leq \tilde{\gamma}_{1(M)}$. The perfect scenario is to pick the best relay ($m = M$). However, the best relay is not always available due to its half-duplex operation mode. In this case, (S) will choose the next best available relay. Consequently, the PRS consists of choosing the mth worst or $(M - m)$th best relay R_m. Taking into account the feedback delays as well as the time-varying channels, the CSI used for the relay selection is different from the actual CSI used for transmission. Hence, the outdated CSI should be assumed instead of the perfect CSI estimation. As a consequence, the instantaneous SNRs used for relay selection and transmission are correlated with time correlation coefficient ρ_m.

The received signal at the mth relay is given by

$$y_{1(m)} = h_m(s + \eta_1) + \nu_1, \tag{4.1}$$

where h_m is the fading amplitude of the RF channel between (S) and R_m, $s \in \mathbb{C}$ is the information signal, $\nu_1 \backsim \mathcal{N}\ (0,\ \sigma_0^2)$ is the AWGN of the RF channel, $\eta_1 \backsim \mathcal{N}\ (0,\ \kappa_1^2 P_1)$ is the distortion noise at the source (S), κ_1 is the impairment level in (S) and P_1 is the average transmitted power from (S).

4.2 End-to-End SNDR: Amplify-and-Forward Relaying

After reception, the relay R_m amplifies the received signal $y_{1(m)}$ with a fixed gain G depending on the average electrical channel fading. The gain G can be defined as follows [16, Eq. (11)]

$$G^2 \triangleq \frac{P_2}{P_1 \mathbb{E}\left[|h_m|^2\right](1+\kappa_1^2)+\sigma_0^2}, \tag{4.2}$$

where P_2 is the average transmitted power from the relay to the destination (D).
Then, the relay R_m converts the electrical signal to the optical one which, is defined as follows

$$y_{opt(m)} = G(1+\eta_e)y_{1(m)}, \tag{4.3}$$

where η_e is the electrical-to-optical conversion coefficient.
At the destination, the signal can be detected following the IM/DD or the heterodyne detection. The signal at the node (D) can be written as follows

$$y_{2(m)} = (\eta_o I_m)^{\frac{r}{2}}[G(1+\eta_e)(h_m(s+\eta_1)+\nu_1)+\eta_2]+\nu_2, \tag{4.4}$$

where η_o is the optical-to-electrical conversion, I_m is the optical channel gain between R_m and D, $\eta_2 \backsim \mathcal{N}\ (0,\ \kappa_2^2 P_2)$ is the distortion noise at the relay R_m, κ_2 is the impairment level in R_m, $\nu_2 \backsim \mathcal{N}\ (0,\ \sigma_0^2)$ is the AWGN of the optical channel.
The SNDR depends on the instantaneous electrical $\gamma_{1(m)}$ and the optical $\gamma_{2(m)}$ SNRs of the two hops. They are respectively defined by

$$\gamma_{1(m)} = \frac{|h_m|^2 P_1}{\sigma_0^2} = |h_m|^2 \mu_1, \tag{4.5}$$

where $\mu_1 = \frac{P_1}{\sigma_0^2}$ is the average SNR of the first hop.
The parameter r takes two values 1 and 2 standing for heterodyne and IM/DD, respectively. The average SNR $\overline{\gamma}_r$ and the average electrical SNR μ_r can be expressed as follows

$$\overline{\gamma}_r = \frac{\mathbb{E}\left[I_m^r\right]}{\mathbb{E}\left[I_m\right]^r}\mu_r, \tag{4.6}$$

$$\mu_r = \frac{\eta^r \mathbb{E}\left[I_m\right]^r}{\sigma_0^2}, \tag{4.7}$$

Hence, the instantaneous optical SNR $\gamma_{2(m)}$ can be obtained by

$$\gamma_{2(m)} = \frac{(\eta_o I_m)^r}{\sigma_0^2}, \tag{4.8}$$

For ideal hardware, the end-to-end SNR is given by [51, Eq. (6)]

$$\gamma_{\text{id}} = \frac{\gamma_{1(m)}\gamma_{2(m)}}{\gamma_{2(m)} + C}, \tag{4.9}$$

In case of non-ideal hardware and after some mathematical manipulations, the end-to-end instantaneous SNDR can be expressed as follows [16, Eq. (13)]

$$\gamma_{\text{ni}} = \frac{\gamma_{1(m)}\gamma_{2(m)}}{\delta\gamma_{1(m)}\gamma_{2(m)} + (1+\kappa_2^2)\gamma_{2(m)} + C}, \tag{4.10}$$

where $\delta \triangleq \kappa_1^2 + \kappa_2^2 + \kappa_1^2\kappa_2^2$ and $C = \mathbb{E}\left[\gamma_{1(m)}\right](1+\kappa_1^2) + 1$.

4.2 End-to-End SNDR: Decode-and-Forward Relaying

In case of DF relaying protocol, the signal is transmitted only if the relay is able to decode it. Therefore, the effective SNDR is the minimum of the set of SNDRs between (source-relay) and (relay-destination). In case of ideal hardware ($\kappa_1 = \kappa_2 = 0$), the end-to-end SNR is expressed as follows [16, Eq. (18)]

$$\gamma_{\text{id}} = \min(\gamma_{1(m)}, \gamma_{2(m)}), \tag{4.11}$$

In case of non-ideal hardware, the end-to-end SNDR is written as follows [16, Eq. (17)]

$$\gamma_{\text{ni}} = \min\left(\frac{\gamma_{1(m)}}{\kappa_1^2\gamma_{1(m)} + 1}, \frac{\gamma_{2(m)}}{\kappa_2^2\gamma_{2(m)} + 1}\right), \tag{4.12}$$

4.2 Channel Model

4.2.3.1 Statistics of the RF channel

Since the channel gain h_m experiences a Rayleigh fading, the instantaneous SNR $\gamma_{1(m)}$ is exponentially distributed. Given that PRS with outdated CSIs is assumed, the CDF

of $\gamma_{1(m)}$ can be obtained by [67, Eq. (9)]

$$\begin{aligned} f_{\gamma_{1(m)}}(\gamma) =& m\binom{M}{m}\sum_{k=0}^{m-1}\binom{m-1}{k}\frac{(-1)^k}{[(M-m+k)(1-\rho_m)+1]\mu_1} \\ &\times \exp\left(-\frac{(M-m+k+1)\gamma}{[(M-m+k)(1-\rho_m)+1]\mu_1}\right), \end{aligned} \tag{4.13}$$

After some mathematical manipulations, the CDF of $\gamma_{1(m)}$ can be expressed as follows

$$\begin{aligned} F_{\gamma_{1(m)}}(\gamma) =& 1 - m\binom{M}{m}\sum_{k=0}^{m-1}\binom{m-1}{k}\frac{(-1)^k}{M-m+k+1} \\ &\times \exp\left(-\frac{(M-m+k+1)\gamma}{[(M-m+k)(1-\rho_m)+1]\mu_1}\right), \end{aligned} \tag{4.14}$$

The constant C mentioned earlier depends on the expression of $\mathbb{E}\left[\gamma_{1(m)}\right]$ which, can be obtained by [66, Eq. (6)]

$$\mathbb{E}\left[\gamma_{1(m)}\right] = m\binom{M}{m}\sum_{k=0}^{m-1}\binom{m-1}{k}(-1)^k\frac{[(M-m+k)(1-\rho_m)+1]\mu_1}{(M-m+k+1)^2}, \tag{4.15}$$

4.2.3.2 Statistics of the optical channel

The FSO fading involves three contributions which, are the turbulence-induced fading (I_{a}), the atmospheric path loss (I_{l}) and the pointing errors (I_{p}). The mth channel gain I_m can be written as follows

$$I_m = I_{\mathrm{a}} I_{\mathrm{l}} I_{\mathrm{p}}, \tag{4.16}$$

Table 4.1 summarizes the parameters of the optical part.
Using the Beers-Lambert law, the path loss can be expressed as follows [21, Eq. (12)]

$$I_{\mathrm{l}} = \exp(-\sigma L), \tag{4.17}$$

The pointing error I_{p} made by Jitter can be given as [24, Eq. (9)]

$$I_{\mathrm{p}} = A_0 \exp\left(-\frac{2R^2}{\omega_{\mathrm{Leq}}^2}\right), \tag{4.18}$$

Table 4.1: Parameters of The FSO Part

Parameter	Definition
σ	Weather attenuation
σ_{s}^2	Jitter variance
σ_{R}^2	Rytov variance
k	Wave number
λ	Wavelength
ξ	Pointing error coefficient
ω_0	Beam waist at the relay
ω_{L}	Beam waist
ω_{Leq}	Equivalent beam waist
L	Length of the optical link
a	Radius of the receiver aperture
A_0	Fraction of the collected power at L = 0
F_0	Radius of curvature
C_n^2	Refractive index of the medium
R	Radial displacement of the beam at the receiver

The $\mathcal{M}$-distribution is a generalized model of fading model and it reflects a wide range of turbulences. This fading is eventually based on a physical model involving three components: the first one is the line-of-sight (LOS) component (U_L), the second term is quasi-forward scattered by the eddies on the propagation axis coupled to the LOS component (U_S^C) and a third component (U_S^G) is caused by the energy scattered to the receiver by off-axis eddies. The special cases of the $\mathcal{M}$-distribution are given by [33, Table I]. Since the atmospheric turbulence fading I_a follows the $\mathcal{M}$-distribution, its PDF can be expressed as follows [33, Eq. (6)]

$$f_{I_a}(I_a) = A \sum_{n=1}^{\beta} a_n I_a^{\frac{\alpha+n}{2}-1} K_{\alpha-n}\left(2\sqrt{\frac{\alpha\beta I_a}{g\beta+\Omega'}}\right), \tag{4.19}$$

where $K_\nu(\cdot)$ is the modified Bessel function of the second kind with order ν, $g = \mathbb{E}\left[|U_S^C|^2\right] = 2b_0(1-\rho)$, $2b_0 = \mathbb{E}\left[|U_S^C|^2 + |U_S^G|^2\right]$ is the average powers of the LOS, $\Omega = \mathbb{E}\left[|U_L^2|\right]$ is the total scatter components, α is a positive parameter related to the effective number of large-scale cells of the scattering process, β is a natural number and it stands for the amount of fading parameter, $\Omega' = \Omega + 2\rho b_0 + 2\sqrt{2\rho b_0 \Omega}\cos(\phi_A - \phi_B)$ represents the average power coming from the coherent component, the parameter ρ ($0 \leq \rho \leq 1$) is the amount of scattering power coupled to the LOS component while the parameters ϕ_A and ϕ_B are the

deterministic phases of the LOS and the coupled-to-LOS component. In addition, the parameter A and a_n are defined as

$$A = \frac{2\alpha^{\frac{\alpha}{2}}}{g^{1+\frac{\alpha}{2}}\Gamma(\alpha)} \left(\frac{g\beta}{g\beta+\Omega'}\right)^{\beta+\frac{\alpha}{2}}, \tag{4.20}$$

$$a_n = \binom{\beta-1}{n-1} \frac{(g\beta+\Omega')^{1-\frac{n}{2}}}{(n-1)!} \left(\frac{\Omega'}{g}\right)^{n-1} \left(\frac{\alpha}{\beta}\right)^{\frac{n}{2}}, \tag{4.21}$$

where $\Gamma(\cdot)$ is the incomplete upper gamma function. After unifying the three FSO components, the PDF of the instantaneous SNR $\gamma_{2(m)}$ can be written as [7, Eq. (9)]

$$f_{\gamma_{2(m)}}(\gamma) = \frac{\xi^2 A}{2^r \gamma} \sum_{n=1}^{\beta} b_n G_{1,3}^{3,0}\left(B\left(\frac{\gamma}{\mu_r}\right)^{\frac{1}{r}} \;\middle|\; \begin{matrix}\tau_1 \\ \tau_2\end{matrix}\right), \tag{4.22}$$

where $G_{p,q}^{m,n}(\cdot)$ is the Meijer G-function, $\tau_1 = \xi^2 + 1$, $\tau_2 = [\xi^2, \alpha, n]$ and the terms b_n and B are given by

$$b_n = a_n \left(\frac{g\beta+\Omega'}{\alpha\beta}\right)^{\frac{\alpha+n}{2}}, \tag{4.23}$$

After some mathematical manipulation, the CDF is given by [7, Eq. (11)]

$$F_{\gamma_{2(m)}}(\gamma) = D \sum_{n=1}^{\beta} c_n G_{r+1,3r+1}^{3r,1}\left(E\frac{\gamma}{\mu_r} \;\middle|\; \begin{matrix}\tau_3 \\ \tau_4\end{matrix}\right), \tag{4.24}$$

where $\tau_3 = [1,\ \Delta(r : \xi^2 + 1)]$, $\tau_4 = [\Delta(r : \xi^2),\ \Delta(r : \alpha),\ \Delta(r : n),\ 0]$, $c_n = b_n r^{\alpha+n-1}$, $E = B^r/r^{2r}$, $D = \xi^2 A/[2^r(2\pi)^{r-1}]$ and $\Delta(j\ ;\ x) \triangleq \frac{x}{j}, \ldots, \frac{x+j-1}{j}$.
Finally, the kth moment of the instantenous SNR $\gamma_{2(m)}$ is given by [7, Eq. (20)]

$$\mathbb{E}\left[\gamma_{2(m)}^k\right] = \frac{r\xi^2 A\Gamma(rk+\alpha)}{2^r(kr+\xi^2)B^{kr}} \sum_{n=1}^{\beta} b_n \Gamma(rk+n)\mu_r^k, \tag{4.25}$$

4.3 End-to-end Outage Probability Analysis

The outage probability is defined as the probability that the end-to-end SNDR falls below an outage threshold γ_{th}. It can be written as

$$P_{\text{out}}(\gamma_{\text{th}}) \triangleq \Pr[\gamma \leq \gamma_{\text{th}}], \tag{4.26}$$

where γ is the effective end-to-end SNDR.

4.3 Amplify-and-Forward Relaying

After substituting the expression of the overall SNDR (4.10) in Eq. (4.26) and using the following identities [53, Eqs. (8.4.3.2), (2.24.1)], the OP can be derived as follows

$$\begin{aligned} P_{\text{out}}(\gamma_{\text{th}}) =& 1 - \frac{m\xi^2 A}{2^r(2\pi)^{r-1}}\binom{M}{m}\sum_{k=0}^{m-1}\sum_{n=1}^{\beta}\binom{m-1}{k}\frac{(-1)^k b_n r^{\alpha+n-1}}{M-m+k+1}e^{-\zeta_1\frac{\gamma_{\text{th}}}{\mu_1}} \\ & \times\ G_{r,3r+1}^{3r+1,0}\left(\zeta_2\frac{\gamma_{\text{th}}}{\mu_1\mu_r}\ \middle|\ \begin{matrix}\tau_5\\ \tau_4\end{matrix}\right), \end{aligned} \tag{4.27}$$

where $\tau_5 = \Delta(r : \xi^2 + 1)$ and ζ_1, ζ_2 are respectively defined as

$$\zeta_1 = \frac{(M-m+k+1)(1+\kappa_2^2)}{[(M-m+k)(1-\rho_m)+1](1-\delta\gamma_{\text{th}})}, \tag{4.28}$$

$$\zeta_2 = \frac{(M-m+k+1)C}{[(M-m+k)(1-\rho_m)+1](1-\delta\gamma_{\text{th}})}\left(\frac{B}{r^2}\right)^r, \tag{4.29}$$

Note that a necessary condition states that the OP is given by Eq. (4.27) only if $1-\delta\gamma_{\text{th}} > 0$, otherwise it is equal to a unity.

To derive the asymptotical high SNR, we refer to the expansion of the Meijer-G function as follows [1, Eq. (07.34.06.0001.01)]

$$G_{r+1,3r+1}^{3r+1,0}\left(\zeta_2\frac{\gamma_{\text{th}}}{\mu_1\mu_r}\ \middle|\ \begin{matrix}\tau_5\\ \tau_4\end{matrix}\right) \underset{\mu_r>>1}{\cong} \sum_{\nu=1}^{3r+1}\frac{\prod_{j=1,j\neq\nu}^{3r+1}\Gamma(\tau_{4,j}-\tau_{4,\nu})}{\prod_{j=1}^{r}\Gamma(\tau_{5,j}-\tau_{4,\nu})}\left(\frac{\zeta_2\gamma_{\text{th}}}{\mu_1\mu_r}\right)^{\tau_{4,\nu}}, \tag{4.30}$$

4.3 Decode-and-Forward Relaying

Without loss of generality, we assume that all relays are able to decode the received signals from the source (S). For non-ideal hardware, the OP for DF relaying can be expressed as follows

$$P_{\text{out}}(\gamma_{\text{th}}) = 1 - \prod_{i=1}^{2}\left(1 - F_{\gamma_{i(m)}}\left(\frac{\gamma_{\text{th}}}{1-\kappa_i^2\gamma_{\text{th}}}\right)\right), \tag{4.31}$$

Note that the CDFs $F_{\gamma_{i(m)}}, i = 1, 2$ are defined only if $\gamma_{\text{th}} < \frac{1}{\kappa_i^2}$, i.e, $\gamma_{\text{th}} < \frac{1}{\max(\kappa_1^2, \kappa_2^2)} = \frac{1}{\delta}$. Hence, the OP is given by Eq. (4.31) if $\gamma_{\text{th}} < \frac{1}{\delta}$, otherwise, it is equal to a unity.
In case of ideal hardware, the expression of the OP is reduced to

$$P_{\text{out}}(\gamma_{\text{th}}) = 1 - \prod_{i=1}^{2} \Big(1 - F_{\gamma_{i(m)}}(\gamma_{\text{th}})\Big), \tag{4.32}$$

The asymptotical high SNR can be derived by using the expansion of the Meijer-G function as follows

$$F_{\gamma_{2(m)}}\left(\frac{\gamma_{\text{th}}}{1-\kappa_2^2\gamma_{\text{th}}}\right) \underset{\mu_r >> 1}{\cong} D \sum_{n=1}^{\beta} \sum_{\nu=1}^{3r} \frac{\prod_{j=1, j\neq\nu}^{3r} \Gamma(\tau_{4,j} - \tau_{4,\nu})\Gamma(\tau_{4,\nu})}{\prod_{j=2}^{r+1} \Gamma(\tau_{5,j} - \tau_{4,\nu})\Gamma(1 + \tau_{4,\nu})} \left(\frac{E\gamma_{\text{th}}}{(1-\kappa_2^2\gamma_{\text{th}})\mu_r}\right)^{\tau_{4,\nu}}, \tag{4.33}$$

4.4 Symbol Error Probability Analysis

For the most coherent linear modulation, the SEP is provided as follows

$$\overline{P_e} = \mathbb{E}\left[\mathcal{Q}(\sqrt{c\gamma})\right], \tag{4.34}$$

where $\mathcal{Q}(\cdot)$ is the Gaussian-Q function and c is a parameter related to the format of the modulation, e.g, $c = 2$ stands for BPSK modulation. After applying an integration by parts on Eq. (4.34), SEP can be expressed as follows

$$\overline{P_e} = \sqrt{\frac{c}{8\pi}} \int_0^{\infty} \frac{e^{-\frac{c}{2}\gamma}}{\sqrt{\gamma}} F_{\gamma}(\gamma) d\gamma, \tag{4.35}$$

4.4 Amplify-and-Forward Relaying

Because of the terms related to the hardware impairments, the derivation of the average SEP is not tractable. In that way, a numerical integration is required to plot the variations of the average SEP. Since the end-to-end OP is constrained by the necessary condition, the upper bound of the integral defined in Eq. (4.35) is equal to $1/\delta$.
For the ideal case ($\kappa_1 = \kappa_2 = 0$) and after using the following identities [27, Eq. (3.381.4)]

and [53, Eq. (2.24.3.1)], the average SEP can be easily derived as follows

$$\begin{aligned}\overline{P_e} =& \frac{1}{2} - \sqrt{\frac{c}{8\pi}} \frac{m\xi^2 A}{2^r (2\pi)^{r-1}} \binom{M}{m} \sum_{k=0}^{m-1} \sum_{n=1}^{\beta} \binom{m-1}{k} \frac{(-1)^k b_n r^{\alpha+n-1}}{M-m+k+1} \sqrt{\frac{2\mu_1}{c\mu_1 + 2\zeta_1}} \\ & \times \; G_{r+1,3r+1}^{3r+1,1}\left(\frac{2\zeta_2}{(c\mu_1 + 2\zeta_1)\mu_r} \;\middle|\; \begin{matrix} \tau_6 \\ \tau_4 \end{matrix} \right),\end{aligned} \tag{4.36}$$

where $\tau_6 = [0.5, \; \tau_5]$. A high SNR asymptote can be derived by using the expansion of the Meijer-G function as follows [1, Eq. (07.34.06.0001.01)]

$$\begin{aligned} G_{r+1,3r+1}^{3r+1,1}\left(\frac{2\zeta_2}{(c\mu_1 + 2\zeta_1)\mu_r} \;\middle|\; \begin{matrix} \tau_6 \\ \tau_4 \end{matrix} \right) \underset{\mu_r >> 1}{\cong} & \sum_{\nu=1}^{3r+1} \frac{\prod_{j=1, j\neq\nu}^{3r+1} \Gamma(\tau_{4,j} - \tau_{4,\nu}) \Gamma(0.5 + \tau_{4,\nu})}{\prod_{j=2}^{r+1} \Gamma(\tau_{6,j} - \tau_{4,\nu})} \\ & \times \; \left(\frac{2\zeta_2}{(c\mu_1 + 2\zeta_1)\mu_r} \right)^{\tau_{4,\nu}}, \end{aligned} \tag{4.37}$$

4.4 Decode-and-Forward Relaying

Similar to the case of the AF relaying, the derivation of the average SEP is complex due to the presence of the terms related to the hardware impairments. Hence, a numerical integration is required. The impact of the hardware impairments on the system performance is the creation of an irreducible floor that saturates the average SEP. Hence, the diversity gain G_d is equal to zero. For the ideal case, since the CDF of the instantaneous SNR consists of complex functions such the Meijer-G function, they do not provide insight into the system performance. Consequently, it is more meaningful to derive the average SEP at high SNR range as follows

$$\overline{P_e} \approx (G_c \overline{\gamma})^{-G_d}, \tag{4.38}$$

where G_d and G_c are the diversity and the coding gains. To achieve this step, we use the technique proposed by [80, 73, 57, 72] to approximate the PDF of the overall SNR as follows

$$f_\gamma(\gamma) = a\gamma^b + o(\gamma), \tag{4.39}$$

From the above approximation, the asymptotical expression of the average SEP can be formulated as follows

$$\overline{P_e} \approx \frac{\prod_{i=1}^{b+1}(2i-1)}{2(b+1)!\,c^{b+1}} \frac{\partial^b f_\gamma}{\partial \gamma^b}(0) = \frac{2^b a \Gamma(b+3/2)}{\sqrt{\pi}(b+1)} (c\overline{\gamma})^{-(b+1)}, \tag{4.40}$$

where a is a constant and b must be a natural number for the first equation in (4.40) and not necessarily an integer for the second equation. As a result, it is required first to derive the approximate PDF to find the diversity order $G_d = b + 1$ and the coding gain G_c. Given that the CDF of the overall SNR for the ideal case is given by Eq. (4.41), it can be approximated at high SNR region as follows

$$F_\gamma(\gamma) \approx F_{\gamma_{1(m)}}(\gamma) + F_{\gamma_{2(m)}}(\gamma), \tag{4.41}$$

After deriving (4.41), the approximate PDF of the end-to-end SNR is given by

$$f_\gamma(\gamma) \approx f_{\gamma_{1(m)}}(\gamma) + f_{\gamma_{2(m)}}(\gamma), \tag{4.42}$$

Since $\gamma_{1(m)}$ is exponentially distributed under the assumption of PRS with outdated CSI, b is equal to zero. On the other side, the high SNR approximation of $f_{\gamma_{2(m)}}$ can be derived by using the expansion of the Meijer-G function as follows

$$f_{\gamma_{2(m)}}(\gamma) \approx \frac{\xi^2 A}{2^r \gamma} \sum_{n=1}^{\beta} \sum_{\nu=1}^{3} \frac{\prod_{j=1, j\neq\nu}^{3} \Gamma(\tau_{2,j} - \tau_{2,\nu})}{\Gamma(\xi^2 + 1 - \tau_{2,\nu})} B^{\tau_{2,\nu}} \left(\frac{\gamma}{\mu_r}\right)^{\frac{\tau_{2,\nu}}{r}}, \tag{4.43}$$

Therefore, the PDF of $\gamma_{2(m)}$ can be reformulated as follows

$$f_{\gamma_{2(m)}}(\gamma) \approx D\gamma^{\min\left(\frac{\xi^2}{r},\ \frac{\alpha}{r},\ \frac{\beta}{r}\right)}, \tag{4.44}$$

where D is a constant parameter. After combining the PDF approximations of $\gamma_{1(m)}$ and $\gamma_{2(m)}$, the PDF of the overall SNR can be derived as follows

$$f_\gamma(\gamma) \approx a\gamma^{\min\left(1,\ \min\left(\frac{\xi^2}{r},\ \frac{\alpha}{r},\ \frac{\beta}{r}\right)\right)}, \tag{4.45}$$

Finally, the diversity gain G_d can be given by

$$G_d = \min\left(1,\ \min\left(\frac{\xi^2}{r},\ \frac{\alpha}{r},\ \frac{\beta}{r}\right)\right), \tag{4.46}$$

While the array gain G_c can be derived as follows

$$G_c = c\left(\frac{2^b a\Gamma(a+3/2)}{\sqrt{\pi}(b+1)}\right)^{-\frac{1}{b+1}}, \tag{4.47}$$

4.5 Ergodic Capacity Analysis

In this section, we will provide the analysis of the ergodic capacity, expressed in bps/Hz. It is defined as the maximum error-free data rate transferred by the system channel.

4.5 Capacity of AF Relaying

The ergodic capacity of AF relaying protocol with ideal hardware has been properly investigated in the literature [22, 74, 82]. Considering the case of hardware impairments, the channel capacity can written as follows

$$\overline{C} \triangleq \mathbb{E}\left[\log_2(1+\varpi\gamma)\right], \tag{4.48}$$

where $\varpi = 1$ indicates the heterodyne detection and $\varpi = \frac{e}{2\pi}$ for IM/DD. The ergodic capacity can be derived by calculating the PDF of the SNDR. However, an exact analytical formulation of Eq. (4.48) is very complex due to the presence of the terms related to the hardware impairments. To calculate the ergodic capacity, we should refer to the numerical integration method.
To quantify the EC, there is a possible way to evaluate an upper bound which, is given by the following theorem.

Theorem 2. *For Asymmetric (Rayleigh/Málaga) fading channels, the ergodic capacity $\overline{C}$ with AF relaying and non-ideal hardware has an upper bound defined by*

$$\overline{C} \leq \log_2\left(1+\frac{\varpi\mathcal{J}}{\delta\mathcal{J}+1}\right), \tag{4.49}$$

where $\mathcal{J}$ is defined as

$$\mathcal{J} \triangleq \mathbb{E}\left[\frac{\gamma_{1(m)}\gamma_{2(m)}}{(1+\kappa_2^2)\gamma_{2(m)}+C}\right], \tag{4.50}$$

After some mathematical manipulations, $\mathcal{J}$ can be derived as follows

$$\mathcal{J} = \frac{\xi^2 A \mathbb{E}\left[\gamma_{1(m)}\right]}{2^r(2\pi)^{r-1}(1+\kappa_2^2)} \sum_{n=1}^{\beta} b_n r^{\alpha+r-1} G_{r+1,3r+1}^{3r+1,1}\left(\left(\frac{B}{r^2}\right)^r \frac{C}{(1+\kappa_2^2)\mu_r} \;\middle|\; \begin{matrix}\tau_5,\ 0\\ \tau_4\end{matrix}\right), \tag{4.51}$$

Although deriving a closed-form of the ergodic capacity is very complex, we can find an approximate simpler form by applying the approximation given by [44, Eq. (27)], [16, Eq. (35)]

$$\mathbb{E}\left[\log_2\left(1+\frac{\psi}{\varphi}\right)\right] \approx \log_2\left(1+\frac{\mathbb{E}\left[\psi\right]}{\mathbb{E}\left[\varphi\right]}\right), \tag{4.52}$$

Now, let's consider a practical and realistic model of hardware impairment to test the resiliency of the proposed relaying system. We assume an ideal source and impaired relays that suffer from non-linear high power amplifier (HPA). We suggest the two HPA models called Soft Envelope Limiter (SEL) and Traveling Wave Tube Amplifier (TWTA) proposed by [44, 11]. In this case, the overall SNDR can be written as follows [11, Eq. (24)]

$$\gamma = \frac{\gamma_{1(m)}\gamma_{2(m)}}{\kappa\gamma_{2(m)}+C}, \tag{4.53}$$

where $C = \mathbb{E}\left[\gamma_{1(m)}\right] + \kappa$ and κ is given by [11, Eq. (25)]

$$\kappa = 1 + \frac{\sigma_\tau^2}{\varepsilon^2 G^2 \sigma_0^2}, \tag{4.54}$$

The parameters ε and σ_τ^2 are derived for SEL and TWTA in [11, Eqs. (18, 19)], respectively. We also define the Input Back-Off (IBO) relative to the amplifier as follows

$$\text{IBO} = \frac{A_{\text{sat}}^2}{\sigma_\tau^2}, \tag{4.55}$$

where A_{sat} is the saturation level of the relay's amplifier. Note that the ideal hardware case can be achieved only if κ converges to one.

In order to derive the average ergodic capacity, we should first find the expression of the CDF of overall SNR. Similar to the derivation steps used to find the OP (4.27), the CDF

of the end-to-end SNDR can be written as follows

$$\begin{aligned} F_{\gamma}(\gamma_{\rm th}) =& 1 - \frac{m\xi^2 A}{2^r(2\pi)^{r-1}}\binom{M}{m}\sum_{k=0}^{m-1}\sum_{n=1}^{\beta}\binom{m-1}{k}\frac{(-1)^k b_n r^{\alpha+n-1}}{M-m+k+1}e^{-\zeta_3\frac{\gamma_{\rm th}}{\mu_1}} \\ & \times\ G_{r,3r+1}^{3r+1,0}\left(\zeta_4\frac{\gamma_{\rm th}}{\mu_1\mu_r}\ \middle|\ \begin{matrix}\tau_5\\ \tau_4\end{matrix}\right), \end{aligned} \tag{4.56}$$

where ζ_3 and ζ_4 are given by

$$\zeta_3 = \frac{(M-m+k+1)\kappa}{[(M-m+k)(1-\rho_m)+1]}, \tag{4.57}$$

$$\zeta_4 = \frac{(M-m+k+1)C}{[(M-m+k)(1-\rho_m)+1]}\left(\frac{B}{r^2}\right)^r, \tag{4.58}$$

After applying the inetgration by parts on (4.48), the ergodic capacity can be reformulated as follows

$$\overline{C} = \frac{\varpi}{\ln(2)}\int_0^{\infty}(1+\varpi\gamma)^{-1}\overline{F}_{\gamma}(\gamma)\ d\gamma, \tag{4.59}$$

where $\overline{F}_{\gamma}(\cdot)$ is the complementary CDF (CCDF) of γ. After replacing the CCDF of (4.27) in (4.52), the ergodic capacity can be derived in closed-form as follows

$$\begin{aligned} \overline{C} =& \frac{m\xi^2 A\varpi\mu_1}{2^r(2\pi)^{r-1}\ln(2)}\binom{M}{m}\sum_{k=0}^{m-1}\sum_{n=1}^{\beta}\binom{m-1}{k}\frac{(-1)^k b_n r^{\alpha+n-1}}{(M-m+k+1)\zeta_3} \\ & \times\ H_{1,0:1,1:r,3r+1}^{0,1:1,1:3r+1,0}\left(\begin{matrix}(0;1,1)\\ -\end{matrix}\ \middle|\ \begin{matrix}(0,1)\\ (0,1)\end{matrix}\ \middle|\ \begin{matrix}(\tau_5,[1]_r)\\ (\tau_6,[1]_{3r+1})\end{matrix}\ \middle|\ \frac{\varpi\mu_1}{\zeta_3},\ \frac{\zeta_4}{\zeta_3\mu_r}\right), \end{aligned} \tag{4.60}$$

where $H_{p_1,q_1:p_2,q_2:p_3,q_3}^{m_1,n_1:m_2,n_2:m_3:n_3}(-|(\cdot,\cdot))$ is the bivariate Fox-H function and $[x]_j$ is the vector containing j elements equal to x.

An efficient Matlab implementation of the bivariate Fox-H function is provided in [64]. To derive the High SNR approximation of the ergodic capacity, we should expand the Meijer-G function in the expression (4.27) and then replace the (CCDF) in Eq. (4.52). After using the identities [53, Eqs. (8.4.2.5), (2.24.3.1)] and [1, Eq. (07.34.06.0001.01)],

the ergodic capacity can be expressed at high SNR region as follows

$$\overline{C} \underset{\mu_r>>1}{\cong} \frac{m\xi^2 A}{\ln(2)2^r(2\pi)^{r-1}} \binom{M}{m} \sum_{k=0}^{m-1} \sum_{n=1}^{\beta} \sum_{\nu=1}^{3r+1} \binom{m-1}{k} \frac{(-1)^k b_n r^{\alpha+n-1}}{M-m+k+1} \times \frac{\prod_{j=1, j\neq\nu}^{3r+1} \Gamma(\tau_{4,j}-\tau_{4,\nu})\Gamma(1+\tau_{4,\nu})}{\prod_{j=1}^{r} \Gamma(\tau_{5,j}-\tau_{4,\nu})} \left(\frac{\mu_1}{\zeta_3}\right)^{\tau_{4,\nu}+1} \left(\frac{\zeta_4}{\mu_1\mu_r}\right)^{\tau_{4,\nu}}, \tag{4.61}$$

4.5 Capacity of DF Relaying

The analysis of the ergodic capacity for the DF relaying is more complicated than the AF relaying protocol. Unlike the AF relaying in term of complexity of processing, the relay must decode and re-encode the information signal which, increases the level of difficulties. If the relay fails to decode the signal, the transmitted signal will be useless. In case of successfull decoding, the relay re-encodes the information and allocates the resources of power and symbols required for the transmission. To avoid further calculus constraints, we assume that all relays are able to decode the signal so that the complexity of processing will be reduced. In addition, we also assume that all relays are assigned equal times of resource allocations and prescheduling.

According to [29, Eq. (45)] and [22, Eq. (11a)] and the expression of the end-to-end SNDR in Eq. (4.12), the upper bound of the ergodic capacity with accounting of hardware impairments [16, Eq. (38)] can be written as follows

$$\overline{C} \leq \min_{i=1,2} \mathbb{E}\left[\log_2\left(1+\frac{c\gamma_{i(m)}}{\kappa_i^2\gamma_{i(m)}+1}\right)\right], \tag{4.62}$$

Eq. (4.62) shows clearly the effects of the hardware impairments in limiting the system performance contrary to the case of the ideal hardware where the system capacity grows infinitely.

4.5 Asymptotic Analysis

For high SNR regime, it is trivial that the end-to-end effective SNDR γ for AF and DF relaying converges to a ceiling γ^* defined as

$$\gamma^* \triangleq \begin{cases} \frac{1}{\kappa_1^2+\kappa_2^2+\kappa_1^2\kappa_2^2} & \text{AF Relaying Protocol,} \\ \frac{1}{\max(\kappa_1^2,\kappa_2^2)} & \text{DF Relaying Protocol,} \end{cases} \tag{4.63}$$

We observe that γ^* is inversely proportional to the hardware impairments κ_1^2 and κ_2^2. This confirms that the hardware impairments deeply affect the system performance and so it must be considered for the system modeling. We also observe that the ceiling for DF relaying is half of the ceiling for AF relaying protocol. This implies that the DF relaying is more resilient to the hardware impairments than the AF protocol.
Regarding the ergodic capacity in a high SNR regime, the hardware impairments saturate the channel capacity. This fact is shown by the following corollary.

Corollary 3. *Suppose that μ_1, μ_r largely increase and the electrical and optical channels are mutually independant with strictly non-negative fading, the ergodic capacity converges to a capacity ceiling defined by $\overline{C^*} = \log_2(1 + \varpi\ \gamma^*)$.*

Proof. Since the SNDR converges to γ^*, the dominated convergence theorem consequently allows to moving the limit inside the logarithm function as shown below

$$\lim_{\mu_1,\mu_r\to\infty} \log_2(1 + \varpi\ \mathbb{E}\left[\gamma\right]) = \log_2(1 + \varpi \lim_{\mu_1,\mu_r\to\infty} \mathbb{E}\left[\gamma\right]) = \log_2(1 + \varpi\gamma^*), \tag{4.64}$$

□

Hence, the ergodic capacity with AF relaying protocol under harware impairments satisfies

$$\lim_{\mu_1,\mu_r\to\infty} \overline{C} = \log_2\left(1 + \frac{\varpi}{\kappa_1^2 + \kappa_2^2 + \kappa_1^2\kappa_2^2}\right), \tag{4.65}$$

For DF relaying and non-ideal harware impairments, the ergodic capacity is upper bounded by

$$\lim_{\mu_1,\mu_r\to\infty} \overline{C} \leq \log_2\left(1 + \frac{\varpi}{\max(\kappa_1^2, \kappa_2^2)}\right), \tag{4.66}$$

If we assume that only the relays are susceptible to the non-linear HPA impairment, the ergodic capacity is saturated by a ceiling that depends only on the amplifier's parameters

as follows [44, Eq. (37)]

$$\overline{C_c} = \log_2\left(1 + \frac{\varpi\varepsilon^2}{\iota - \varepsilon^2}\right), \tag{4.67}$$

where ι is called the clipping factor. Further details about the non-linear HPA modeling are found in [19, 11].

4.6 Numerical Results

This section provides numerical results obtained by using the mathematical formulations of the previous section. The electrical channel is subject to the correlated Rayleigh fading which, can be generated using the algorithm in [81]. The turbulence-induced fading is modeled by $\mathcal{M}$-distribution, which, can be generated by using the formula [33, Eq. (2)], $I = XY$, where $X \backsim \mathcal{G}(\alpha, 1)$ and $Y \backsim \mathcal{SR}(g, \beta, \rho, \Omega', \Delta\Phi)$ are mutually independent random variables. In addition, the pointing error is simulated by generating the radial displacement R following the Rayleigh distribution and then applying Eq. (18). Since the path loss is deterministic, it can be generated using relation (17). Unless otherwise stated, Table 4.2 presents the main simulation parameters.

Table 4.2: Simulation Parameters

Parameter	Value
C_n^2	2.8 10^{-14} $\mathrm{m}^{-2/3}$
L	1 km
λ	1550 nm
γ_{th}	7 dB
F_0	-10 m
a	5 cm
w_0	5 mm
b_0	0.596
Ω	1.32
α	4.2
β	5
ρ	0.6
ρ_m	0.7
M, m	3
$\kappa_1,\ \kappa_2$	0.3
Modulation	CBPSK

Fig. 4.2 shows the OP dependence on the average SNR for AF and DF relaying protocols. We note that for low SNR, the performance of ideal and non-ideal hardware shows

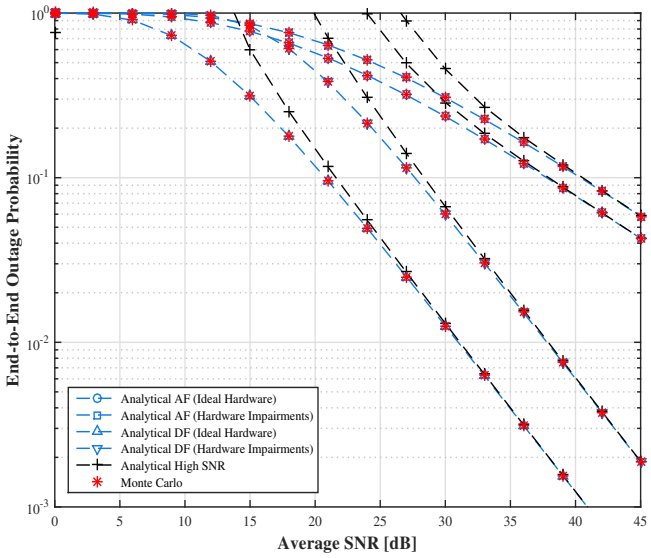

Figure 4.2: Outage probability for ideal and non-ideal hardware under IM/DD detection.

a slight deviation from each other. In this case, the hardware impairments has a small impact on the outage performance and so the assumption of neglecting the effect of the impairments can be valid. As the SNR increases toward 30 dB, the performance deteriorates and so the approximation of neglecting the hardware impairments is no longer valid. Although the impairments factor has an inavoidable effect on the system performance, the DF relaying protocol appears to be more resilient than the AF protocol. In fact, we observe that even though a DF relaying system operates under hardware impairments, it outperforms an AF relaying system with ideal hardware. This result as expected since the distortion noise of the first RF channels is carried on the second optical channels for AF protocol.

Fig. 4.3 shows the OP performance as a function of the average SNR for AF relaying protocol. The curve variations show that there is a small performance loss caused by the hardware impairments for the low threshold $\gamma_{\text{th}} = 2$ dB. Whereas, there are substantial losses when the outage threshold increases to 5 dB. Regarding the detection method, the graph is absolutely in agreement with previous work. As expected, the relaying system works better with heterodyne detection than using IM/DD method.

The dependence of the OP for DF relaying protocol on the average SNR is given by Fig. 4.4. As expected, the outage performance is better under the moderate turbulence condition and suddenly deteriorate as the turbulence becomes strong and severe. This

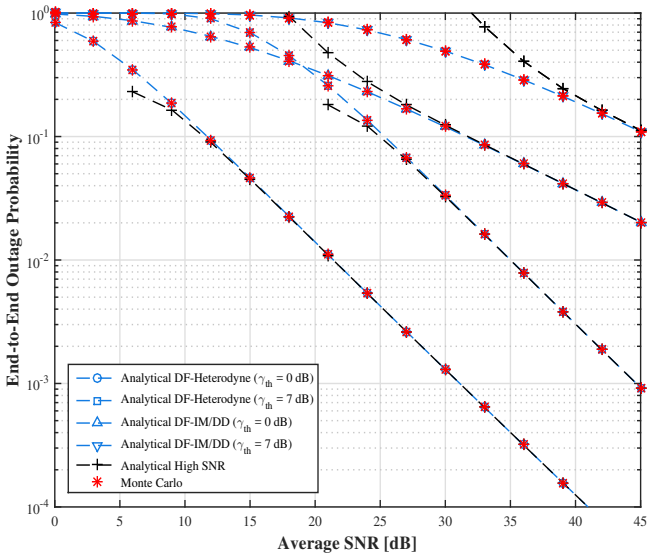

Figure 4.3: Outage probability for IM/DD and heterodyne detections using different γ_{th}.

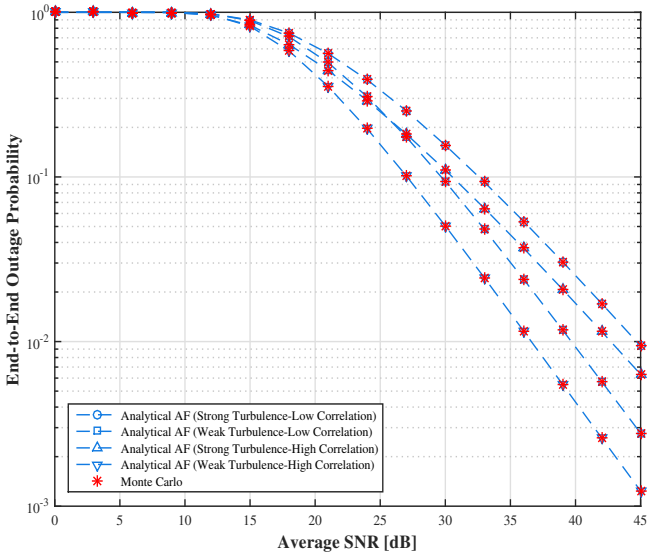

Figure 4.4: Outage probability for various correlation and turbulences.

result is clearly observed, especially for the case of full correlation of CSIs ($\rho = 1$). It turned out that the system substantially depends on the state of the optical channels. As the correlation ρ between the CSI used for relay selection and the CSI used for trans-

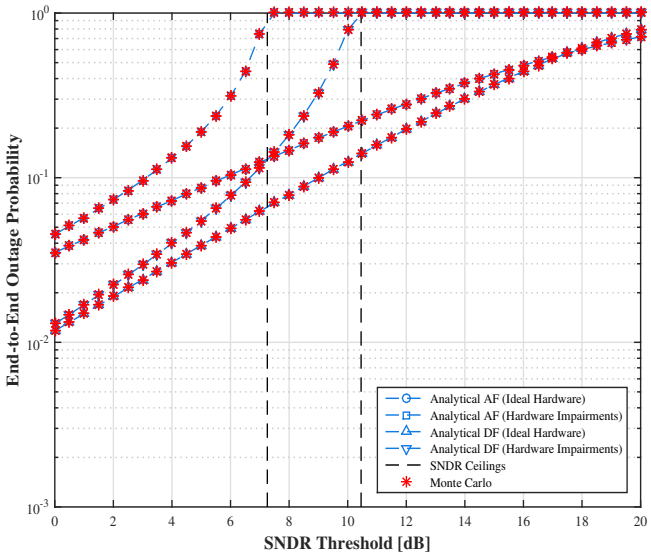

Figure 4.5: Outage probability versus the SNDR threshold for ideal and non-ideal hardware.

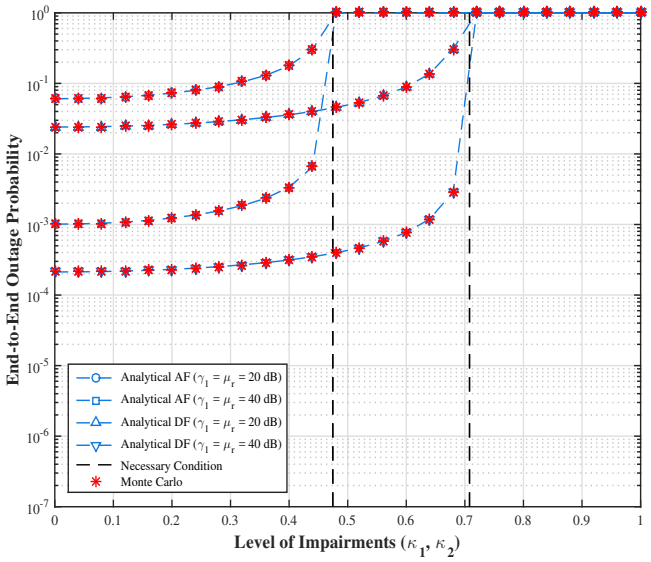

Figure 4.6: Outage probability for various levels of hardware impairments.

mission increases, i.e., the two CSIs become more and more correlated, the selection of the best relay is certainly achieved ($m = M$). In this case, the system works under the perfect condition specially under moderate turbulence condition. As the time correlation

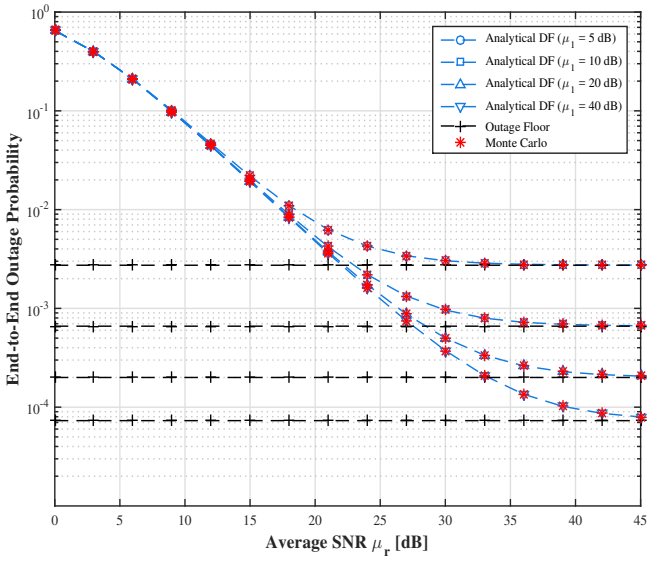

Figure 4.7: Outage probability versus the average optical SNR for different μ_1.

decreases, the selection of the best relay is no longer achieved and so the system certainly operates with a worse relay.

Fig. 4.5 shows the OPs of AF and DF relaying protocols as a function of the threshold γ_{th} (dB) for ideal and non-ideal hardware ($\kappa_1 = \kappa_2 = 0.3$). For small outage threshold, the OPs are slightly deteriorated by the hardware impairments. For high outage threshold, the system with ideal harware smoothly converges toward 1, while the non-ideal system is subject to a rapid convergence to the SNDR ceiling. As we concluded before, DF relaying protocol is more robust to hardware impairments and the relative SNDR ceiling is higher than of AF relaying scheme. For practical use when dealing with non-ideal hardware, DF relaying sufficiently proves its superiority over AF relaying scheme to acquire the hardware imperfections caused by low quality of the materials. The variations of the OP for AF and DF protocols with respect to the level of the impairments for two different average SNRs $\mu_1 = \mu_2 = \{20, 40\}$dB are shown in Fig. 4.6. Considering the case 40 dB and requiring that the OP is under $10^{-}2$, we can identify two operating regimes

1. AF relaying protocol with $\kappa_1 = \kappa_2 \leq 0.44$.

2. DF relaying protocol with $\kappa_1 = \kappa_2 \leq 0.70$.

The various acceptable levels of impairments prove that DF relaying protocol is more resistant to the hardware impairments and thus, it can operate with low quality of the

hardware for practical use. Fig. 4.6 also shows the necessary condition we mentioned earlier which,, is an upper bound on the impairments level that can achieve an outage probability inferior to 1.

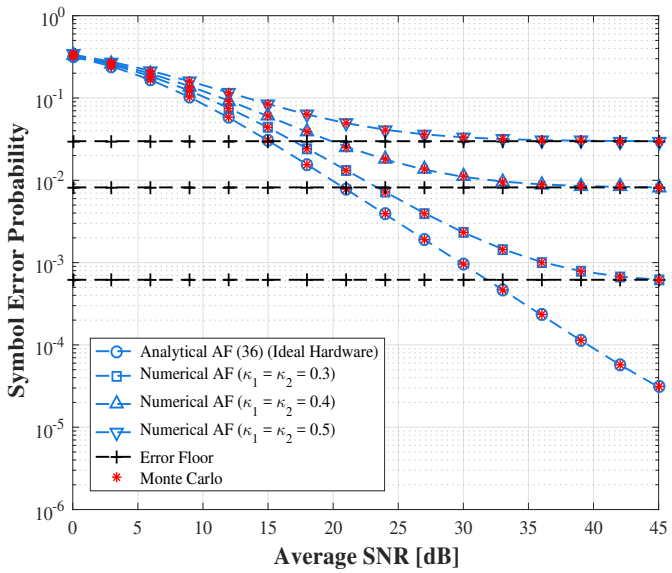

Figure 4.8: Symbol error probability for various levels of hardware impairments.

Fig. 4.7 shows the impact of the average RF SNR on the outage performance. In fact, the system saturates as the average transmitted power over the first hop is constant. The limitation is mainly observed by the creation of the outage floor that substantially degrades the system performance. Another important metric that is considered is the error performance. The degradation caused by the hardware impairments is confirmed again by the saturation of the error performance shown by Fig. 4.8. We observe the creation of an error floor that limits the system performance and this floor becomes more severe as the average SNR increases. The error performance is also investigated for different weather states in Fig. 4.9. For clear air, the weather is quiet and the scattering loss is negligible or small. Given that the high frequency signals are greatly disturbed by the fog, clouds and dust particles, the FSO signal depends not only on the rain which, is the major attenuating factor but also on the rate of the rainfall as shown by the figure. In fact, the rain droplets cause a substantial scattering in different directions that mainly attenuate the signal power during the propagation and this phenomena can be explained in more details according to the Rayleigh model of scattering.

Fig. 4.10 shows the dependence of the ergodic capacity on the average SNR for ideal

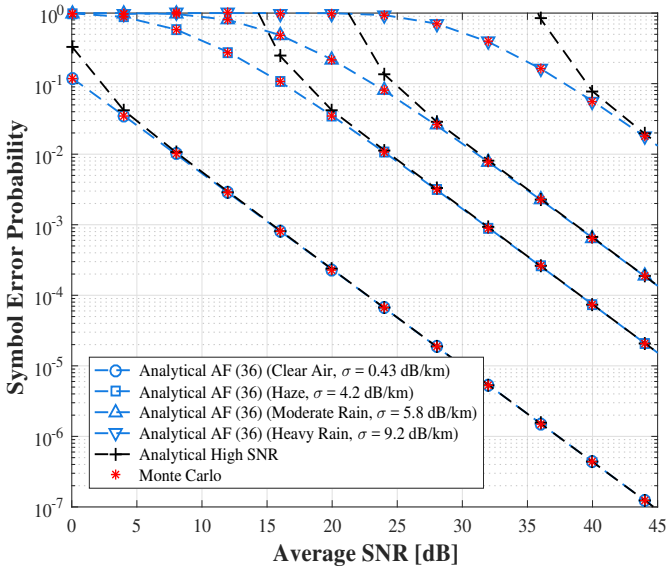

Figure 4.9: Symbol error probabilty probability for various weather attenuation coefficients.

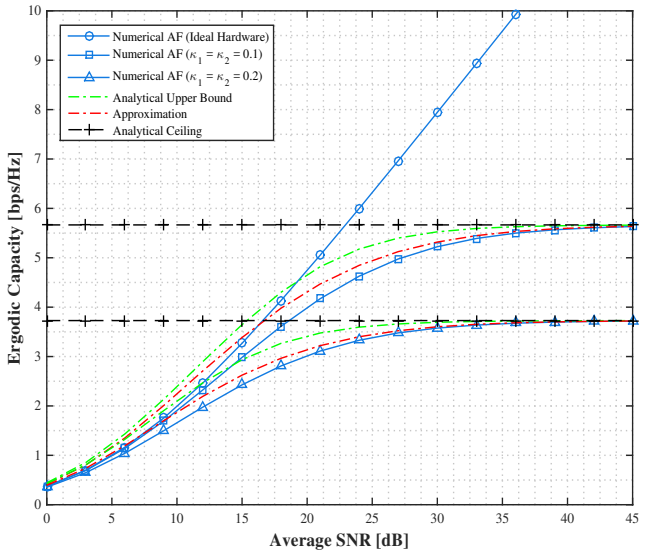

Figure 4.10: Ergodic capacity for different values of the hardware impairments.

and non-ideal harware. We observe that the hardware impairments level is acceptable at low SNR, but it becomes very severe as the SNR increases. Specifically, the ergodic capacity saturates and converges to the capacity ceiling C^* as shown by corollary 1, which,

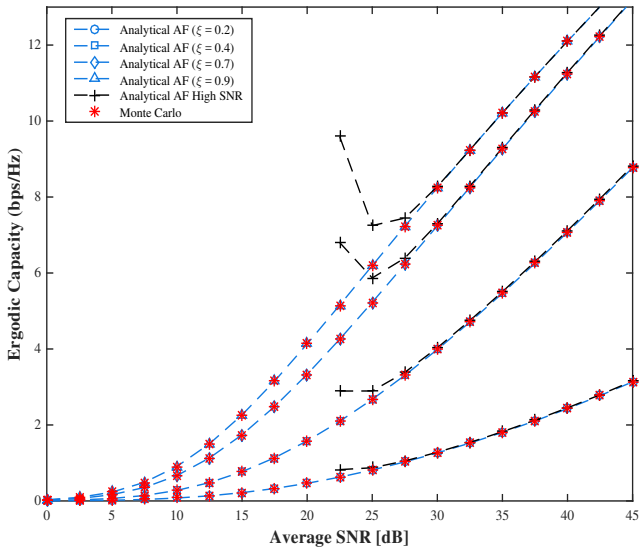

Figure 4.11: Ergodic capacity for different values of the pointing error coefficients.

is inversely proportional to κ_1 and κ_2. Fig. 4.10 also presents the capacity upper bound proved by Theorem 1 and the approximation (52). Although the exact, the approximate and the upper bound of the ergodic capacity show a slight deviation from each other at low SNR regime, they are asymptotically exact as the average SNR largely increases. Fig. 4.11 provides the variations of the ergodic capacity against the average SNR for different values of the pointing error coefficients. We observe that the system works better as the pointing error coefficient decreases. In fact, as this coefficient ξ decreases, the pointing error effect becomes more severe. For a given average SNR of 30 dB, the system capacity achieves the following rates 1, 3.9, 7 and 8 bps/Hz for the pointing error coefficients equal to 0.2, 0.4, 0.7 and 0.9, respectively. Thereby, the ergodic capacity gets better as the pointing error coefficient becomes higher.

Fig. 4.12 shows the variations of the ergodic capacity versus the average SNR for different values of IBO. Clearly, we observe that the ergodic capacity saturates by the ceilings that are caused by the hardware impairments as shown by the figure. In addition, these ceilings disappear for an IBO = 30 dB as shown in Fig. 4.3 but the performances are limited for the case of lower values of IBO. For the following values of IBO equaling to 0, 3, 5 and 7 dB, the system capacity is saturated by the following ceiling values 3, 4.9, 6.6 and 9.8 bps/Hz, respectively. Note that these ceilings are inversely proportional to the values of the IBO. In fact, as the IBO increases, the saturation amplitude of the

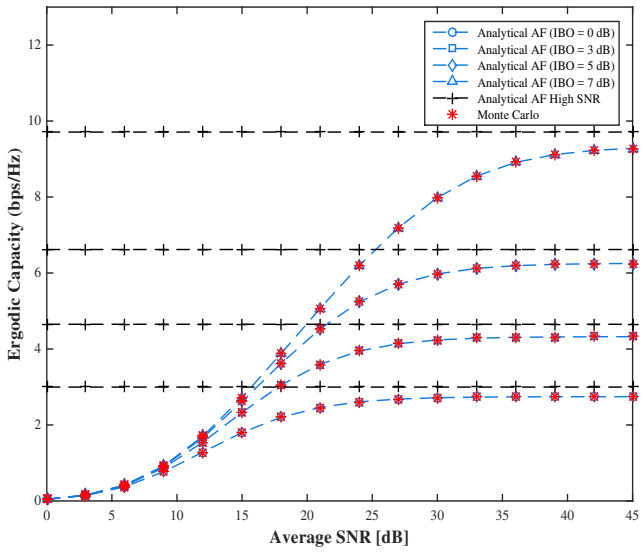

Figure 4.12: Ergodic capacity of AF relaying for different values of the relay's amplifier IBO.

relay amplifier increases and thus the distortion effect is reduced. However, as the IBO decreases, i.e, the relay amplifier level becomes lower, the non-linear distortion impact becomes more severe and the channel capacity substantially saturates. Note that the capacity ceiling depends only on the hardware impairment parameters like the clipping factor and the scale of the input signal and not on the system parameters such as the number of relays and the channels' parameters, etc.

4.7 Conclusion

In this work, we introduced a general model of impairments to a mixed RF/FSO system for AF and DF relaying protocols and we observed that it has a small impact on the system for low SNRs but this effect becomes more severe as the SNR increases. In addition, we proved that the correlation has a deep impact on the system performance but importantly, the system depends to a large extent on the state of the optical channel in terms of the turbulence intensity, the weather attenuation and the pointing error. Furthermore, we proved that the DF relaying is more efficient than AF protocol and so it is more convenient for practical use. Also, we investigated the impact of the non-linear HPA on the system performance and we concluded that the system works better for higher values of IBO.

Chapter 5: On the Joint Effects of HPA Non-Linearity and IQ Imbalance on Mixed RF/FSO Relaying Systems

5.1 Introduction

In this chapter, we present the performance analysis of asymmetric dual-hop RF/FSO system with multiple relays. The RF channels follow the correlated Rayleigh fading while the optical links are subject to the Gamma-Gamma fading. To select the candidate relay to forward the communication, we assume Partial Relay Selection (PRS) with outdated Channel State Information (CSI). Unlike the vast majority of work in this area, we introduce the impairments to the relays and the destination. We will propose three impairment models called Soft Envelope Limiter (SEL), Traveling Wave Tube Amplifier (TWTA) and IQ Imbalance in order to compare the resilience of our system with the RF one against the hardware impairments. Closed-from of the outage probability (OP) is derived in terms of Meijer's G function as well as the upper bound of the ergodic capacity (EC). The Bit Error Rate (BER) and the exact EC are evaluated numerically. Finally, analytical and numerical results are presented and validated by Monte Carlo simulation.

5.2 System and Channels Models

Our system consists of source (S), destination (D) and N parallel relays wirelessly connected to the S and D shown by Fig. 5.1. For a given transmission, the source S receives periodically the CSIs ($\gamma_{1(l)}$ for $l = 1 \dots N$) of the first hop from the N relays and sorts them in an increasing order of magnitude as follows: $\gamma_{1(1)} \leq \gamma_{1(2)} \leq \dots \leq \gamma_{1(N)}$. The perfect scenario is to select the best relay *($m = N$)* but this best one is not always available. In this case, S will select the next best available relay. Consequently, PRS protocol selects the mth worst or *(N - m)*th best relay $R_{(m)}$. Given that the feedback sent from the relays to S is susceptible to the delay, the CSI at the time of selection is different from the CSI at the instant of transmission. In this case, outdated CSI should be assumed instead of perfect CSI estimation. Hence, the instantaneous CSI used for relay selection $\tilde{\gamma}_{1(m)}$ and the instantaneous CSI $\gamma_{1(m)}$ used for transmission are correlated with the time correlation coefficient ρ.

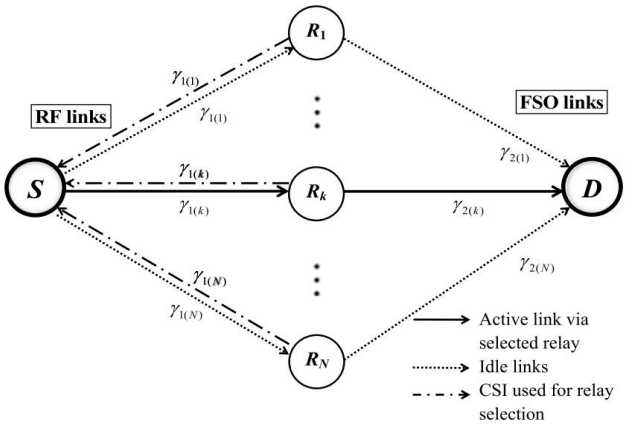

Figure 5.1: Mixed RF/FSO system with partial relay selection

The received signal at the mth relay is given by

$$y_{1(m)} = h_m s + \nu_1, \tag{5.1}$$

where $s \in \mathbb{C}$ is the information signal, h_m is the RF fading between S and $R_{(m)}$ and $\nu_1 \backsim \mathcal{CN}\ (0,\, \sigma_0^2)$ is the AWGN of the RF channel.

5.2 Relay's Power Amplifier non-linearity

PA non-linearity impairment is introduced to the relays. The amplification of the signal happens in two time slots. In the first slot, the received signal at the relay $R_{(m)}$ is amplified by a proper gain G as $\phi_m = G y_{1(m)}$. The gain G can be defined as

$$G = \sqrt{\frac{\sigma^2}{\mathbb{E}\left[|h_m|^2\right] P_1 + \sigma_0^2}}, \tag{5.2}$$

where $\mathbb{E}\left[\cdot\right]$ is the expectation operator, P_1 is the average transmitted power from S and σ^2 is the mean power of the signal at the output of the relay block. In the second time slot, the signal passes through a non-linear circuit $\psi_m = f(\phi_m)$.

The PA (Power Amplifier) of the relay is assumed to be memoryless. A memoryless PA is characterized by both Amplitude to Amplitude (AM/AM) and Amplitude to Phase (AM/PM) characteristics. The functions AM/AM and AM/PM transform the signal distortion respectively to $A_m(|\phi_m|)$ and $A_p(|\phi_m|)$ and then the output signal of the non-linear PA circuit is given by

$$\psi_m = A_m(|\phi_m|)\ e^{j(\arg(\phi_m) + A_p(|\phi_m|))}, \tag{5.3}$$

where $\arg(\phi_m)$ is the polar angle of the complex signal ϕ_m. The characteristic functions of the SEL and TWTA impairments models are respectively given by [20]

$$A_m(|\phi_m|) = \begin{cases} |\phi_m| & \text{if } |\phi_m| < A_{sat} \\ A_{sat} & \text{otherwise} \end{cases}, \quad A_p(|\phi_m|) = 0,$$

$$A_m(|\phi_m|) = \frac{A_{sat}^2 |\phi_m|}{A_{sat}^2 + |\phi_m|^2}, \quad A_p(|\phi_m|) = \frac{\Phi_0 \ |\phi_m|^2}{A_{sat}^2 + |\phi_m|^2}, \tag{5.4}$$

A_{sat} is called the input saturation magnitude and Φ_0 controls the maximum phase rotation. From a given saturation level A_{sat}, the relay's power amplifier operates at an input back-off (IBO), which is defined by IBO $= \frac{A_{sat}^2}{\sigma^2}$.

According to Bussgang Linearization theory [20], the output of the non-linear PA circuit linearly depends on both the linear scale δ of the input signal and a non-linear distortion d which is uncorrelated with the input signal and follows the circularly complex Gaussian random variable $d \backsim \mathcal{CN}(0, \ \sigma_d^2)$. Then, the AM/AM characteristic $A_m(|\phi_m|)$ can be expressed as follows

$$A_m(|\phi_m|) = \delta \ x + d, \tag{5.5}$$

Regarding the SEL NLPA model, δ and σ_d^2 can be written as follows

$$\begin{aligned} \delta &= 1 - \exp\left(-\frac{A_{sat}^2}{\sigma^2}\right) + \frac{\sqrt{\pi} A_{sat}}{2\sigma^2} \ \operatorname{erfc}\left(\frac{A_{sat}}{\sigma}\right), \\ \sigma_d^2 &= \sigma^2 \ \left[1 - \exp\left(-\frac{A_{sat}^2}{\sigma^2}\right) - \delta^2\right], \end{aligned} \tag{5.6}$$

The clipping factor ξ of the SEL model is given by

$$\xi = 1 - \exp\left(-\frac{A_{sat}^2}{\sigma^2}\right), \tag{5.7}$$

For the TWTA model, if the AM/PM effect of the characteristic $A_p(|\phi_m|)$ is neglected (i.e., $\Phi_0 \approx 0$), δ and σ_d^2 can be written as follows

$$\begin{aligned} \delta &= \frac{A_{sat}^2}{\sigma^2}\left[1 + \frac{A_{sat}^2}{\sigma^2} \exp\left(\frac{A_{sat}^2}{\sigma^2}\right) + \operatorname{Ei}\left(-\frac{A_{sat}^2}{\sigma^2}\right)\right], \\ \sigma_d^2 &= -\frac{A_{sat}^4}{\sigma^2}\left[\left(1 + \frac{A_{sat}^2}{\sigma^2}\right) e^{\frac{A_{sat}^2}{\sigma^2}} \operatorname{Ei}\left(-\frac{A_{sat}^2}{\sigma^2}\right) + 1\right] - \sigma^2\delta^2, \end{aligned} \tag{5.8}$$

where Ei$(\cdot)$ is the exponential integral function.
The clipping factor of the TWTA is given by

$$\xi = -\frac{A_{sat}^4}{\sigma^4}\left[\left(1+\frac{A_{sat}^2}{\sigma^2}\right)\exp\left(\frac{A_{sat}^2}{\sigma^2}\right)\mathrm{Ei}\left(-\frac{A_{sat}^2}{\sigma^2}\right)+1\right], \tag{5.9}$$

Then at the relay $R_{(m)}$, the RF amplified signal is converted to an optical one which is given by [51]

$$r_m = G(1+\eta\psi_m), \tag{5.10}$$

where η is the electrical-to-optical conversion coefficient.

5.2 In-Phase and quadrature-phase imbalance at the destination

In case of perfect IQ mismatch, the received signal at the destination can be expressed as follows

$$y_{2(m)} = I_m G\eta\psi_m + \nu_2, \tag{5.11}$$

where I_m is the optical irradiance between the relay $R_{(m)}$ and the destination D, η is the optical-to-electrical conversion coefficient, and$\nu_2 \backsim \mathcal{CN}\ (0,\ \sigma_0^2)$ is the AWGN of the optical channels.
Given that the destination is affected by IQ imbalance, the received signal is given by

$$\hat{y}_{2(m)} = \omega_1 y_{2(m)} + \omega_2 (y_{2(m)})^*, \tag{5.12}$$

where $(y_{2(m)})^*$ is called the mirror signal introduced by the IQ imbalance at D and the coefficients ω_1 and ω_2 are respectively given by

$$\omega_1 = \frac{1+\zeta e^{-j\theta}}{2}, \quad \omega_2 = \frac{1-\zeta e^{j\theta}}{2}, \tag{5.13}$$

where θ and ζ are respectively the phase and the magnitude imbalance. This impairment is modeled by the Image-Leakage Ratio (ILR), which is given by ILR $= \left|\frac{\omega_1}{\omega_2}\right|^2$.
For an ideal D, $\theta = 0, \zeta = 1, \omega_1 = 1, \omega_2 = 0$, and ILR $= 0$.

5.2 Channels Models

Since the RF channels are subject to correlated Rayleigh fading, the probability density function (PDF) and the cumulative distribution function (CDF) of the instantaneous RF

SNR $\gamma_{1(m)}$ are respectively given by [51]

$$f_{\gamma_{1(m)}}(x) = m\binom{N}{m}\sum_{n=0}^{m-1}\frac{(-1)^n}{[(N-m+n)(1-\rho)+1]\overline{\gamma}_1} \times \binom{m-1}{n}\exp\left(-\frac{(N-m+n+1)x}{((N-m+n)(1-\rho)+1)\overline{\gamma}_1}\right), \tag{5.14}$$

$$F_{\gamma_{1(m)}}(x) = 1 - m\binom{N}{m}\sum_{n=0}^{m-1}\frac{(-1)^n}{N-m+n+1} \times \binom{m-1}{n}\exp\left(-\frac{(N-m+n+1)x}{((N-m+n)(1-\rho)+1)\overline{\gamma}_1}\right), \tag{5.15}$$

Since the instantaneous SNR $\gamma_{2(m)}$ experiences Gamma-Gamma fading, its PDF is given by

$$f_{\gamma_{2(m)}}(x) = \frac{(\alpha\beta)^{\frac{\alpha+\beta}{2}}x^{\frac{\alpha+\beta}{4}-1}}{\Gamma(\alpha)\Gamma(\beta)\overline{\gamma}_2^{\frac{\alpha+\beta}{4}}}K_{\alpha-\beta}\left(2\sqrt{\alpha\beta\sqrt{\frac{x}{\overline{\gamma}_2}}}\right), \tag{5.16}$$

where $K_\nu(\cdot)$ is the ν-th order modified Bessel function of the second kind, α and β are respectively the small-scale and large-scale of the scattering process in the atmospheric environment. These parameters are given by

$$\alpha = \left(\exp\left[\frac{0.49\sigma_R^2}{(1+1.11\sigma_R^{\frac{12}{5}})^{\frac{7}{6}}}\right]-1\right)^{-1}, \quad \beta = \left(\exp\left[\frac{0.51\sigma_R^2}{(1+0.69\sigma_R^{\frac{12}{5}})^{\frac{5}{6}}}\right]-1\right)^{-1}, \tag{5.17}$$

where σ_R^2 is called Rytov variance which is a metric of the atmospheric turbulence intensity.

5.2 End-to-end signal-to-noise-plus-distortion ratio (SNDR)

The average SNR of the first hop is given by

$$\overline{\gamma}_1 = \frac{P_1|h_m|^2}{\sigma_0^2}, \tag{5.18}$$

While the average SNR $\overline{\gamma}_2$[1] of the second hop can be expressed as

$$\overline{\gamma}_2 = \frac{\mathbb{E}\left[I_m^2\right]}{\mathbb{E}\left[I_m\right]^2}\mu_2, \tag{5.19}$$

where μ_2 is the average electrical SNR given by

$$\mu_2 = \frac{\eta^2\mathbb{E}\left[I_m\right]^2}{\sigma_0^2}, \tag{5.20}$$

According to [44, Eq. (16)], the end-to-end SNDR is given by Eq. (5.25).

5.3 Performance Analysis

In this section, we present the analysis of the OP, the BER and the EC. We will show that the OP and BER are limited by irreducible floors and the EC is finite and saturated by a ceiling at the high SNRs values. The floors and the ceiling are certainly caused by the hardware impairments originating from the relays and the destination.

5.3 Outage Probability Analysis

The outage probability is defined as the probability that the end-to-end SNDR falls below a given outage threshold γ_{th}. It can be written as follows

$$P_{\text{out}}(\gamma_{\text{th}}) \triangleq \Pr[\gamma_{\text{e2e}} < \gamma_{\text{th}}], \tag{5.21}$$

where $\Pr(\cdot)$ is the probability notation. The analytical expression of the SNDR given by Eq. (5.25) should be placed in Eq. (5.21). After some algebraic manipulations, the OP can be expressed by Eq. (5.26). Note that the CDF $F_{\gamma_{1(m)}}$ is defined only if $1-\text{ILR}\gamma_{\text{th}} > 0$, otherwise it is equal to unity. The term κ is the ratio between the received SNR and the average transmitted SNDR at the relay which is given by

$$\kappa = 1 + \frac{\sigma_d^2}{\delta^2 G^2 \sigma_0^2}, \tag{5.22}$$

Note that the OP is equal to Eq. (24) for $\gamma_{\text{th}} < \frac{1}{\text{ILR}}$, otherwise, it is equal to a unity. Since the expression of the outage probability involves complex function such as the

[1]The average SNR $\overline{\gamma}_2$ is defined as $\overline{\gamma}_2 = \eta^2\mathbb{E}\left[I_m^2\right]/\sigma_0^2$, while the average electrical SNR μ_2 is given by $\mu_2 = \eta^2\mathbb{E}\left[I_m\right]^2/\sigma_0^2$. Therefore, the relation between the average SNR and the average electrical SNR is trivial given that $\frac{\mathbb{E}\left[I_m^2\right]}{\mathbb{E}[I_m]^2} = \sigma_{\text{si}}^2 + 1$, where σ_{si}^2 is the scintillation index [50].

Meijer-G function, we need to derive an asymptotic high SNR expression to unpack engineering insights about the system gain. Given that the outage performance saturates at high SNR by the outage floor caused by the hardware impairments, it is trivial to conclude that the diversity gain G_d is equal to zero. For an ideal hardware and after expanding the Meijer-G function at high SNR using [1, Eq. (07.34.06.0001.01)], it can be shown that the diversity gain is given by

$$G_d = \min\left(1,\ \frac{\alpha}{2},\ \frac{\beta}{2}\right), \tag{5.23}$$

5.3 Average Bit Error Rate

The BER can be expressed as follows

$$\overline{P_e} = \frac{q^p}{2\Gamma(p)} \int_0^\infty \gamma^{p-1} e^{-q\gamma}\ F_{\gamma_{\mathrm{e2e}}}(\gamma)\ d\gamma, \tag{5.24}$$

where $F_{\gamma_{\mathrm{e2e}}}(\cdot)$ is the CDF of γ_{e2e}, p and q are the parameters that indicate the modulation format, respectively. As we mentioned earlier, the mathematical terms related to the impairments render the integral calculus very complex. As a result, deriving a closed-form of the BER is not possible. In this case, a numerical integration is required. Note that a floor occurs at high SNRs values which prevents the BER from converging to zero. This floor will be shown graphically later in the section of numerical results.

$$\gamma_{e2e} = \frac{\gamma_{1(m)}\gamma_{2(m)}}{\mathrm{ILR}\gamma_{1(m)}\gamma_{2(m)} + (1+\mathrm{ILR})\kappa\gamma_{2(m)} + (1+\mathrm{ILR})(\mathbb{E}\left[\gamma_{1(m)}\right] + \kappa)}, \tag{5.25}$$

$$\begin{aligned} P_{\mathrm{out}}(\gamma_{\mathrm{th}}) =& 1 - \frac{2^{\alpha+\beta-2}}{\pi\Gamma(\alpha)\Gamma(\beta)} m \binom{N}{m} \sum_{n=0}^{m-1} \binom{m-1}{n} \frac{(-1)^n}{N-m+n+1} \\ &\times\ \exp\left(-\frac{(N-m+n+1)\kappa(1+\mathrm{ILR})\gamma_{\mathrm{th}}}{((N-m+n)(1-\rho)+1)(1-\mathrm{ILR}\gamma_{\mathrm{th}})\overline{\gamma}_1}\right) \\ &\times\ G_{0,5}^{5,0}\left(\begin{matrix}-\\ \frac{\alpha}{2}, \frac{\alpha+1}{2}, \frac{\beta}{2}, \frac{\beta+1}{2}, 0\end{matrix}\middle|\ \frac{(\alpha\beta)^2(\mathbb{E}\left[\gamma_{1(m)}\right] + \kappa)(N-m+n+1)\gamma_{\mathrm{th}}}{16((N-m+n)(1-\rho)+1)(1-\mathrm{ILR}\gamma_{\mathrm{th}})\overline{\gamma}_1\overline{\gamma}_2}\right), \end{aligned} \tag{5.26}$$

5.3 Ergodic Capacity

The ergodic capacity, expressed in bit/s/Hz, is defined as the maximum error-free data transferred by the channel of the system. It can be written as follows

$$\overline{C} \triangleq \frac{1}{2}\mathbb{E}\left[\log_2(1+\gamma_{\text{e2e}})\right], \tag{5.27}$$

The capacity can be calculated by deriving the PDF of the SNDR. However, an exact closed-form is very difficult due to the mathmatical terms related to the impairments. To evaluate the system capacity, we should refer to the numerical integration.
In spite of the difficulty to calculate an exact closed-form of the EC, we can derive a simpler expression by referring to the approximation given by [44, Eq. (27)]

$$\mathbb{E}\left[\log_2\left(1+\frac{\psi}{\varphi}\right)\right] \approx \log_2\left(1+\frac{\mathbb{E}\left[\psi\right]}{\mathbb{E}\left[\varphi\right]}\right), \tag{5.28}$$

For high SNR values, the SNDR converges to γ^* defined by

$$\lim_{\overline{\gamma}_1,\overline{\gamma}_2\to\infty} \gamma_{\text{e2e}} = \frac{1}{\frac{(1+\text{ILR})\xi}{\delta}-1} = \gamma^*, \tag{5.29}$$

Corollary 4. *Suppose that $\overline{\gamma}_1$ and $\overline{\gamma}_2$ converge to infinity and the electrical and optical channels are independent, the ergodic capacity converges to a capacity ceiling defined by*

$$\overline{C}^* = \frac{1}{2}\log_2(1+\gamma^*), \tag{5.30}$$

Proof. Since the SNDR converges to γ^* as the average SNRs of the first and second hop largely increase, the dominated convergence theorem allows moving the limit inside the logarithm function. □

If the relaying system is linear, i.e, the system is only impaired by IQ imbalance, the SNDR and the average capacity are saturated at the high SNR regime as follows

$$\gamma^* = \frac{1}{\text{ILR}}, \quad \overline{C}^* = \frac{1}{2}\log_2\left(1+\frac{1}{\text{ILR}}\right), \tag{5.31}$$

To characterize the EC, it is possible to derive the expression of the upper bound stated by the following theorem.

Theorem 3. *For asymmetric (Rayleigh/Gamma-Gamma) fading channels, the ergodic*

capacity $\overline{C}$ *for non-ideal hardware is upper bounded by*

$$\overline{C} \leq \frac{1}{2}\log_2\left(1+\frac{\mathcal{J}}{ILR\ \mathcal{J}+1}\right), \tag{5.32}$$

where $\mathcal{J}$ is given by

$$\mathcal{J} = \mathbb{E}\left[\frac{\gamma_{1(m)}\gamma_{2(m)}}{\mathrm{ILR}\gamma_{2(m)}+\tau}\right], \tag{5.33}$$

where $\tau = (1+\mathrm{ILR})\kappa\gamma_{2(m)} + (1+\mathrm{ILR})(\mathbb{E}\left[\gamma_{1(m)}\right]+\kappa)$.
After some mathematical manipulations, $\mathcal{J}$ is given by

$$\begin{aligned}\mathcal{J} = &\frac{m\binom{N}{m}(\alpha\beta)^{\frac{\alpha+\beta}{2}}\left(\frac{\mathbb{E}\left[\gamma_{1(m)}\right]+\kappa}{\kappa}\right)^{\frac{\alpha+\beta}{4}}}{2\pi(1+\mathrm{ILR})\kappa\Gamma(\alpha)\Gamma(\beta)\overline{\gamma}_2^{\frac{\alpha+\beta}{4}}}\\ &\times\sum_{n=0}^{m-1}\binom{m-1}{n}\frac{(-1)^m((N-m+n)(1-\rho)+1)\overline{\gamma}_1}{(N-m+n+1)^2}\\ &\times\ G_{1,5}^{5,1}\left[\frac{(\alpha\beta)^2(\mathbb{E}\left[\gamma_{1(m)}\right]+\kappa)}{16\kappa\overline{\gamma}_2}\ \middle|\ \begin{matrix}\kappa_0\\ \kappa_1\end{matrix}\right],\end{aligned} \tag{5.34}$$

where κ_0, κ_1 are given by

$$\begin{aligned}\kappa_0 &= -\frac{\alpha+\beta}{4},\\ \kappa_1 &= \left[\frac{\alpha-\beta}{4}, \frac{\alpha-\beta+2}{4}, \frac{\beta-\alpha}{4}, \frac{\beta-\alpha+2}{4}, -\frac{\alpha+\beta}{4}\right],\end{aligned} \tag{5.35}$$

5.4 Numerical results

This section presents analytical and numerical [1] results of the OP, BER and EC obtained from the mathematical expressions mentioned in the previous section.
Since the RF channel experiences correlated Rayleigh fading, it can be generated using the algorithm in [81]. The atmospheric turbulence follows Gamma-Gamma fading, which can be generated by using the formula, $I = I_X I_Y$, where I_X and I_Y are independent random variables, which follow Gamma distribution.

[1]For all cases, 10^9 realizations of the random variables were generated to perform the Monte Carlo simulation in MATLAB.

Table 5.1: Simulation Parameters

Parameters	Values
Outage threshold γ_{th} [dB]	10
Time correlation ρ	0.9
Number of relays N	7
Rank of selected relay k	7
Rytov variance σ_R^2	0.16
Modulation	BPSK

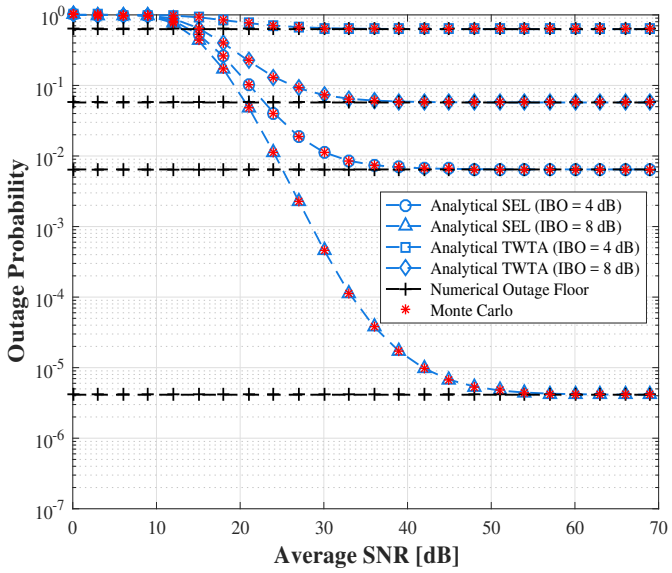

Figure 5.2: Outage probability versus the average SNR for different values of IBO

The dependence of the OP with respect to the average SNR for the case of SEL and TWTA NLPA models are shown in Fig. 5.2. For ILR = -15 dB, this value can be obtained by 1 dB of amplitude imbalance and 15° of phase imbalance. We observe that when the relays's system are impaired by SEL, the OP is lower compared to the case of the TWTA impairment. For example, for SNR = 60 dB and IBO = 8 dB, the OPs under the effect of SEL and TWTA are respectively equal to 4 10^{-6} and 6 10^{-2}. Moreover, we observe that the system performs better as long as the IBO value increases. As the average SNR per hop increases, the outage floors appear for both cases SEL and TWTA but the system performs better under the effect of SEL than TWTA. Therefore the TWTA has more severe impact on the system performance than the SEL. In addition, our system apprears to be more resilient to the hardware imperfections compared to the system assumed in [44]. In fact, for (IBO, ILR, γ_{th}, SNR) equal to (8, -15, 10, 45)[dB] and under the joint

effect of SEL and IQ imbalance, the OP of our system is equal to 7 10^{-6}. However, the OP of the system suggested by Maletic *et al.* in [44] is equal to 6 10^{-3} shown by Fig. 4 of this reference. The factors that achieve this significant enhancement of our system over the classical RF system [44] are essentially the FSO technology and the diversity of the RF part characterized by the multiple relays.

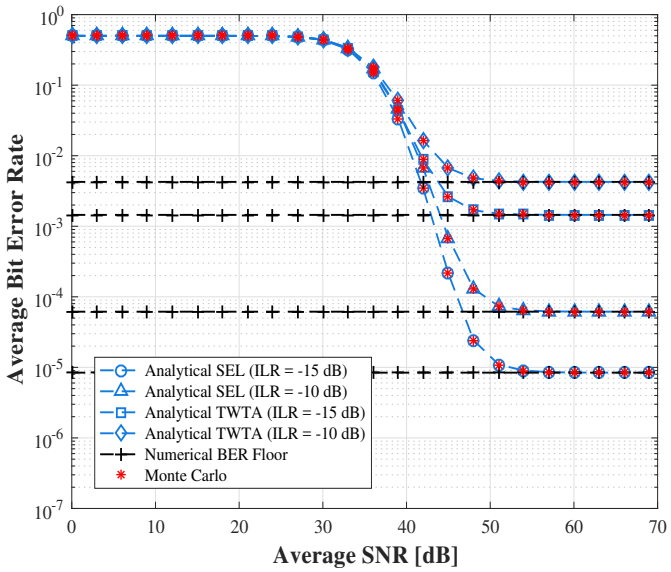

Figure 5.3: Average Bit Error Rate versus the average SNR for different values of ILR

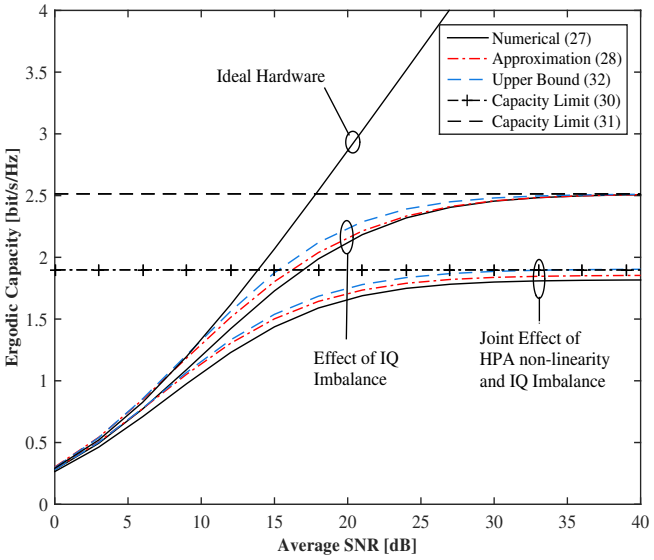

Figure 5.4: Exact, approximate and upper bound of the ergodic capacity versus the average SNR

Fig. 5.3 shows the variations of the BER against the average SNR per hop for different values of the ILR. We clearly observe that the BER is limited by an irreducible floor caused by the joint effect of HPA non-linearity and IQ imbalance. As the ILR value increases, the destination is more susceptible to impairments and hence the BER performance deteriorates further. As a comparison with the work done by [44], for ILR = -15 dB, IBO = 5 dB, BPSK modulation and assuming the TWTA impairment, the mixed RF/FSO system outperforms the classical RF suggested by [44]. In fact, for an average SNR equal to 45 dB and ILR = -15 dB, the BER performance of our system is equal to 7 10^{-3}, however, the BER of the RF system is approximately equal to 1.9 10^{-2} shown by Fig. 9 of [44]. Regarding the impact of the SEL impairments, our system again performs better and proves its high resiliency against the imperfections than the RF system. In fact, for the same previous configuration of ILR, IBO and modulation format, the BER is equal to 2 10^{-4} while the BER for RF system is equal to 1.3 10^{-3}. Note that even our system is impaired by TWTA, the most severe impairments, there is no significant difference between the BER of mixed RF/FSO and the BER of the full RF system under the effect of the SEL, the less severe impairments. We conlude that our mixed RF/FSO system is more robust to the impairments than the previous RF system due to the advantages brought by the FSO technique.

The variations of the EC versus the average SNR hop assuming linear and non-linear relaying (SEL model) with an impaired destination are shown in Fig. 5.4. As expected, the system operating with linear relaying outperforms the system performance in the case of non-linear relaying. As the impairments at the relays disappear, the saturation level of the capacity increases but the capacity is still limited by a ceiling superior than the ceiling of the capacity under the joint effect of the NLPA relaying and IQI. The significant difference between the two ECs at high SNR shows clearly the deleterious effect of the high power amplifier non-linearities on the system performance.

Note that the capacity ceiling is independent on the system parameters and it depends only on the impairments parameters (ILR, IBO), that is why the ceiling level is still the same for the ceiling suggested by [44]. The main advantage of our system compared with the RF system, is that even though the two systems are limited by the same ceiling level, the mixed RF/FSO system capacity increases faster than the capacity of the RF system.

5.5 Conclusion

In this work, we provided the analysis of various models of impairments and their effects on the system performance. We introduced the SEL and TWTA as HPA non-

linearities affecting the relays and we assume that D is impaired by IQ imbalance. We studied the effects of these hardware imperfections on the system performance in terms of OP, BER and EC. We concluded that the system performs better as the IBO increases and the ILR decreases. Moreover, it turned out that the TWTA has more severe impact on the system performance than the SEL model. Furthermore, even though the performance deteriorates under the effects of the imperfections, we noted that the introduction of the FSO technique makes the mixed RF/FSO system more resilient to the hardware impairments than the previous RF relaying system. As future directions, unlike the previous work that developed various techniques for the impairments compensation, we intend to develop an algorithm/technique that must remove completely, or at least to a large extent, the residual impairments which still cause the performance deteriorations.

Chapter 6: Hybrid Rayleigh and Double-Weibull Over Impaired RF/FSO System with Outdated CSI

"Hybrid Rayleigh and Double-Weibull over impaired RF/FSO system with outdated CSI," *2017 IEEE International Conference on Communications (ICC)*, Paris, 2017, pp. 1-6.

6.1 Introduction

In this chapter, we present a global framework of a dual-hop RF/FSO system with multiple relays operating in the mode of amplify-and-forward (AF) with fixed gain. Partial relay selection (PRS) protocol with outdated channel state information (CSI) is assumed since the channels of the first hop are time-varying. The optical irradiance of the second hop are subject to the Double-Weibull model while the RF channels of the first hop experience the Rayleigh fading. The signal reception is achieved either by heterodyne or intensity modulation and direct detection (IM/DD). In addition, we introduce an aggregate model of hardware impairments to the source (S) and the relays since they are not perfect nodes. In order to quantify the impairment impact on the system, we derive closed-form, approximate, upper bound and high signal-to-noise ratio (SNR) asymptotic of the outage probability (OP) and the ergodic capacity (EC). Finally, analytical and numerical results are in agreement using Monte Carlo simulation.

6.2 System and Channels Models

6.2 System Model

The system consists of S, D and N parallel relays wirelessly linked to S and D. In order to pick a relay of rank m, PRS with outdated CSI based on the partial knowledge of the CSIs channels of the first hop is assumed. This protocol states that for each transmission, S receives the CSIs ($\gamma_{1(l)}$ for l = 1,... N) of the RF channels from the relays via local feedback. Once the CSIs are received, S sorts the values of the CSIs in an increasing order of amplitude as: $\gamma_{1(1)} \leq \gamma_{1(2)} \leq \ldots \leq \gamma_{1(N)}$. Based on this sorting, S selects the relay with the highest RF SNR which is clearly the relay of last rank N. Given that the relays operate in the half-duplex mode, the best relay of rank N may not be

always available to forward the signal. In this case, S will select the next best relay and so on so forth. In addition, the relay with the last rank is not always the best one even after the selection. In fact, the channels are time-varying and the feedback propagation from the relays to S are very slow. In this case, the CSIs are susceptible to significant variations and so their values before and after the selection are not the same. It turned out that the estimation of the channels is not perfect and hence, the relay selection is achieved based on the outdated CSIs. To model this imperfect channel estimation, we associate a time correlation coefficient ρ between the outdated and the updated CSIs. Thereby, the best relay is not necessarily the one of the last rank since the selection is based on the outdated CSI.

Assume that S selects the relay of rank m, the received signal at the relay is given by

$$y_{1(m)} = h_m(s + \eta_1) + \nu_1, \tag{6.1}$$

where h_m is the RF channel fading, $s \in \mathbb{C}$ is the information signal, $\nu_1 \backsim \mathcal{CN}\ (0,\ \sigma_0^2)$ is the AWGN of the RF channel, $\eta_1 \backsim \mathcal{CN}\ (0,\ \kappa_1^2 P_1)$ is the distortion noise at S, κ_1 is the impairment level at S and P_1 is the average transmitted power from S.

Once the signal is completely received by the relay R_m, it is amplified by a fixed gain G that depends on the average electrical SNR of the RF channels. This gain can be expressed as follows

$$G^2 \triangleq \frac{P_2}{P_1 \mathbb{E}\left[|h_m|^2\right](1 + \kappa_1^2) + \sigma_0^2}, \tag{6.2}$$

where P_2 is the average transmitted power from the relay to D and $\mathbb{E}\left[\cdot\right]$ is the expectation operator.

The amplified signal at the output of the relay is given by

$$y_{opt(m)} = G(1 + \eta_e) y_{1(m)}, \tag{6.3}$$

where η_e is the electrical-to-optical conversion coefficient.

Finally the received signal at the destination can be expressed as follows

$$y_{2(m)} = (\eta_o I_m)^{\frac{r}{2}} [G(1 + \eta_e)(h_m(s + \eta_1) + \nu_1) + \eta_2] + \nu_2, \tag{6.4}$$

where η_o is the optical-to-electrical conversion coefficient, I_m is the optical irradiance between R_m and D, $\eta_2 \backsim \mathcal{CN}\ (0,\ \kappa_2^2 P_2)$ is the distortion noise at the relay R_m, κ_2 is the impairment level at R_m, $\nu_2 \backsim \mathcal{CN}\ (0,\ \sigma_0^2)$ is the AWGN of the optical channel and $r = 1$,

2 stands for heterodyne and IM/DD detections respectively.

6.2 End-to-End Signal-to-Noise plus Distortion Ratio (SNDR)

The SNDR depends on both the electrical $\gamma_{1(m)}$ and optical $\gamma_{2(m)}$ SNRs of the two hops which can be defined by

$$\gamma_{1(m)} = \frac{|h_m|^2 P_1}{\sigma_0^2} = |h_m|^2 \overline{\gamma}_1, \tag{6.5}$$

where $\overline{\gamma}_1 = \frac{P_1}{\sigma_0^2}$ is the average SNR of the first hop.

$$\gamma_{2(m)} = \frac{|I_m|^r \eta_o^r P_2}{\sigma_0^2} = |I_m|^r \overline{\gamma}_r, \tag{6.6}$$

where $\overline{\gamma}_r = \frac{\eta_o^r P_2}{\sigma_0^2}$ is the average electrical SNR of the second hop. Finally, the SNDR can be expressed as follows

$$\gamma_{\text{ni}} = \frac{|h_m|^2 |I_m|^r}{\delta |h_m|^2 |I_m|^r + |I_m|^r (1+\kappa_2^2)\frac{\sigma_0^2}{P_1} + \frac{\sigma_0^2}{P_1 G^2}}, \tag{6.7}$$

After some algebraic manipulations, the SNDR can be expressed as follows

$$\gamma_{\text{ni}} = \frac{\gamma_{1(m)}\gamma_{2(m)}}{\delta\gamma_{1(m)}\gamma_{2(m)} + (1+\kappa_2^2)\gamma_{2(m)} + C}, \tag{6.8}$$

where $\delta \triangleq \kappa_1^2 + \kappa_2^2 + \kappa_1^2\kappa_2^2$ and $C = \mathbb{E}\left[\gamma_{1(m)}\right](1+\kappa_1^2) + 1$.
Note that for ideal case, the end-to-end SNR is given by

$$\gamma_{\text{id}} = \frac{\gamma_{1(m)}\gamma_{2(m)}}{\gamma_{2(m)} + \mathbb{E}\left[\gamma_{1(m)}\right] + 1}, \tag{6.9}$$

6.2 Channels Model

6.2.3.1 Statistics of the electrical channels

We model the relation between the outdated and updated CSIs as follows

$$h_{1(m)} = \sqrt{\rho}\tilde{h}_{1(m)} + \sqrt{1-\rho}w_{1(m)}, \tag{6.10}$$

where $h_{1(m)}$ and $\tilde{h}_{1(m)}$ are the updated and outdated CSIs respectively and $w_{1(m)}$ follows the circularly symmetric complex gaussian distribution with the same variance of the channel gain $\tilde{h}_{1(m)}$.
The coefficient ρ is given by the Jakes' autocorrelation model [31] as follows

$$\rho = J_0(2\pi f_d T_d), \tag{6.11}$$

where $J_0(\cdot)$ is the zeroth order Bessel function of the first kind [27, Eq. (8.411)], T_d is the time delay between the current CSI and the delayed version and f_d is the maximum Doppler frequency of the channels.
Since the RF channels experience the Rayleigh fading, the instantaneous electrical SNR $\gamma_{1(m)}$ follows the correlated exponential distribution. The PDF can be expressed as follows

$$\begin{aligned} f_{\gamma_{1(m)}}(x) =& \sum_{n=0}^{m-1} \binom{m-1}{n} \frac{(-1)^n}{[(N-m+n)(1-\rho)+1]\overline{\gamma}_1} \\ & \times \; m\binom{N}{m} \exp\left(-\frac{(N-m+n+1)x}{[(N-m+n)(1-\rho)+1]\overline{\gamma}_1}\right), \end{aligned} \tag{6.12}$$

After some mathematical manipulations, the CDF of $\gamma_{1(m)}$ can be expressed as follows

$$\begin{aligned} F_{\gamma_{1(m)}}(x) =& 1 - m\binom{N}{m} \sum_{n=0}^{m-1} \binom{m-1}{n} \frac{(-1)^n}{N-m+n+1} \\ & \times \; \exp\left(-\frac{(N-m+n+1)x}{[(N-m+n)(1-\rho)+1]\overline{\gamma}_1}\right), \end{aligned} \tag{6.13}$$

The constant C mentioned earlier depends on the expression of $\mathbb{E}\left[\gamma_{1(m)}\right]$, which can be obtained as

$$\mathbb{E}\left[\gamma_{1(m)}\right] = m\binom{N}{m} \sum_{n=0}^{m-1} \binom{m-1}{n} (-1)^n \frac{[(N-m+n)(1-\rho)+1]\overline{\gamma}_1}{(N-m+n+1)^2}, \tag{6.14}$$

6.2.3.2 Statistics of the optical channels

The PDF of the random variable X that follows the Weibull distribution can be written as follows

$$f_X(x) = \frac{\beta_1 x^{\beta_1 - 1}}{\Omega_1} \; \exp\left(-\frac{x^{\beta_1}}{\Omega_1}\right), \tag{6.15}$$

where $\Omega_1 > 0$ is the average fading power of the optical fading and $\beta_1 > 0$ describes the strength of the irradiance fluctuations.

According to the scintillation theory, it is possible to model the irradiance as the product of two independent random variables X, Y following the Weibull distribution. Since the irradiance is modelled by the Double-Weibull, the PDF of $I = XY$ can be obtained by [18, Eq. (5)]

$$f_I(I) = \frac{\beta_2 k\sqrt{kl}}{(2\pi)^{\frac{k+l}{2}-1} I} G_{k+l,0}^{0,k+l}\left(\begin{matrix} \Lambda_0 \\ - \end{matrix} \middle| \left(\frac{\Omega_2 k}{I^{\beta_2}}\right)^k (\Omega_1 l)^l \right), \tag{6.16}$$

where $\Lambda_0 = [\Delta(l;0), \Delta(k;0)]$, $G_{p,q}^{m,n}(\cdot)$ is the Meijer's G-function, $\Delta(j;x) \triangleq \frac{x}{j}, \ldots, \frac{x+j-1}{j}$ and l, k are positive integers satisfying

$$\frac{l}{k} = \frac{\beta_2}{\beta_1}, \tag{6.17}$$

where $\beta_1, \beta_2 > 0$ are the parameters describing the strength of the optical irradiance from large and small scale turbulent eddies. In addition, $\Omega_1, \Omega_2 > 0$ are the average power of the channels.

The CDF of the optical irradiance can be expressed as follows

$$F_I(I) = \frac{\sqrt{kl}}{(2\pi)^{\frac{k+l}{2}-1}} G_{1,k+l+1}^{k+l,1}\left(\begin{matrix} 1 \\ \Lambda_1, 0 \end{matrix} \middle| \frac{I^{\beta_1 l}}{(\Omega_1 l)^l (\Omega_2 k)^k} \right), \tag{6.18}$$

where $\Lambda_1 = [\Delta(l;1), \Delta(k;1)]$.

The normalized variances σ_i^2 and the average fading powers Ω_i of the large and small scale atmospheric turbulence are given by

$$\sigma_i^2 = \frac{\Gamma(1+\frac{2}{\lambda_i})}{\Gamma(1+\frac{2}{\lambda_i})^2} - 1, \tag{6.19}$$

$$\Omega_i = \left(\frac{1}{\Gamma(1+\frac{1}{\beta_i})} \right)^{\beta_i}, \tag{6.20}$$

where $i = 1, 2$ and $\sigma_X^2 = \sigma_1^2, \sigma_Y^2 = \sigma_2^2$. λ_i can be determined by $\lambda_i = \sigma_i^{-1.0852}$.

Now, we substitute the analytical expression of the optical channel I_m by $\left(\frac{\gamma_{2(m)}}{\bar{\gamma}_r}\right)^{\frac{1}{r}}$ in Eq. (6.18) and after some mathematical manipulations, the PDF and the CDF of the

instantaneous SNR $\gamma_{2(m)}$ can be respectively written as follows

$$f_{\gamma_{2(m)}}(\gamma_{2(m)}) = \frac{\beta_2 k\sqrt{kl}}{r\gamma_{2(m)}(2\pi)^{\frac{k+l}{2}-1}} G_{k+l,0}^{0,k+l}\left(\begin{matrix} \Lambda_0 \\ - \end{matrix} \middle| (\Omega_1 l)^l (\Omega_2 k)^k \left(\frac{\overline{\gamma}_r}{\gamma_{2(m)}}\right)^{\frac{\beta_2 k}{r}} \right), \tag{6.21}$$

$$F_{\gamma_{2(m)}}(\gamma_{2(m)}) = \frac{\sqrt{kl}}{(2\pi)^{\frac{k+l}{2}-1}} G_{1,k+l+1}^{k+l,1}\left(\begin{matrix} 1 \\ \Lambda_1, 0 \end{matrix} \middle| \frac{1}{(\Omega_1 l)^l (\Omega_2 k)^k} \left(\frac{\gamma_{2(m)}}{\overline{\gamma}_r}\right)^{\frac{\beta_1 l}{r}} \right), \tag{6.22}$$

The n-th moment of the random variable X is given by

$$\mathbb{E}\left[X^n\right] = \Omega_1^{\frac{n}{\beta_1}} \Gamma\left(1 + \frac{n}{\beta_1}\right), \tag{6.23}$$

After some mathematical manipulations, the n-th moment of the instantaneous SNR $\gamma_{2(m)}$ can be written as follows

$$\mathbb{E}\left[\gamma_{2(m)}^n\right] = \overline{\gamma}_r^n \Omega_1^{\frac{nr}{\beta_1}} \Omega_2^{\frac{nr}{\beta_2}} \Gamma\left(1 + \frac{nr}{\beta_1}\right) \Gamma\left(1 + \frac{nr}{\beta_2}\right), \tag{6.24}$$

6.3 Performance Analysis

In this section we present the analysis of the system performance in terms of the OP and EC. We will derive the expressions of the OP and the upperbound of the EC in terms of the Meijer's G-function. We will also evaluate the system performance in particular at the high SNR regime and we will show that the EC and the SNDR are saturated by the ceilings created by the hardware impairments.

6.3 Outage Probability Analysis

The outage probability is defined as the probability that the end-to-end SNDR falls below an outage threshold γ_{th}. It can be written as follows

$$P_{\text{out}}(\gamma_{\text{th}}) \triangleq \Pr\{\gamma_{\text{ni}} < \gamma_{\text{th}}\}, \tag{6.25}$$

where $\Pr(\cdot)$ is the probability notation. Then, we substitute the expression of the SNDR in Eq. (6.25) and after applying some mathematical manipulations, the OP can be written as follows

$$P_{\text{out}}(\gamma_{\text{th}}) = \int_0^\infty F_{\gamma_{1(m)}}\left(\frac{(1+\kappa_2^2)\gamma_{\text{th}}}{1-\delta\gamma_{\text{th}}} + \frac{C\gamma_{\text{th}}}{(1-\delta\gamma_{\text{th}})\gamma_{2(m)}}\right) f_{\gamma_{2(m)}}(\gamma_{2(m)})\, d\gamma_{2(m)}, \tag{6.26}$$

Note that the CDF $F_{\gamma_{1(m)}}$ is defined only if $1-\delta\gamma_{\text{th}} > 0$, otherwise it is equal to a unity. Using the identity given by [53, Eq. (2.24.3.1)] and after some mathematical manipulations, the OP can be derived as follows

$$\begin{aligned} P_{\text{out}}(\gamma_{\text{th}}) =& 1 - \binom{N}{m} \frac{mk\sqrt{\beta_2 l} r^{\mu-1}}{(2\pi)^{\frac{\beta_2 l + r(k+l)-3}{2}}} \sum_{n=0}^{m-1} \frac{(-1)^n}{N-m+n+1} \\ &\times \exp\left(-\frac{(N-m+n+1)(1+\kappa_2^2)\gamma_{\text{th}}}{[(N-m+n)(1-\rho)+1](1-\delta\gamma_{\text{th}})\overline{\gamma}_1}\right) \\ &\times \binom{m-1}{n} G_{r(k+l)+\beta_2 k, 0}^{0, r(k+l)+\beta_2 k}\left(\begin{matrix}\Lambda_2 \\ - \end{matrix}\middle| \zeta\right), \end{aligned} \tag{6.27}$$

where μ, Λ_2, ζ, τ, and ξ are respectively given by

$$\mu = -\sum_{j=0}^{k+l} \Lambda_0(j) + \frac{k+l}{2} + 1, \tag{6.28}$$

$$\Lambda_2 = [\Delta(r; \Lambda_0), \Delta(\beta_2 k; 1)], \tag{6.29}$$

$$\zeta = \left((\Omega_1 l)^l (\Omega_2 k)^k r^{k+l}\right)^r \left(\frac{\beta_2 k \overline{\gamma}_1 \overline{\gamma}_r}{\tau\xi}\right)^{\beta_2 k}, \tag{6.30}$$

$$\tau = \frac{C\gamma_{\text{th}}}{1-\delta\gamma_{\text{th}}}, \tag{6.31}$$

$$\xi = \frac{N-m+n+1}{(N-m+n)(1-\rho)+1} \tag{6.32}$$

The OP is equal to Eq. (6.27) for $\gamma_{\text{th}} < \frac{1}{\delta}$, otherwise, it is equal to a unity.

6.3 Ergodic Capacity Analysis

The ergodic capacity, expressed in bps/Hz, is defined as the maximum error-free data rate transferred by the system channel. It can be written as follows

$$\overline{C} = \mathbb{E}\left[\log_2(1 + c\gamma_{\text{ni}})\right], \tag{6.33}$$

where $c = 1$ indicates the heterodyne detection and $c = \frac{e}{2\pi}$ for IM/DD. The ergodic capacity can be derived by evaluating the PDF of the SNDR. However, an exact analytical expression is not solvable. To evaluate the ergodic capacity, a numerical evaluation is required.

It is possible to derive a simpler form of an upper bound which is given by the following theorem.

Theorem 4. *For Asymmetric (Rayleigh/Double-Weibull) channels, the system capacity* $\overline{C}$ *with AF relaying protocol and hardware impairments is upper bounded by*

$$\overline{C} \leq \log_2\left(1 + c\frac{\mathcal{J}}{\mathcal{J}\delta + 1}\right), \tag{6.34}$$

where $\mathcal{J}$ is given by

$$\mathcal{J} = \frac{\beta_2 k\sqrt{kl}r^{\mu-1}\mathbb{E}\left[\gamma_{1(m)}\right]}{(2\pi)^{\beta_2 k + r\frac{k+l}{2}-2}(1+\kappa_2^2)} G_{r(k+l)+\beta_2 k,\beta_2 k}^{\beta_2 k, r(k+l)+\beta_2 k}\left(\begin{matrix}\Lambda_2 \\ \Delta(\beta_2 k;1)\end{matrix}\middle| \varrho\right), \tag{6.35}$$

where ϱ is given by

$$\varrho = ((\Omega_1 l)^l(\Omega_2 k)^k r^{k+l})^r \left(\frac{(1+\kappa_2^2)\overline{\gamma}_r}{C}\right)^{\beta_2 k}, \tag{6.36}$$

Although deriving a closed-form of the ergodic capacity is very complex, we can find an approximate simpler form by applying the approximation given by [16, Eq. (35)]

$$\mathbb{E}\left[\log_2\left(1 + \frac{\psi}{\varphi}\right)\right] \approx \log_2\left(1 + \frac{\mathbb{E}\left[\psi\right]}{\mathbb{E}\left[\varphi\right]}\right), \tag{6.37}$$

For high SNR regime, the behavior of the SNDR is expressed as

$$\lim_{\overline{\gamma}_1,\overline{\gamma}_r\to\infty} \gamma_{\text{ni}} = \frac{1}{\delta}, \tag{6.38}$$

We observe that the SNDR converges to a ceiling $\gamma^* = \frac{1}{\delta}$.

Corollary 5. *For larger values of* $\overline{\gamma}_1$ *and* $\overline{\gamma}_r$ *and mutually independent RF and optical fadings, the average channel capacity converges to a ceiling defined by* $C^* = \log_2(1 + c\gamma^*)$.

Proof. Applying the dominated convergence theorem and given that the SNDR is limited by γ^*, the limit can be moved inside the logarithm function as shown below

$$\lim_{\overline{\gamma}_1,\overline{\gamma}_r\to\infty} \log_2(1 + c\gamma_{\text{ni}}) = \log_2(1 + c\lim_{\overline{\gamma}_1,\overline{\gamma}_r\to\infty} \gamma_{\text{ni}}) = \log_2(1 + c\gamma^*), \tag{6.39}$$

□

6.4 Numerical Results

This section provides numerical results obtained by using the mathematical formulations of the previous section.

The electrical channel is subject to the correlated Rayleigh fading which can be generated using the algorithm in [81]. The atmospheric turbulence is modeled by the Double-Weibull fading, which can be generated by using the formula, $I = XY$, where X and Y are mutually independent Weibull random variables.

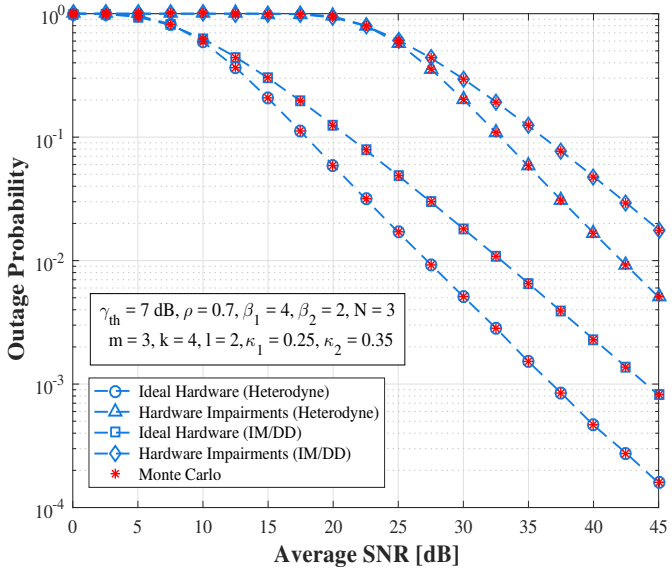

Figure 6.1: Outage probability versus the average SNR for ideal and non-ideal hardware under IM/DD and heterodyne detection

Fig. 6-1 shows the dependence of the OP with respect to the average SNR. We observe that the heterodyne detection outperforms the IM/DD method for our system. Moreover, the impact of the hardware impairments are clearly observed compared to the ideal hardware case. For low SNR, the impairments have small impact on the performance and so it can be neglected as we mentioned earlier. As the average SNR increases, the impact of the impairments becomes more severe enough to be of high importance and must not be neglected.

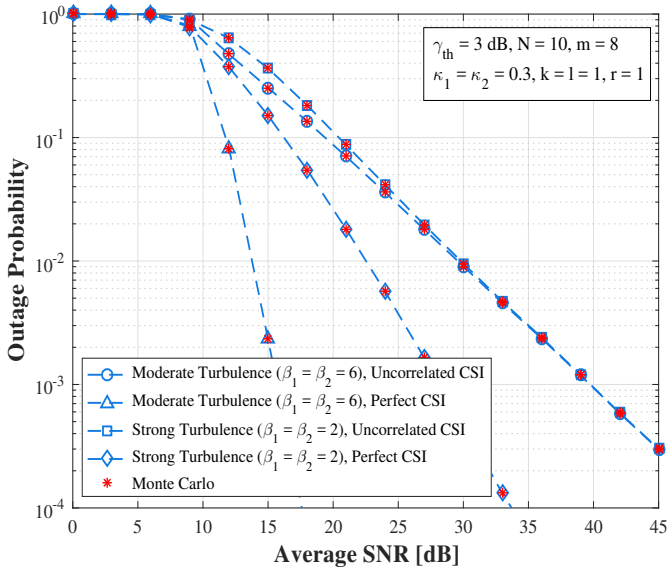

Figure 6.2: Outage probability versus the average SNR for different values of the correlation coefficient ρ under moderate and strong turbulences

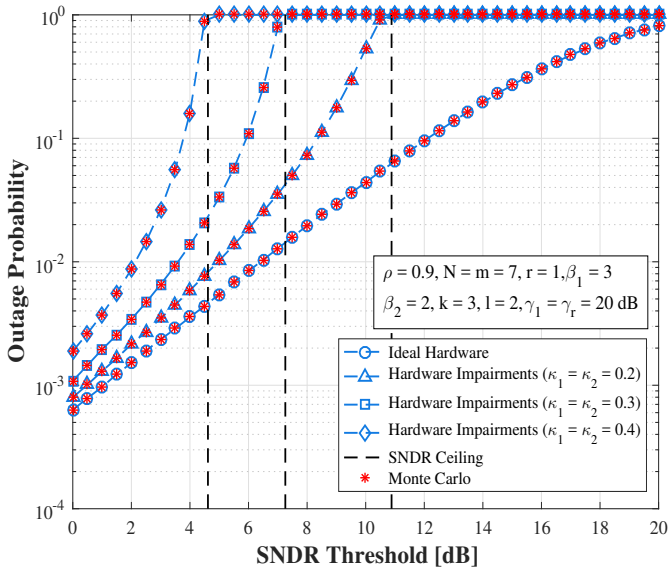

Figure 6.3: Outage probability versus the SNDR threshold for ideal and non-ideal hardware

The dependence of the OP for AF relaying protocol on the average SNR is given by Fig. 6-2. As expected, the outage performance is better under the moderate turbulence condition and suddenly deteriorates as the turbulence becomes strong and severe. This result is clearly observed, especially for the case of full correlation of CSIs ($\rho = 1$). It turns out that

the system substantially depends on the state of the optical channels. As the correlation ρ between the CSI used for relay selection and the CSI used for transmission increases, i.e., the two CSIs become more and more correlated, the selection of the best relay is certainly achieved ($m = N$). In this case, the system works under the perfect condition especially under moderate turbulence condition. As the time correlation decreases, the selection of the best relay is no longer achieved and so the system certainly operates with a worse relay. In addition, we note that the correlation has a severe impact on the performance. In fact, for the case of completely outdated CSI ($\rho = 0$), we observe a substantial degradation of the performance for moderate and strong turbulence conditions and the curves most likely look the same. In other words, considering either moderate or strong turbulence conditions has no remakable impact on the performance in case of uncorrelated CSIs. This observation proves that the system depends to a large extent on the correlation between the CSIs rather than the state of the optical channels. This is nothing but to say that is important to achieve perfect CSI channels estimation than to focus on the atmospheric turbulence conditions.

Fig. 6-3 presents the variations of the outage probability versus the outage threshold γ_{th} [dB] for different values of the level of impairments (κ_1, κ_2). For lower values of γ_{th}, the performance under the hardware impairments slightly deviates from the case of an ideal system. However, as the outage threshold increases, the outage performance experiences a rapid convergence to unity and this convergence becomes more faster as the impairment level grows up. In fact, we observe that for the given values of the impairment level 0.2, 0.3 and 0.4, the system saturates at the following SNDR thresholds 4.6, 7.5 and 10.8 dB respectively, while the ideal system saturates very slowly for an outage threshold greater than 20 dB.

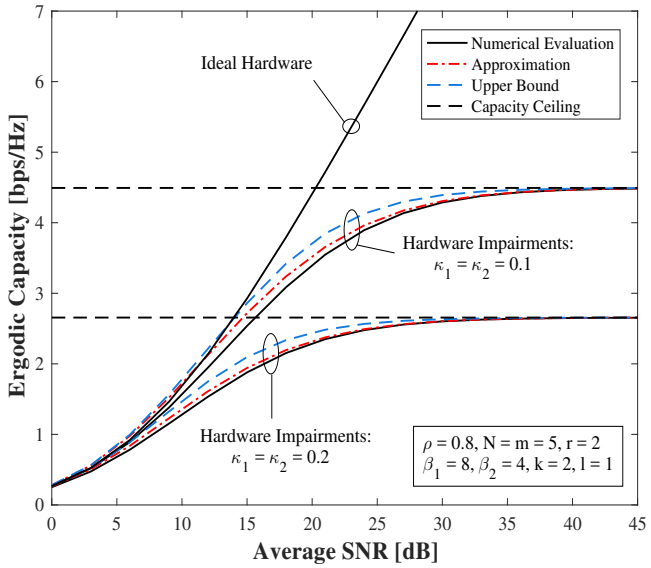

Figure 6.4: Ergodic capacity versus the SNDR threshold for ideal and non-ideal hardware

The variations of the EC versus the average SNR is given by Fig. 6-4. For the ideal hardware case, as the SNR increases, the EC grows indefinitely. Regarding the non-ideal hardware, the impairments have small impact on the system for low SNRs, but it becomes very deleterious at high SNRs. In fact, the EC converges to a capacity ceiling C^*, as shown by corollary 1, which is inversely proportional to the level of the impairments, i.e, as the impairment level increases, the ceiling decreases. The approximate form and the upper bound of the EC are also shown in Fig. 6-4. Although they deviate from the exact EC at low SNRs, they are asymptotically in agreement and converge to the capacity ceiling C^*.

6.5 Conclusion

In this work, we investigate the performance analysis of a mixed RF/FSO system with multiple relays employing the amplify-and-forward relaying scheme. Partial relay selection with outdated CSI is adopted to pick one relay for forwarding the signal. Because of its accuracy compared to the Log-Normal and Double-Gamma distributions, Double-Weibull fading is used as a model of the optical irradiance. We conclude that for moderate turbulence, both the correlation coefficient and the detection method have significant impacts on the system. We observe that the system performs better under the heterodyne mode than IM/DD. We also note that as the time correlation increases, the channel estimation enhances and the performance improves substantially. However, as the correlation becomes very low, the turbulences have no longer impact on the perfor-

mance and the system depends only on the CSIs correlation. Furthermore, we introduce a general model of hardware impairments to the source and the relays. We conclude that for lower values of the average SNR, the hardware impairments have no observable impacts on the system. However, as the average SNR grows largely, the impairments impact becomes noticeable by a quick saturation of the outage probability and the ergodic capacity. Finally, as an extention of this work, we intend to study the effects of some specified hardware impairments such as the HPA non-linearities and the IQ imbalance on the mixed RF/FSO system and to quantify the impacts of the different parameters of each hardware impairments on some performance metrics of the system.

Chapter 7: Mixed RF/FSO Cooperative Relaying Systems with Co-Channel Interference

"Mixed RF/FSO Cooperative Relaying Systems with Co-Channel Interference," in *IEEE Transactions on Communications.*

7.1 Introduction

In this chapter, we provide a global framework analysis of a dual-hop mixed Radio Frequency (RF)/Free Space Optical (FSO) system with multiple branches/relays wherein the first and second hops, respectively, consist of RF and FSO channels. To cover various cases of fading, we propose generalized channels' models for RF and FSO channels that follow the Nakagami-m and the Double Generalized Gamma (DGG) distributions, respectively. Moreover, we suggest Channel State Information (CSI)-assisted relaying or variable relaying gain based Amplifiy-and-Forward (AF) amplification. Partial relay selection with outdated CSI is assumed as a relay selection protocol based on the knowledge of the RF CSI. In order to derive the end-to-end Signal-to-Interference-plus-Noise Ratio (SINR) statistics such as the Cumulative Distribution Function (CDF), the Probability Density Function (PDF), the higher order moments, the amount of fading and the Moment Generating Function (MGF), the numerical values of the fading severity parameters are only valid for integer values. Based on these statistics, we derive closed-forms of the outage probability, the bit error probability, the ergodic capacity and the outage capacity in terms of Meijers'-G, univariate, bivariate and trivariate Fox-H functions. Capitalizing on these expressions, we derive high SNR asymptotes to unpack valuable engineering insights of the system performance. Monte Carlo simulation is used to confirm the analytical expressions.

7.2 System and CSIs Models

7.2 System Model

The proposed system consists of M parallel relays wirelessly connected to S and D. Partial relay selection based on the knowledge of the RF channels is assumed to select one relay among the set. This protocol states that for a given communication, S periodically

receives CSI feedback ($\gamma_{1(n)}$ for n = *1,... M*) from the relays, sorts them in an increasing order of magnitude and then select the branch/relay with the highest CSI. Hence, partial relay selection consists of selecting the m-th worst or *(M - m)*-th best relay $R_{(m)}$. Once S receives the feedback, a processing time is required for resources allocation, prescheduling, etc. Given that the channels are time-varying, the received CSIs rapidly change after the processing time and hence the selection is achieved based on an outdated CSI. To model the relation between the updated and outdated CSIs, we define the time correlation coefficient ρ as follows

$$\gamma_{1(\mathrm{m})} = \sqrt{\rho}\ \hat{\gamma}_{1(\mathrm{m})} + \sqrt{1-\rho}\ w, \tag{7.1}$$

where $\gamma_{1(\mathrm{m})}$ is the instantaneous CSI of the mth RF channel, $w \backsim \mathcal{N}(0, \sigma^2_{\gamma_{1(\mathrm{m})}})$, $\sigma^2_{\gamma_{1(\mathrm{m})}}$ is the variance of the m-th channel/CSI $\gamma_{1(\mathrm{m})}$. Note that the subscript of $\gamma_{1(\mathrm{m})}$ contains "1(m)" to indicate the mth channel of the first hop. The same notation is adopted for the channels of the second hop as $\gamma_{2(\mathrm{m})}$. The correlation coefficient ρ is given by the Jakes' autocorrelation model as follows [31]

$$\rho = J_0(2\pi f_d T_d), \tag{7.2}$$

where $J_\nu(\cdot)$ is the ν-th order Bessel function of the first kind, T_d is the time delay between the current and the delayed CSI versions, and f_d is the maximum Doppler frequency of the channels.

The received RF signal at the m-th relay is given by

$$y_{1(\mathrm{m})} = h_{1(\mathrm{m})} x + \sum_{n=1}^{M_R} f_n d_n + \nu_{\mathrm{SR}}, \tag{7.3}$$

where $h_{1(\mathrm{m})}$ is the m-th channel gain of the first hop, x is the information signal, d_n is the modulation symbol of the n-th interferer with an average power $\mathbb{E}\left[|d_n|^2\right] = P_{R_n}$, M_R is the number of interferers, f_n is the fading between the n-th interferer and the selected relay and ν_{SR} is the additive white Gaussian noise (AWGN) of the RF channels with variance σ_0^2.

The received signal at D can be expressed as follows

$$y_{2(\mathrm{m})} = (\eta I_{2(\mathrm{m})})^{\frac{r}{2}} G h_{\mathrm{SR}} x + (\eta I_{2(\mathrm{m})})^{\frac{r}{2}} G \sum_{n=1}^{M_R} f_n d_n + (\eta I_{2(\mathrm{m})})^{\frac{r}{2}} G \nu_{\mathrm{SR}} + \nu_{\mathrm{RD}}, \tag{7.4}$$

where η is the electrical-to-optical conversion coefficient, G is the relaying gain, $I_{2(\mathrm{m})}$ is the m-th FSO channel, ν_{RD} is the AWGN of the FSO channels with variance σ_0^2, $r = 1$ and $r = 2$ represent the heterodyne detection and IM/DD, respectively. An illustrative system model is given by Fig. 7.1, where the mmWave channels connect the different mobile users to the base stations. The FSO links play the role of back-hauling to connect the various networks such as the ISP (Internet Service Provider), mobile network, and enterprise network to the main data centers.

7.2 CSIs Model

Since the outdated RF CSI $\backsim \mathcal{G}(m_{\mathrm{SR}}, \Omega_{\mathrm{SR}}/m_{\mathrm{SR}})$, the PDF and CDF of the instantaneous SNR are expressed as follows

$$f_{\hat{\gamma}_{1(\mathrm{m})}}(\gamma) = \frac{\alpha_{\mathrm{SR}}^{m_{\mathrm{SR}}} \gamma^{m_{\mathrm{SR}}-1}}{\Gamma(m_{\mathrm{SR}})} e^{-\alpha_{\mathrm{SR}}\gamma}, \tag{7.5}$$

$$F_{\hat{\gamma}_{1(\mathrm{m})}}(\gamma) = 1 - \frac{\Gamma(m_{\mathrm{SR}}, \alpha_{\mathrm{SR}}\gamma)}{\Gamma(m_{\mathrm{SR}})}, \tag{7.6}$$

where $\alpha_{\mathrm{SR}} = \dfrac{m_{\mathrm{SR}}}{\Omega_{\mathrm{SR}}}$.
To simplify the mathematical derivations, we assume that m_{SR} is an integer and hence the CDF can be reformulated as follows

$$F_{\hat{\gamma}_{1(\mathrm{m})}}(\gamma) = 1 - e^{-\frac{m_{\mathrm{SR}}\gamma}{\overline{\gamma}_{\mathrm{SR}}}} \sum_{n=1}^{m_{\mathrm{SR}}-1} \frac{1}{n!} \left(\frac{m_{\mathrm{SR}}\gamma}{\overline{\gamma}_{\mathrm{SR}}} \right)^n, \tag{7.7}$$

where $\overline{\gamma}_{\mathrm{SR}}$ is the average SNR of the RF link.

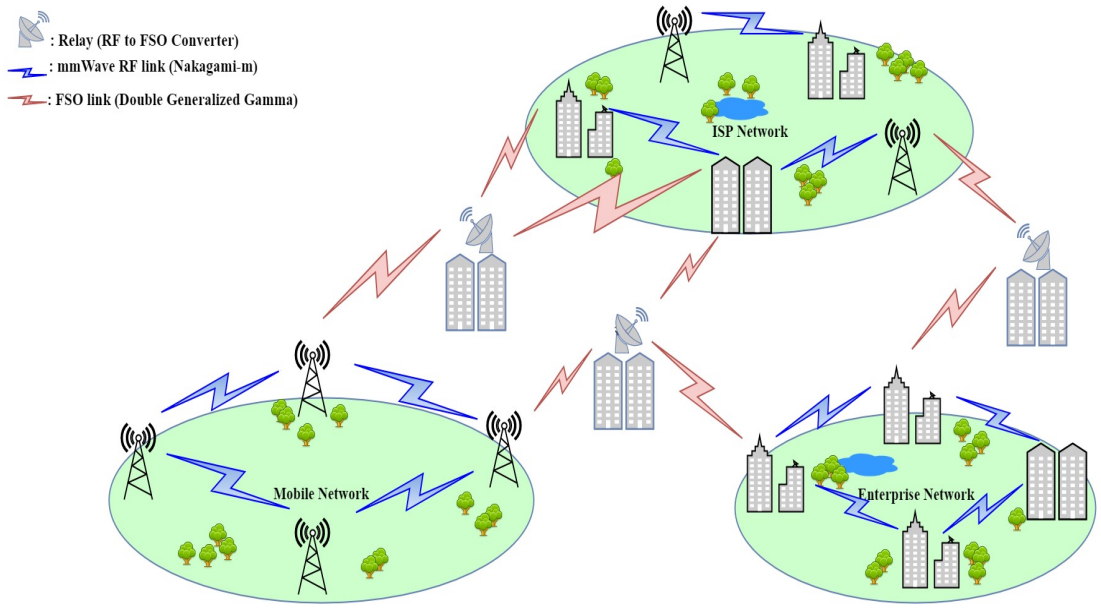

Figure 7.1: Mixed RF/FSO Relaying System

The outdated and current instantaneous SNRs are jointly Nakagami-m distributed with the joint PDF expressed as follows

$$f_{\gamma_{1(\mathrm{m})},\hat{\gamma}_{1(\mathrm{m})}}(x,y)=\left(\frac{m_{\mathrm{SR}}}{\overline{\gamma}_{\mathrm{SR}}}\right)^{m_{\mathrm{SR}}+1}\frac{\left(\frac{xy}{\rho}\right)^{\frac{m_{\mathrm{SR}}-1}{2}}}{(1-\rho)\Gamma(m_{\mathrm{SR}})}e^{-\frac{m_{\mathrm{SR}}}{\overline{\gamma}_{\mathrm{SR}}}\left(\frac{x+y}{1-\rho}\right)}\,I_{m_{\mathrm{SR}}-1}\left(\frac{2m_{\mathrm{SR}}\sqrt{\rho xy}}{\overline{\gamma}_{\mathrm{SR}}(1-\rho)}\right), \quad (7.8)$$

After some mathematical manipulations, the PDF of the current instantaneous SNR is given by [65, Eq. (3.11)]

$$\begin{aligned}f_{\gamma_{1(\mathrm{m})}}(\gamma)=&\frac{m_{\mathrm{SR}}}{\Gamma(m_{\mathrm{SR}})}\binom{M}{m_{\mathrm{SR}}}\sum_{n=0}^{m_{\mathrm{SR}}-1}\sum_{i=0}^{j(m_{\mathrm{SR}}-1)}\sum_{v=0}^{i}\binom{m_{\mathrm{SR}}-1}{n}\binom{i}{v}\left(\frac{m_{\mathrm{SR}}}{\overline{\gamma}_{\mathrm{SR}}}\right)^{m_{\mathrm{SR}}+v}\Xi^{i,j}_{m_{\mathrm{SR}}-1}\\&\times\frac{(-1)^n\rho^v\Gamma(m_{\mathrm{SR}}+i)\gamma^{m_{\mathrm{SR}}+v-1}}{(1+j(1-\rho))^{m_{\mathrm{SR}}+v+i}(1-\rho)^{v-i}\Gamma(m_{\mathrm{SR}}+v)}\exp\left[-\frac{m_{\mathrm{SR}}(j+1)\gamma}{(1+j(1-\rho))\overline{\gamma}_{\mathrm{SR}}}\right],\end{aligned} \quad (7.9)$$

where $I_\nu(\cdot)$ denotes the ν-th order modified Bessel function of first kind and the coefficients $\Xi^{i,j}_m$ are defined and evaluated recursively as $\left(\sum_{i=0}^{m}\frac{x^i}{i!}\right)^j\triangleq\sum_{i=0}^{j(m-1)}\Xi^{i,j}_m x^i$, $\Xi^{i,j}_m\triangleq\sum_{n=n_1}^{n_2}\frac{\Xi^{n_1,j-1}_m}{(i-n_1)!}x^i$, $n_1=\max(0,i-m_{\mathrm{SR}})$, $n_2=\min(i,(j-1)(m_{\mathrm{SR}}-1))$[68].

The instantaneous SNR of each interferer $\gamma_{\mathrm{R,k}}\backsim\mathcal{G}(m_{\mathrm{R,k}},1/\beta_{\mathrm{R}})$ where $\beta_{\mathrm{R}}\triangleq\frac{m_{\mathrm{R,k}}\sigma_0^2}{\Omega_{\mathrm{R,k}}P_{\mathrm{R_k}}}$, $(m_{\mathrm{R,k}},\Omega_{\mathrm{R,k}})$ are Nakagami-m parameters between the k-th interferer and the relay. It

has been shown in [43] that the sum of L independent and identically distributed (i.i.d) Gamma random variables with shape parameter σ and scale parameter α is a Gamma random variable with parameters σL and α. The PDF of the total Interference-to-Noise Ratio (INR) $\gamma_{\mathrm{R}} \triangleq \sum_{k=1}^{M_{\mathrm{R}}} \gamma_{\mathrm{R,k}}$ can be expressed as follows

$$f_{\gamma_{\mathrm{R}}}(\gamma) = \frac{\beta_R^{m_{\mathrm{R}}}}{\Gamma(m_{\mathrm{R}})} \gamma^{m_{\mathrm{R}}-1} e^{-\beta_{\mathrm{R}}\gamma}, \tag{7.10}$$

where $m_{\mathrm{R}} \triangleq \sum_{k=1}^{M_{\mathrm{R}}} m_{\mathrm{R,k}}$.

The FSO fading encompasses the turbulence-induced fading (I_{a}), the atmospheric path loss (I_{l}) and the pointing errors (I_{p}). The m-th channel gain $I_{2(m)}$ can be written as follows

$$I_{2(m)} = I_{\mathrm{a}} I_{\mathrm{l}} I_{\mathrm{p}}, \tag{7.11}$$

The table below summarizes the parameters of the optical part.

Table 7.1: Parameters of The FSO Part

Parameter	Definition
σ	Weather attenuation
σ_{s}^2	Jitter variance
σ_{R}^2	Rytov variance
k	Wave number
λ	Wavelength
ξ	Pointing error coefficient
ω_0	Beam waist at the relay
ω_{L}	Beam waist
ω_{Leq}	Equivalent beam waist
L	Length of the optical link
a	Radius of the receiver aperture
A_0	Fraction of the collected power at L = 0
F_0	Radius of curvature
C_n^2	Refractive index of the medium
R	Radial displacement of the beam at the receiver

Using the Beers-Lambert law, the path loss can be expressed as follows [21, Eq. (12)]

$$I_{\mathrm{l}} = \exp(-\sigma L), \tag{7.12}$$

The pointing error $I_{\rm p}$ made by Jitter can be given as [24, Eq. (9)]

$$I_{\rm p} = A_0 \exp\left(-\frac{2R^2}{\omega_{\rm Leq}^2}\right), \tag{7.13}$$

The atmoshperic turbulence fading $I_{\rm a}$ consists of small scale (I_x) and large scale (I_y) where $I_x \backsim \mathcal{GG}(\alpha_1, m_1, \Omega_1)$ and $I_y \backsim \mathcal{GG}(\alpha_2, m_2, \Omega_2)$, m_1 and m_2 are the shaping parameters defining the atmospheric turbulence fading. Moreover, $\alpha_1, \alpha_2, \Omega_1$, and Ω_2 are defined using the variances of the small and large scale fluctuations from [34, Eqs. (8.a), (8.b), (9), (10)]. Thereby, the PDF of the turbulence-induced fading $I_{\rm a}$ can be given by [34, Eq. (4)]

$$f_{I_{\rm a}}(I_{\rm a}) = \frac{\alpha_2 p^{m_2+\frac{1}{2}} q^{m_1-\frac{1}{2}} (2\pi)^{1-\frac{p+q}{2}}}{\Gamma(m_1)\Gamma(m_2) I_{\rm a}} G_{p+q,0}^{0,p+q}\left(\frac{p^p q^q \Omega_1^q \Omega_2^p}{m_1^q m_2^p I_a^{\alpha_2 p}} \;\middle|\; \begin{matrix} \Delta(q:1-m_1),\ \Delta(p:1-m_2) \\ - \end{matrix}\right), \tag{7.14}$$

where $G_{p,q}^{m,n}(\cdot)$ is the Meijer-G function, p and q are positive integers satisfying $\frac{p}{q} = \frac{\alpha_1}{\alpha_2}$ and $\Delta(j\ ;\ x) \triangleq \frac{x}{j}, \ldots, \frac{x+j-1}{j}$. In case of the heterodyne detection, the average SNR μ_1 is given by $\mu_1 = \frac{\eta \mathbb{E}\left[I_{2(\rm m)}\right]}{\sigma_0^2}$. Regarding the IM/DD detection, the average electrical SNR μ_2 is given by $\mu_2 = \frac{(\eta \mathbb{E}\left[I_{2(\rm m)}\right])^2}{\sigma_0^2}$, while the instantaneous optical SNR is $\gamma_{2(\rm m)} = \frac{(\eta I_{2(\rm m)}^2)}{\sigma_0^2}$. Unifying the two detection schemes and applying the transformation of the random variable $\gamma_{2(\rm m)} = \frac{(\eta I_{2(m)})^r}{\sigma_0^2}$, the unified PDF of the m-th instantaneous SNR $\gamma_{2(\rm m)}$ can be expressed as follows

$$f_{\gamma_{2(\rm m)}}(\gamma) = \frac{\xi^2 p^{m_2-\frac{1}{2}} q^{m_1-\frac{1}{2}} (2\pi)^{1-\frac{p+q}{2}}}{r\Gamma(m_1)\Gamma(m_2)\gamma} G_{p+q+\alpha_2 p,\alpha_2 p}^{0,p+q+\alpha_2 p}\left(\frac{p^p q^q \Omega_1^q \Omega_2^p}{m_1^p m_2^q} (A_0 I_l)^{\alpha_2 p} \left(\frac{\mu_r}{\gamma}\right)^{\frac{\alpha_2 p}{r}} \;\middle|\; \begin{matrix} \kappa_1 \\ \kappa_2 \end{matrix}\right), \tag{7.15}$$

where $\kappa_1 = \Delta(\alpha_2 p : 1-\xi^2),\ \Delta(q:1-m_1),\ \Delta(p:1-m_2)$, and $\kappa_2 = \Delta(\alpha_2 p : -\xi^2)$.
The average SNR $\overline{\gamma}_r$ can be expressed as follows

$$\overline{\gamma}_r = \frac{\mathbb{E}\left[I^r\right]}{\mathbb{E}\left[I\right]^r} \mu_r, \tag{7.16}$$

The average electrical SNR μ_r can be expressed as follows

$$\mu_r = \frac{\eta^r \mathbb{E}\left[I\right]^r}{\sigma_0^2}, \tag{7.17}$$

After some mathematical manipulation, the CDF can be expressed as follows

$$F_{\gamma_{2(\mathrm{m})}}(\gamma) = \frac{\xi^2 p^{m_2-\frac{3}{2}} q^{m_1-\frac{1}{2}} (2\pi)^{1-\frac{p+q}{2}}}{\alpha_2 \Gamma(m_1)\Gamma(m_2)} G_{p+q+2\alpha_2 p, 2\alpha_2 p}^{\alpha_2 p, p+q+\alpha_2 p}\left(\frac{p^p q^q \Omega_1^q \Omega_2^p}{m_1^p m_2^q} (A_0 I_l)^{\alpha_2 p} \left(\frac{\mu_r}{\gamma}\right)^{\frac{\alpha_2 p}{r}} \;\middle|\; \begin{matrix} \kappa_3 \\ \kappa_4 \end{matrix} \right), \tag{7.18}$$

where $\kappa_3 = \kappa_1,\ [1]_{\alpha_2 p},\ \kappa_4 = [0]_{\alpha_2 p},\ \kappa_2$, and $[x]_j$ is defined as the vector of length j and its components are equal to x.

7.3 End-to-End SINR Statistics

For CSI-assisted relaying, the overall SINR (γ_{e2e}) can be expressed as follows

$$\gamma_{\mathrm{e2e}} = \frac{\gamma_{1(\mathrm{m})}\gamma_{2(\mathrm{m})}}{\gamma_{1(\mathrm{m})} + \gamma_{2(\mathrm{m})} + \gamma_{2(\mathrm{m})}\gamma_{\mathrm{R}} + \gamma_{\mathrm{R}} + 1} = \frac{\gamma_{1(\mathrm{m})}^{\mathrm{eff}}\gamma_{2(\mathrm{m})}}{\gamma_{1(\mathrm{m})}^{\mathrm{eff}} + \gamma_{2(\mathrm{m})} + 1}, \tag{7.19}$$

where $\gamma_{1(\mathrm{m})}^{\mathrm{eff}}$ is the effective RF SNR including both the interferer and the RF fadings, which can be expressed as

$$\gamma_{1(\mathrm{m})}^{\mathrm{eff}} = \frac{\gamma_{1(\mathrm{m})}}{\gamma_{\mathrm{R}} + 1}, \tag{7.20}$$

Given that $\gamma_{1(\mathrm{m})}$ and γ_{R} are independent, the CDF of $\gamma_{1(\mathrm{m})}^{\mathrm{eff}}$ is given by

$$F_{\gamma_{1(\mathrm{m})}^{\mathrm{eff}}}(\gamma) = \Pr[\gamma_{\mathrm{e2e}} \le \gamma] = \Pr[\gamma_{1(\mathrm{m})} \le \gamma(1+\gamma_{\mathrm{R}})] = \int_0^\infty F_{\gamma_{1(\mathrm{m})}}(\gamma(1+\gamma_{\mathrm{R}})) f_{\gamma_{\mathrm{R}}}(\gamma_{\mathrm{R}})\, d\gamma_{\mathrm{R}}, \tag{7.21}$$

Using the identity [27, Eq. (3.381.4)], and after some mathematical manipulations, the CDF of $\gamma_{1(\mathrm{m})}^{\mathrm{eff}}$ can be expressed as follows

$$F_{\gamma_{1(\mathrm{m})}^{\mathrm{eff}}}(\gamma) = \sum_{n=0}^{m-1} \sum_{i=0}^{j(m_{\mathrm{SR}}-1)} \sum_{v=0}^{i} \mathcal{A}_0 \left[1 - \sum_{l=0}^{m_{\mathrm{SR}}+v-1} \sum_{s=0}^{l} \mathcal{A}_2 \gamma^l (\mathcal{A}_1\gamma + \beta_{\mathrm{R}})^{-(s+m_{\mathrm{R}})} e^{-\mathcal{A}_1\gamma} \right], \tag{7.22}$$

where $\mathcal{A}_0$, $\mathcal{A}_1$, and $\mathcal{A}_2$ are given by

$$\mathcal{A}_0 = \binom{M}{m}\binom{m-1}{n}\binom{i}{v}\frac{m\ \Xi^{i,j}_{m_{\mathrm{SR}}-1}\Gamma(m_{\mathrm{SR}}+i)(-1)^n\rho^v(1-\rho)^{i-v}}{\Gamma(m_{\mathrm{SR}})[1+j(1-\rho)^i](j+1)^{m_{\mathrm{SR}}+v}}, \tag{7.23}$$

$$\mathcal{A}_1 = \frac{m_{\mathrm{SR}}(j+1)}{[1+j(1-\rho)]\overline{\gamma}_1}, \tag{7.24}$$

$$\mathcal{A}_2 = \binom{l}{s}\frac{\beta_{\mathrm{R}}^{m_{\mathrm{R}}}\Gamma(m_{\mathrm{R}}+s)\mathcal{A}_1^l}{l!\Gamma(m_{\mathrm{R}})}, \tag{7.25}$$

7.3 Cumulative Distribution Function

Since the CDF of γ_{e2e} is not tractable, we refer to the following approximation

$$\gamma_{\mathrm{e2e}} \cong \frac{\gamma^{\mathrm{eff}}_{1(\mathrm{m})}\gamma_{2(\mathrm{m})}}{\gamma^{\mathrm{eff}}_{1(\mathrm{m})}+\gamma_{2(\mathrm{m})}} \cong \min(\gamma^{\mathrm{eff}}_{1(\mathrm{m})}, \gamma_{2(\mathrm{m})}), \tag{7.26}$$

The approximate CDF can be expressed as follows

$$F_{\gamma_{\mathrm{e2e}}}(\gamma) = 1 - \Pr(\min(\gamma^{\mathrm{eff}}_{1(\mathrm{m})}, \gamma_{2(\mathrm{m})}) \geq \gamma) = F^{\mathrm{eff}}_{\gamma_{1(\mathrm{m})}}(\gamma) + F_{\gamma_{2(\mathrm{m})}}(\gamma) - F^{\mathrm{eff}}_{\gamma_{1(\mathrm{m})}}(\gamma)F_{\gamma_{2(\mathrm{m})}}(\gamma), \tag{7.27}$$

7.3 Probability Density Function

After some mathematical manipulations, the PDF of $\gamma^{\mathrm{eff}}_{1(\mathrm{m})}$ can be expressed as

$$f_{\gamma_{1(\mathrm{m})}}(\gamma) = \sum_{n=0}^{m-1}\sum_{i=0}^{j(m_{\mathrm{SR}}-1)}\sum_{v=0}^{i}\sum_{u=0}^{m_{\mathrm{SR}}+v}\mathcal{A}_5\gamma^{m_{\mathrm{SR}}+v-1}e^{-\mathcal{A}_1\gamma}, \tag{7.28}$$

where $\mathcal{A}_5$ is given by

$$\begin{aligned}\mathcal{A}_5 =& \binom{M}{m}\binom{m-1}{n}\binom{i}{v}\binom{m_{\mathrm{SR}}+v}{u}\left(\frac{m_{\mathrm{SR}}}{\overline{\gamma}_1}\right)^{m_{\mathrm{SR}}+v} \\ &\times \frac{m(-1)^n\beta_{\mathrm{R}}^{m_{\mathrm{R}}}\rho^v(1-\rho)^{i-v}}{[1+j(1-\rho)]^{m_{\mathrm{SR}}+v+i}(\mathcal{A}_1+\beta_{\mathrm{R}})^{m_{\mathrm{R}}+u-1}} \\ &\times \frac{\Gamma(m_{\mathrm{SR}}+i)\Gamma(m_{\mathrm{R}}+u)}{\Gamma(m_{\mathrm{SR}})\Gamma(m_{\mathrm{R}})\Gamma(m_{\mathrm{SR}}+v)},\end{aligned} \tag{7.29}$$

After deriving the CDF (7.27), the PDF can be expressed as follows

$$f_{\gamma_{\mathrm{e2e}}}(\gamma) = f_{\gamma_{1(\mathrm{m})}}(\gamma) + f_{\gamma_{2(\mathrm{m})}}(\gamma) - f_{\gamma_{1(\mathrm{m})}}(\gamma) F_{\gamma_{2(\mathrm{m})}}(\gamma) - F_{\gamma_{1(\mathrm{m})}}(\gamma) f_{\gamma_{2(\mathrm{m})}}(\gamma), \tag{7.30}$$

To simplify the derivation, we reformulate the CDF of $\gamma_{2(\mathrm{m})}$ as follows

$$F_{\gamma_{2(\mathrm{m})}}(\gamma) = \mathcal{A}_3 \; G_{p+q+2\alpha_2 p, 2\alpha_2 p}^{\alpha_2 p, p+q+\alpha_2 p}\left(\mathcal{A}_4 \gamma^{-\frac{\alpha_2 p}{r}} \;\middle|\; \begin{matrix} \kappa_3 \\ \kappa_4 \end{matrix} \right), \tag{7.31}$$

where $\mathcal{A}_3$ and $\mathcal{A}_4$ are defined by

$$\mathcal{A}_3 = \frac{\xi^2 p^{m_2 - \frac{3}{2}} q^{m1 - \frac{1}{2}} (2\pi)^{1 - \frac{p+q}{2}}}{\alpha_2 \Gamma(m_1)\Gamma(m_2)}, \tag{7.32}$$

$$\mathcal{A}_4 = \left(\frac{q\Omega_1}{m_1} \right)^q \left(\frac{p\Omega_2}{m_2} \right)^p (A_0 I_l)^{\alpha_2 p} \mu_r^{\frac{\alpha_2 p}{r}}, \tag{7.33}$$

We also reformulate the PDF of $\gamma_{2(\mathrm{m})}$ as follows

$$f_{\gamma_{2(\mathrm{m})}}(\gamma) = \frac{\mathcal{A}_6}{\gamma} G_{p+q+\alpha_2 p, \alpha_2 p}^{0, p+q+\alpha_2 p}\left(\mathcal{A}_4 \gamma^{-\frac{\alpha_2 p}{r}} \;\middle|\; \begin{matrix} \kappa_1 \\ \kappa_2 \end{matrix} \right), \tag{7.34}$$

where $\mathcal{A}_6$ is given by

$$\mathcal{A}_6 = \frac{\xi^2 p^{m_2 - \frac{1}{2}} q^{m_1 - \frac{1}{2}} (2\pi)^{1 - \frac{p+q}{2}}}{r \Gamma(m_1)\Gamma(m_2)}, \tag{7.35}$$

7.3 Moments

The ν-th moment is defined as follows

$$\mathbb{E}\left[\gamma^\nu\right] = \int_0^\infty \gamma^\nu f_\gamma(\gamma) d\gamma, \tag{7.36}$$

After replacing the PDF expression (7.30) in Eq. (7.36), the moments are expressed as follows

$$\mathbb{E}\left[\gamma^\nu\right] = \mathcal{I}_1 + \mathcal{I}_2 - \mathcal{I}_3 - \mathcal{I}_4, \tag{7.37}$$

Using the identity [27, Eq. (3.381.4)], the term $\mathcal{I}_1$ can be expressed as follows

$$\mathcal{I}_1 = \int_0^\infty \gamma^\nu f_{\gamma_{1(\mathrm{m})}}(\gamma) d\gamma = \sum_{n=0}^{m-1} \sum_{i=0}^{j(m_{\mathrm{SR}}-1)} \sum_{v=0}^{i} \sum_{u=0}^{m_{\mathrm{SR}}+v} \frac{\mathcal{A}_5}{\mathcal{A}_1^{m_{\mathrm{SR}}+\nu+v}} \Gamma(m_{\mathrm{SR}}+v+\nu), \tag{7.38}$$

After changing the variable of integration ($x = \gamma^{-\frac{\alpha_2 p}{r}}$) and using the identity [53, Eq. (2.24.2.1)], the term $\mathcal{I}_2$ can be obtained by Eq. (7.39).

After changing the variable of integration ($x = \gamma^{-1}$) and using the identity [53, Eq. (2.24.1.1)], the term $\mathcal{I}_3$ is given by Eq. (7.40), where $\zeta_1 = \sum_{j=1}^{2\alpha_2 p} \kappa_{4,j} - \sum_{j=1}^{p+q+2\alpha_2 p} \kappa_{3,j} + \frac{p+q}{2} + 1,$, $\kappa_5 = \Delta(r : \alpha_2 p : 1-\xi^2),\ \Delta(r : q : 1-m_1),\ \Delta(r : p : 1-m_2),\ \Delta(r : \alpha_2 p : 1)$, and $\kappa_6 = \Delta(\alpha_2 p : m_{\mathrm{SR}}+v+\nu),\ \Delta(r : \alpha_2 p : 0),\ \Delta(r : \alpha_2 p : -\xi^2)$.

After reproducing the same derivation steps as $\mathcal{I}_2$ and using the identities [53, Eq. (8.4.3.1)], [1, Eq. (07.35.03.0001.01), (07.35.26.0003.01)], and [47, Eq. (2.3)], the term $\mathcal{I}_4$ can be expressed by Eq. (7.41).

$$\mathcal{I}_2 = \int_0^\infty \gamma^\nu f_{\gamma_{2(\mathrm{m})}}(\gamma) d\gamma = \frac{r\mathcal{A}_6}{\alpha_2 p \mathcal{A}_4^{\frac{r\nu}{\alpha_2 p}+2}} \frac{\prod_{j=1}^{p+q+\alpha_2 p} \Gamma\left(-\frac{r\nu}{\alpha_2 p} - \kappa_{1,j} - 1\right)}{\prod_{j=1}^{\alpha_2 p} \Gamma\left(-\frac{r\nu}{\alpha_2 p} - \kappa_{2,j} - 1\right)}, \tag{7.39}$$

$$\begin{aligned}\mathcal{I}_3 = \int_0^\infty \gamma^\nu f_{\gamma_{1(\mathrm{m})}}(\gamma) F_{\gamma_{2(\mathrm{m})}}(\gamma) d\gamma = \sum_{n=0}^{m-1} \sum_{i=0}^{j(m_{\mathrm{SR}}-1)} \sum_{v=0}^{i} \sum_{u=0}^{m_{\mathrm{SR}}+v} \frac{\mathcal{A}_3 \mathcal{A}_5 r^{\zeta_1} (\alpha_2 p)^{\frac{2(m_{\mathrm{SR}}+v+\nu)-1}{2}}}{\mathcal{A}_1^{m_{\mathrm{SR}}+v+\nu} (2\pi)^{\frac{\alpha_2 p+(r-1)(p+q)-1}{2}}} \\ \times G_{r(p+q+\alpha_2 p),(r+1)\alpha_2 p}^{\alpha_2 p, r(p+q+\alpha_2 p)} \left(\left(\mathcal{A}_4 r^{p+q}\right)^r \left(\frac{\mathcal{A}_1}{\alpha_2 p}\right)^{\alpha_2 p} \;\middle|\; \begin{matrix} \kappa_5 \\ \kappa_6 \end{matrix} \right),\end{aligned} \tag{7.40}$$

$$\begin{aligned}\mathcal{I}_4 = \int_0^\infty \gamma^\nu F_{\gamma_{1(\mathrm{m})}}(\gamma) f_{\gamma_{2(\mathrm{m})}}(\gamma) d\gamma = \\ \sum_{n=0}^{m-1} \sum_{i=0}^{j(m_{\mathrm{SR}}-1)} \sum_{v=0}^{i} \mathcal{A}_0 \left[\mathcal{I}_2 + \frac{r\mathcal{A}_6}{\alpha_2 p} \sum_{l=0}^{m_{\mathrm{SR}}+v-1} \sum_{s=0}^{l} \frac{\mathcal{A}_2 \mathcal{A}_1^{-(n+l)}}{\beta_{\mathrm{R}}^{s+m_{\mathrm{R}}} \Gamma(s+m_{\mathrm{R}})} \right. \\ \left. \times H_{1,0:1,1:p+q+\alpha_2 p,\alpha_2 p}^{0,1:1,1:0,p+q+\alpha_2 p} \left(\begin{matrix} (1-l-\nu;1,1) \\ - \end{matrix} \middle|^{(1-s-m_{\mathrm{R}},1)}_{(0,1)} \middle|^{(\kappa_1,[-\frac{r}{\alpha_2 p}]_{p+q+\alpha_2 p})}_{(\kappa_2,[-\frac{r}{\alpha_2 p}]_{\alpha_2 p})} \middle| \frac{1}{\beta_{\mathrm{R}}}, \frac{\mathcal{A}_4^{-\frac{r}{\alpha_2 p}}}{\mathcal{A}_1} \right) \right],\end{aligned} \tag{7.41}$$

where $H_{p_1,q_1:p_2,q_2:p_3,q_3}^{m_1,n_1:m_2,n_2:m_3,n_3}(\cdot)$ is the bivariate Fox-H function. An efficient implementation of this function is provided by [40, 64].

7.3 Moment Generating Function

The moment generating function can be expressed in terms of the CDF as follows [78, Eq. (12)]

$$\mathcal{M}_\gamma(t) = \mathbb{E}\left[e^{t\gamma}\right] = t\int_0^\infty e^{t\gamma} F_\gamma(\gamma) d\gamma, \tag{7.42}$$

After replacing the CDF (7.27) in Eq. (7.42), the MGF can be expressed as the summation of three terms $\mathcal{J}_1$, $\mathcal{J}_2$, and $\mathcal{J}_3$.

Using the identities [27, Eq. (3.381.4)], [8, Eq. (2.3.6.9)] and after some mathematical manipulation, the term $\mathcal{J}_1$ can be given by Eq. (7.43).

where $\Psi(\cdot:\cdot\,;\,\cdot)$ is the Tricomi confluent hypergeometric function.

After applying the identity [53, Eq. (2.24.3.1)], the term $\mathcal{J}_2$ can be obtained by Eq. (7.44).

where $\kappa_7 = \Delta(\alpha_2 p : 1),\ \Delta(r : \alpha_2 p : 0),\ \Delta(r : \alpha_2 p : -\xi^2)$.

Following the same derivation steps for $\mathcal{I}_4$, the term $\mathcal{J}_3$ can be given by Eq. (7.45).

$$\begin{aligned}\mathcal{J}_1 =& \sum_{n=0}^{m-1}\sum_{i=0}^{j(m_{\mathrm{SR}}-1)}\sum_{v=0}^{i}\mathcal{A}_0\left[1-\sum_{l=0}^{m_{\mathrm{SR}}+v-1}\sum_{s=0}^{l} t\mathcal{A}_2\beta_{\mathrm{R}}^{l-m_R-s+1}\frac{\Gamma(l+1)}{\mathcal{A}_1^{l+1}}\right.\\ &\left.\times\ \Psi\left(l+1, l+2-m_{\mathrm{R}}-s; \frac{\beta_{\mathrm{R}}(\mathcal{A}_1+t)}{\mathcal{A}_1}\right)\right],\end{aligned} \tag{7.43}$$

$$\mathcal{J}_2 = \frac{\mathcal{A}_3 r^{\zeta_1}\sqrt{\alpha_2 p}}{(2\pi)^{\frac{\alpha_2 p+(r-1)(p+q)-1}{2}}} G_{r(p+q+\alpha_2 p),(r+1)\alpha_2 p}^{\alpha_2 p, r(p+q+\alpha_2 p)}\left(\left(\mathcal{A}_4 r^{p+q}\right)^r\left(\frac{t}{\alpha_2 p}\right)^{\alpha_2 p}\ \middle|\ \begin{matrix}\kappa_5\\ \kappa_7\end{matrix}\right), \tag{7.44}$$

$$\begin{aligned}\mathcal{J}_3 =& \sum_{n=0}^{m-1}\sum_{i=0}^{j(m_{\mathrm{SR}}-1)}\sum_{v=0}^{i} t\mathcal{A}_0\left[\mathcal{J}_2 + \sum_{l=0}^{m_{\mathrm{SR}}+v-1}\sum_{s=0}^{l}\frac{r\mathcal{A}_2\mathcal{A}_3}{\alpha_2 p\beta_{\mathrm{R}}^{s+m_{\mathrm{R}}}(\mathcal{A}_1+t)^{l+1}\Gamma(m_{\mathrm{R}}+s)}\right.\\ &\left. H_{1,0:1,1:p+q+\alpha_2 p,\alpha_2 p}^{0,1:1,1:0,p+q+\alpha_2 p}\left(\begin{matrix}(-l;1,1)\\ -\end{matrix}\ \middle|\begin{matrix}(1-s-m_{\mathrm{R}},1)\\ (0,1)\end{matrix}\middle|\begin{matrix}(\kappa_1,[-\frac{r}{\alpha_2 p}]_{p+q+\alpha_2 p})\\ (\kappa_2,[-\frac{r}{\alpha_2 p}]_{\alpha_2 p})\end{matrix}\middle|\frac{\mathcal{A}_1}{\beta_{\mathrm{R}}(\mathcal{A}_1+t)},\ \frac{\mathcal{A}_4^{-\frac{r}{\alpha_2 p}}}{\mathcal{A}_1+t}\right)\right],\end{aligned} \tag{7.45}$$

7.4 Performance Analysis

7.4 End-to-End Outage Probability

The end-to-end outage probability is the probability that the overall SINR falls below a given threshold γ_{T}. For CSI-assisted relaying, the outage probability can be given using (7.27).

$$P_{\mathrm{out}}(\gamma_{\mathrm{T}}) = \Pr[\gamma \leq \gamma_{\mathrm{T}}] = F_{\gamma_{\mathrm{e2e}}}(\gamma_{\mathrm{T}}), \tag{7.46}$$

7.4 High SNR Analysis

To get the diversity gain G_{d}, we derive the asymptotic high SNR by expanding the Meijer-G function in (31) using [1, Eq. (07.34.06.0044.01)]. The expression is given by Eq. (7.46).

For infinite RF, and FSO average SNR, and after applying partial fraction expansion on (7.22), it can be shown that the diversity gain G_{d} is given by Eq. (7.47).

Note that the diversity gain for partial relay selection of the RF branches is equal to m_{SR} regardless of the correlation coefficient value ρ, unlike the case of opportunistic relay selection protocol wherein the correlation affects the diversity gain.

$$G_{\mathrm{d}} = \min\left(\frac{\xi^2}{r}, \frac{m_1\alpha_1}{r}, \frac{m_2\alpha_2}{r}, m_{\mathrm{SR}}\right), \tag{7.47}$$

7.4 Higher-Order Amount of Fading

The amount of fading is mathematically defined as follows

$$AF_{\gamma}^{(\nu)} = \frac{\mathbb{E}\left[\gamma^{\nu}\right]}{\mathbb{E}\left[\gamma\right]^{\nu}} - 1, \tag{7.48}$$

Replacing (7.37) in (7.48) yields to the ν-th order of the amount of fading.

7.4 Average Bit Error Probability

For the most binary modulations, the bit error probability is expressed as follows

$$\overline{P_{\mathrm{e}}} = \frac{\delta^{\tau}}{2\Gamma(\tau)} \int_0^{\infty} \gamma^{\tau-1} e^{-\delta\gamma} F_{\gamma}(\gamma) d\gamma, \tag{7.49}$$

where τ and δ are the parameters of the modulation, which can be summarized in Table 7.2.

Table 7.2: Parameters of Binary Modulations

Modulation	δ	τ
Coherent Binary Frequency Shift Keying (CBFSK)	0.5	0.5
Non-Coherent Binary Frequency Shift Keying (NBFSK)	0.5	1
Coherent Binary Phase Shift Keying (CBPSK)	1	0.5
Differential Binary Phase Shift Keying (DBPSK)	1	1

For CSI-assisted relaying of the proposed system, the bit error rate can be given by replacing (7.27) in (7.49). In this case, it can be expressed as follows

$$\overline{P_{\mathrm{e}}} = \mathcal{T}_1 + \mathcal{T}_2 - \mathcal{T}_3, \tag{7.50}$$

Using the identities [27, Eq. (3.381.4)] and [8, Eq. (2.3.6.9)], the term $\mathcal{T}_1$ can be derived as follows

$$\begin{aligned}\mathcal{T}_1 =& \frac{\delta^{\tau}}{2\Gamma(\tau)} \int_0^{\infty} \gamma^{\tau-1} e^{-\delta\gamma} F_{\gamma_{1(\mathrm{m})}}(\gamma) d\gamma \\ =& \sum_{n=0}^{m-1} \sum_{i=0}^{j(m_{\mathrm{SR}}-1)} \sum_{v=0}^{i} \frac{\mathcal{A}_0}{2t} \left[1 - \sum_{l=0}^{m_{\mathrm{SR}}+v-1} \sum_{s=0}^{l} \frac{\mathcal{A}_2 \delta^{\tau} \beta_{\mathrm{R}}^{l+\tau-m_{\mathrm{R}}-s} \Gamma(l+1)}{\mathcal{A}_1^{l+\tau} \Gamma(\tau)} \right. \\ & \left. \times \Psi\left(l+\tau, l+\tau-m_{\mathrm{R}}-s+1; \frac{\beta_{\mathrm{R}}(\mathcal{A}_1+\delta)}{\mathcal{A}_1} \right) \right],\end{aligned} \tag{7.51}$$

After changing the variable of integration ($x = \gamma^{-1}$), and using [53, Eq. (2.24.1.1)], and [1, Eqs. (01.03.26.0004.01), (07.34.16.0002.01)], the term $\mathcal{T}_2$ can be derived as follows

$$\begin{aligned}\mathcal{T}_2 =& \frac{\delta^{\tau}}{2\Gamma(\tau)} \int_0^{\infty} \gamma^{\tau-1} e^{-\delta\gamma} F_{\gamma_{2(\mathrm{m})}}(\gamma) d\gamma = \frac{\mathcal{A}_3 r^{\zeta_1} (\alpha_2 p)^{(l+\tau-1)}}{2(2\pi)^{\frac{\alpha_2 p+(r-1)(p+q)-1}{2}} \Gamma(\tau)} \\ & \times \; G_{r(p+q+\alpha_2 p),(r+1)\alpha_2 p}^{\alpha_2 p, r(p+q+\alpha_2 p)} \left(\left(\mathcal{A}_4 r^{p+q}\right)^r \left(\frac{\delta}{\alpha_2 p} \right)^{\alpha_2 p} \;\middle|\; \begin{matrix} \kappa_5 \\ \kappa_8 \end{matrix} \right),\end{aligned} \tag{7.52}$$

where $\kappa_8 = \Delta(\alpha_2 p : \tau),\ \Delta(r : \alpha_2 p : 0),\ \Delta(r : \alpha_2 p : -\xi^2)$.
After reproducing the same derivation steps for $\mathcal{I}_4$, term $\mathcal{T}_3$ can be expressed by (7.56).

7.4 Ergodic Capacity

The channel capacity, expressed in (bit/s/Hz), is defined as the maximum error-free data rate transmitted by the system. It can be written as follows

$$\overline{C} = \mathbb{E}\left[\log_2(1+\varpi\gamma)\right] = \int_0^\infty \log_2(1+\varpi\gamma) f_\gamma(\gamma) d\gamma, \tag{7.53}$$

$\varpi = 1$ or $\frac{e}{2\pi}$, respectively, for heterodyne and IM/DD detection.
After replacing the PDF (30) in (54), the ergodic capacity can be expressed as follows

$$\overline{C} = \mathcal{C}_1 + \mathcal{C}_2 - \mathcal{C}_3 - \mathcal{C}_4, \tag{7.54}$$

After applying [53, Eqs. (8.4.6.5), (2.24.3.1)], and [1, Eqs. (07.35.03.0001.01)
, (07.35.26.0003.01)], the term $\mathcal{C}_1$ can be derived in terms of the univariate Fox-H function (7.57).
Reproducing the same proceduces for $\mathcal{C}_1$, the term $\mathcal{C}_2$ can be obtained by (7.58).
Using the identities [1, Eq. (07.35.03.0001.01), (07.35.26.0003.01)],
[53, Eqs. (8.4.3.1), (8.4.6.5)], and [47, Eq. (2.3)] and after some mathematical manipulations, the term $\mathcal{C}_3$ can be derived by (7.59).
The term $\mathcal{C}_4$ can be derived in terms of the trivariate Fox-H function (7.60).
The Python implementation of the multivariate Fox-H function is given by [28].

7.4 End-to-End Outage Capacity

The outage capacity is defined as the probability that the overall throughput falls below a given outage rate $\mathcal{C}_{\mathrm{T}}$. This metric is very important since it clearly describes the average throughput outage of the proposed system. Mathematically, the outage rate can be expressed as follows

$$\mathcal{R}(\mathcal{C}_{\mathrm{T}}) = \Pr[\overline{C} \leq \mathcal{C}_{\mathrm{T}}] = F_\gamma\left(\frac{2^{\mathcal{C}_T}-1}{\varpi}\right), \tag{7.55}$$

After replacing the CDF (7.27) in (7.55), the outage rate is finally derived. Note that $\overline{\kappa} = [1]_{\mathrm{length}(\kappa)} - \kappa$.

$$\mathcal{T}_3 = \frac{\delta^\tau}{2\Gamma(\tau)} \int_0^\infty \gamma^{\tau-1} e^{-\delta\gamma} F_{\gamma_{1(\mathrm{m})}}(\gamma) F_{\gamma_{2(\mathrm{m})}}(\gamma) d\gamma$$

$$= \sum_{n=0}^{m-1} \sum_{i=0}^{j(m_{\mathrm{SR}}-1)} \sum_{v=0}^{i} \mathcal{A}_0 \left[\mathcal{T}_2 + \sum_{l=0}^{m_{\mathrm{SR}}+v-1} \sum_{s=0}^{l} \frac{r\delta^\tau \mathcal{A}_2 \mathcal{A}_3}{2\alpha_2 p \beta_{\mathrm{R}}^{m_{\mathrm{R}}+s} (\mathcal{A}_1+\delta)^{l+\tau} \Gamma(\tau)\Gamma(m_{\mathrm{R}}+s)} \right.$$

$$\left. H_{1,0:1,1:p+q+2\alpha_2 p, 2\alpha_2 p}^{0,1:1,1:\alpha_2 p, p+q+\alpha_2 p} \left(\begin{matrix} (1-l-\tau;1,1) \\ - \end{matrix} \middle| \begin{matrix} (1-s-m_{\mathrm{R}},1) \\ (0,1) \end{matrix} \middle| \begin{matrix} (\kappa_3, [-\frac{r}{\alpha_2 p}]_{p+q+2\alpha_2 p}) \\ (\kappa_4, [-\frac{r}{\alpha_2 p}]_{2\alpha_2 p}) \end{matrix} \middle| \frac{\mathcal{A}_1}{\beta_{\mathrm{R}}(\mathcal{A}_1+\delta)}, \frac{\mathcal{A}_4^{-\frac{r}{\alpha_2 p}}}{\mathcal{A}_1+\delta} \right) \right], \tag{7.56}$$

$$\mathcal{C}_1 = \int_0^\infty \log_2(1+\varpi\gamma) f_{\gamma_{1(\mathrm{m})}}(\gamma) d\gamma$$

$$= \sum_{n=0}^{m-1} \sum_{i=0}^{j(m_{\mathrm{SR}}-1)} \sum_{v=0}^{i} \sum_{u=0}^{m_{\mathrm{SR}}+v} \frac{\mathcal{A}_5}{\log(2)\mathcal{A}_1^{m_{\mathrm{SR}}+v}} H_{3,2}^{1,3} \left(\begin{matrix} (1-m_{\mathrm{SR}}-v,1)(1,1)(1,1) \\ (1,1)(0,1) \end{matrix} \middle| \frac{\varpi}{\mathcal{A}_1} \right), \tag{7.57}$$

$$\mathcal{C}_2 = \int_0^\infty \log_2(1+\varpi\gamma) f_{\gamma_{2(\mathrm{m})}}(\gamma) d\gamma$$

$$= -\frac{r\mathcal{A}_6}{\alpha_2 p \log(2)} H_{p+q+\alpha_2 p+2, \alpha_2 p+2}^{2, p+q+\alpha_2 p+1} \left(\begin{matrix} (\kappa_1, [-\frac{r}{\alpha_2 p}]_{p+q+\alpha_2 p+2})(0,1)(0,1) \\ (0,1)(0,1)(\kappa_2, [-\frac{r}{\alpha_2 p}]_{\alpha_2 p+2}) \end{matrix} \middle| \frac{\mathcal{A}_4^{-\frac{r}{\alpha_2 p}}}{\varpi} \right), \tag{7.58}$$

$$\mathcal{C}_3 = \int_0^\infty \log_2(1+\varpi\gamma) f_{\gamma_{1(\mathrm{m})}}(\gamma) F_{\gamma_{2(\mathrm{m})}}(\gamma) d\gamma = -\frac{r}{\alpha_2 p \log(2)} \sum_{n=0}^{m-1} \sum_{i=0}^{j(m_{\mathrm{SR}}-1)} \sum_{v=0}^{i} \sum_{u=0}^{m_{\mathrm{SR}}+v} \frac{\mathcal{A}_3 \mathcal{A}_5}{\mathcal{A}_1^{m_{\mathrm{SR}}+v}}$$

$$\times \; H_{1,0:2,2:p+q+2\alpha_2 p, 2\alpha_2 p}^{0,1:1,2:\alpha_2 p, p+q+\alpha_2 p} \left(\begin{matrix} (1-m_{\mathrm{SR}}-v;1,1) \\ - \end{matrix} \middle| \begin{matrix} (1,1)(1,1) \\ (1,1)(0,1) \end{matrix} \middle| \begin{matrix} (\kappa_3, [-\frac{r}{\alpha_2 p}]_{p+q+2\alpha_2 p}) \\ (\kappa_4, [-\frac{r}{\alpha_2 p}]_{2\alpha_2 p}) \end{matrix} \middle| \frac{\varpi}{\mathcal{A}_1}, \frac{1}{\mathcal{A}_1 \mathcal{A}_4^{\frac{\alpha_2 p}{r}}} \right), \tag{7.59}$$

$$\mathcal{C}_4 = \int_0^{\infty} \log_2(1+\varpi\gamma) F_{\gamma_{1(\mathrm{m})}}(\gamma) f_{\gamma_{2(\mathrm{m})}}(\gamma) d\gamma$$

$$= \sum_{n=0}^{m-1} \sum_{i=0}^{j(m_{\mathrm{SR}}-1)} \sum_{v=0}^{i} \left[\mathcal{C}_2 - \sum_{l=0}^{m_{\mathrm{SR}}+v-1} \sum_{s=0}^{l} \frac{\mathcal{A}_1^{l+1} \mathcal{A}_2 \mathcal{A}_3}{\beta_{\mathrm{R}}^{m_{\mathrm{R}}+s} \Gamma(m_{\mathrm{R}}+s)\log(2)} H^{0,1:2,0:2,1:0,p+q+\alpha_2 p}_{1,0:0,2:2,2:p+q+2\alpha_2 p,2\alpha_2 p} \right.$$
$$\left. \left(\begin{matrix} (-l;-1,-1,-\frac{\alpha_2 p}{r}) \\ - \end{matrix} \middle| \begin{matrix} - \\ (1,-1)(0,1)(0,1) \end{matrix} \middle| \begin{matrix} (0,1)(1,1) \\ (0,1)(0,1) \end{matrix} \middle| \begin{matrix} (\overline{\kappa}_2, [-\frac{r}{\alpha_2 p}]_{\alpha_2 p}) \\ (\overline{\kappa}_1, [-\frac{r}{\alpha_2 p}]_{p+q+\alpha_2 p}) \end{matrix} \middle| \frac{\beta_{\mathrm{R}}}{\mathcal{A}_1^2}, \frac{\mathcal{A}_1^{-1}}{\varpi}, \frac{\mathcal{A}_4^{-\frac{\alpha_2 p}{r}}}{\mathcal{A}_1} \right) \right], \tag{7.60}$$

7.5 Numerical Results and Discussions

In this section, we compare the analytical expressions of the system performance against Monte Carlo simulations. The correlated RF CSI is generated using relation (7.1), while the atmospheric turbulence samples are generated using the product of two independent random variables ($I_a = I_{aX} \times I_{aY}$) following the Generalized Gamma distribution. In addition, the pointing error samples are generated by firstly generating the radial displacement R following the Rayleigh distribution with scale equal to the jitter standard deviation (σ_s) and then we generate the samples using (7.13). Since the path loss is deterministic, it can be generated using relation (7.12). Table 7.3 summarizes the main simulation parameters.

Table 7.3: Main Simulation Parameters

Parameter	Value
L	1 km
λ	1550 nm
F_0	-10 m
a	5 cm
ω_0	5 mm
σ_s	3.75 cm
σ	0.5 dB/km
p	2
q	2
m_1	3
m_2	3
M_{R}	5
m_{R}	5

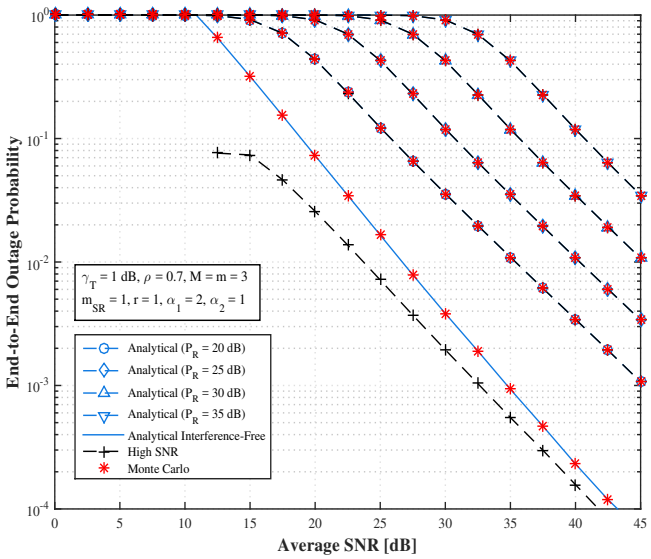

Figure 7.2: Effects of the interferers' powers on the outage probability.

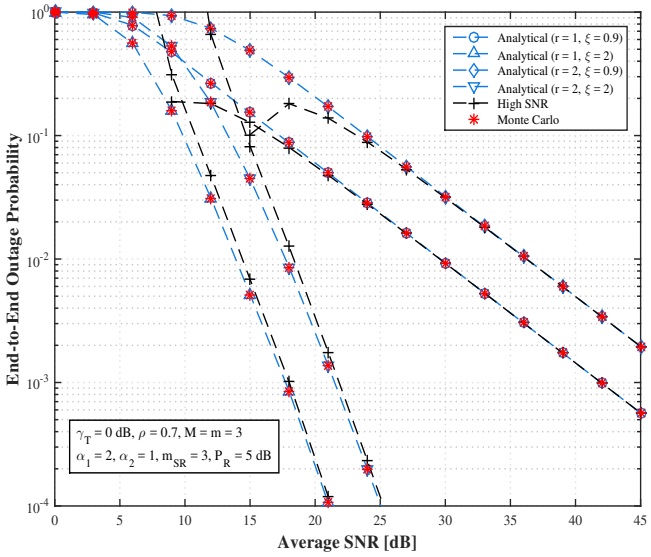

Figure 7.3: Effects of the pointing error on the outage performance.

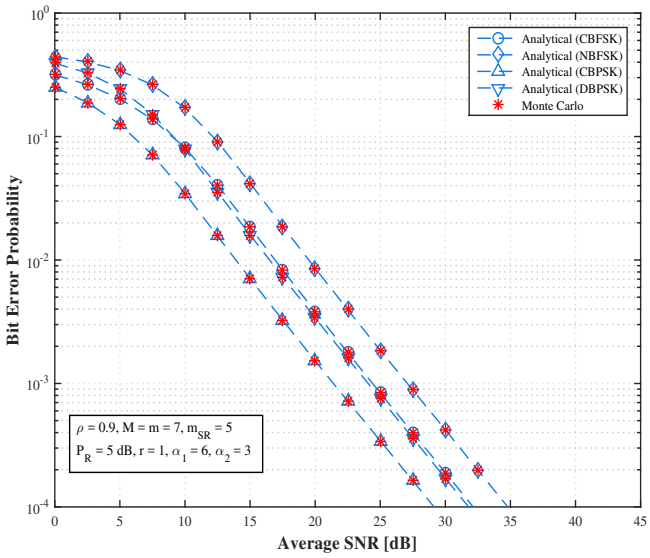

Figure 7.4: Bit error probability for various binary modulation schemes.

Fig. 7.2 shows the end-to-end outage performance for various profiles of interferers. As a special case, we assume that the RF channels experience Rayleigh fading ($m_{\mathrm{SR}} = 1$). We observe that more interferers's powers yields worse outage performance. In this case, to improve the network coverage and scalability in farthest areas, it is better to implement useful techniques to eliminate or reduce the interference impacts such as partial interference cancellation. The interference-free case illustrates the best performance compared to the other ones.

The impacts of the pointing error on the outage probability for heterodyne and IM/DD detection modes are illustrated by Fig. 7.3. As expected, the system works better under the coherent detection rather than IM/DD for negligeable pointing error. In addition, the system performance is very sensitive to the pointing error coefficients. In fact, we observe that as the pointing error coefficient ξ decreases (severe pointing error fading), the effect becomes more pronounced and the performance gets worse. We also note that for severe pointing fading, the system performance assuming coherent detection is worse compared to the case of IM/DD for less pointing error fading. Thereby, the coverage reliability depends to a large extent on the misalignment between the relays and the front photodetector.

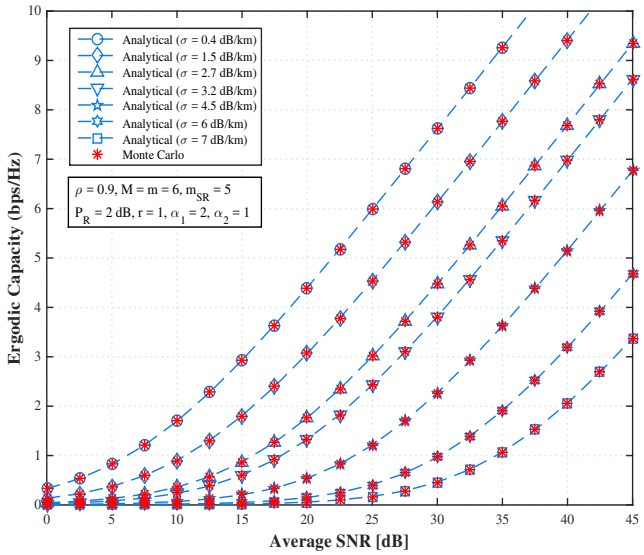

Figure 7.5: Effects of the atmospheric path loss on the average capacity.

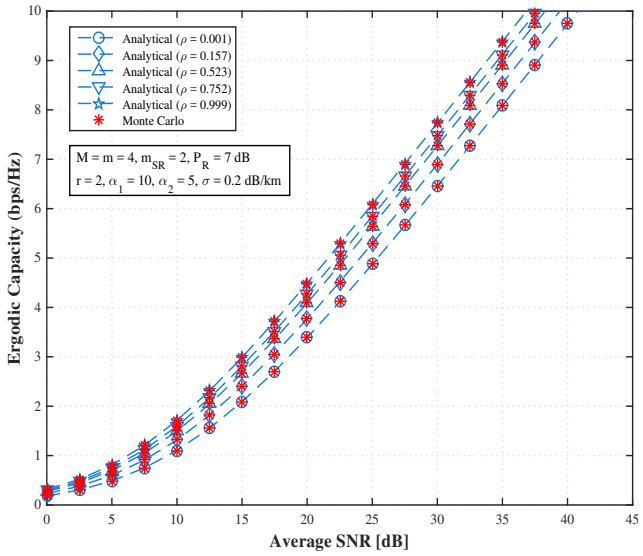

Figure 7.6: Effects of the time correlation on the ergodic capacity.

Fig. 7.4 shows the variations of the bit error probability for various binary modulation schemes. The graph clearly shows the agreement between the derived analytical results and the Monte Carlo simulation. Therefore, these results confirm the accuracy of the performance metrics derived of the proposed system. Furthermore, we note that the best performance is achieved by CBPSK, however, it becomes completely bad for NBFSK

modulation.

Fig. 7.5 illustrates the variations of the average capacity for different values of the atmospheric weather attenuation (path loss). We observe that for a lower path loss value of roughly 0.4 dB/km, which describes a clear air weather, the system achieves better throughput. As the path loss becomes moderate for rainy weather around 2.7 and 4.5 dB/km, the system still operates in acceptable conditions but with lower throughput compared to the case of clear air condition. However, as the atmospheric attenuation becomes more severe, which is the case of foggy weather, the average capacity substantially gets worse. We also observe that for an average SNR around 45 dB, the throughput is roughly 3.2 bps/Hz for severe path loss (σ = 7 dB/km) while for moderate path loss (σ = 4.5 dB/km), the achievable rate is around 6.8 bps/Hz. Consequently, the effect of the atmospheric attenuation on the system throughput is substantially pronounced mainly at high SNR.

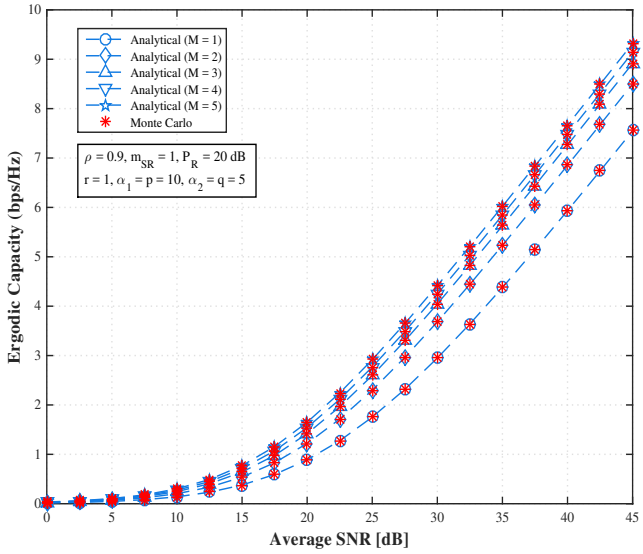

Figure 7.7: Average capacity performance for various number of relays.

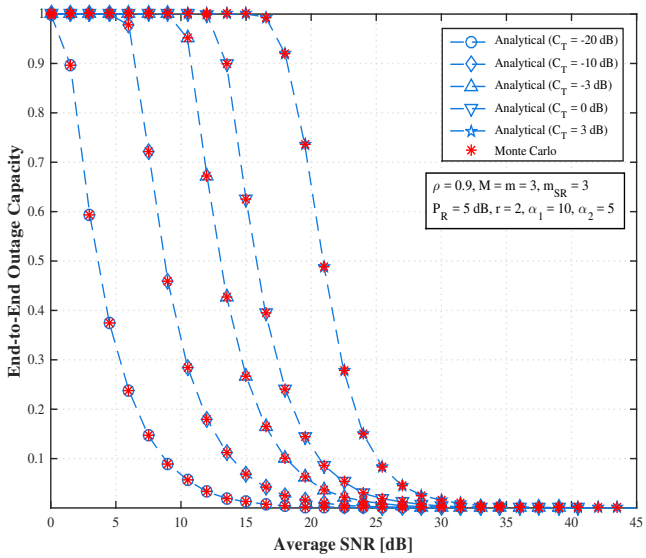

Figure 7.8: Effects of the capacity threshold on the end-to-end outage rate.

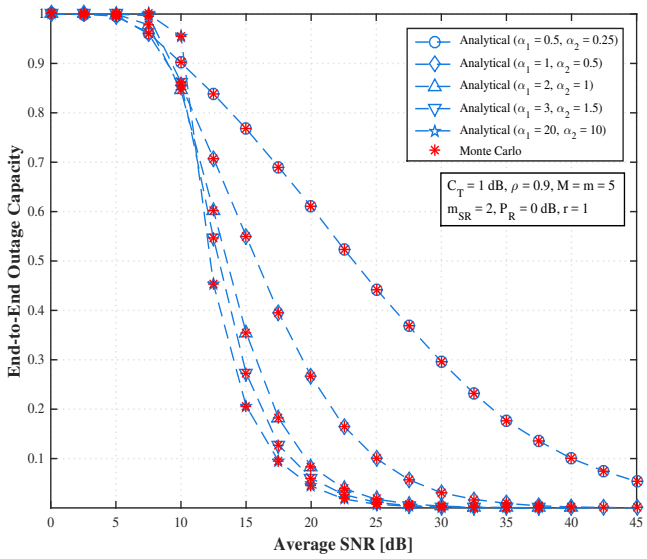

Figure 7.9: End-to-end outage capacity under various turbulence conditions.

Fig. 7.6 illustrates the effects of the time correlation coefficient ρ on the ergodic capacity. We observe that the average rate gets better as the correlation between the RF CSIs increases. In fact, for higher correlation, the source gets better estimation of the channels' coefficients and based on that, the best branch will be selected for the transmission. However, as the RF CSIs become completely outdated ($\rho \cong 0.001$), the source gets bad estimation of the channels' coefficients and hence the selection of the best branch

is uncertainly achieved. Generally speaking, the throughput basically improves as the instantaneous CSI of the branch becomes stronger. Consequently, to realize a stable and satisfied average throughput, a better channel estimation (higher correlation) must be achieved first.

The variations of the ergodic capacity for various number of relays is illustrated by Fig. 7.7. We clearly note that a large number of relays yields better throughput. In fact, increasing the number of the relays means that the source has better chance to select a branch with a stronger CSI. Therefore, to serve the densified cells without throughput perturbation, the number of the relays implemented must be large enough to deal with power shortages/outages that may occur. Moreover, for a given throughput equal to 3 bps/Hz, the proposed system requires 30 dB and 25 dB for M = 1 and 5, respectively. Thereby, the system achieves a power gain of 5 dB.

Another important metric used to evaluate the system performance is the outage capacity, whose variations with respect to the outage threshold, and the atmospheric turbulence are shown in figures 7.8, and 7.9, respectively. We clearly note in Fig. 7-8 that a lower threshold yields better throughput coverage. However, as the throushold becomes stronger, the throughput quickly saturates and reaches the bottleneck. In addition, the variations of the outage capacity for various atmospheric turbulence conditions are illustrated by Fig. 7.9. As expected, weaker atmospheric turbulence conditions (higher values of α_1 and α_2) yield lower outage throughput. For moderate turbulence ($\alpha_1 = 3$ and $\alpha_2 = 1.5$), the system still achieves acceptable performance but a little worse compared to the case of weak turbulence. However, as the turbulences become severe ($\alpha_1 = 0.5$ and $\alpha_2 = 0.25$), the average throughput is not stable anymore and experiences a substantial outage/shortage yielding the worst performance. As a result, the system performance depends to a large extent on the state of the optical channel.

7.6 Conclusion

In this work, we proposed a dual-hop mixed RF/FSO system with multiple relays under the effects of the co-channel interference. Partial relay selection with outdated CSI is assumed as a protocol to select the best branch/relay. The results show that the coverage reliability is very sensitive to the interferers' powers. Moreover, a large number of relays and higher correlation substantially improves the system throughput under weak and moderate atmospheric conditions. However, the contributions of these parameters become less pronounced as the state of the optical channel (path loss, pointing error and atmospheric turbulences) becomes unstable. The most challenging part of FSO system is

the strong dependence on the severity of fading and that possible enhancements are very limited. As an extention of this work, we intend to propose sophisticated techniques to mitigate or compensate for the loss introduced by the FSO channel disturbance.

Chapter 8: Conclusion

8.1 Summary

An extensive analysis was conducted on the performance of an asymmetric radio frequency (RF)-free-space optical (FSO) dual-hop transmission system with various different developments towards generalization, unification, and practical applicability in each subsequent study/work relative to the previous chapter. At first, the single FSO link was unified by integrating all the previous related work on single FSO link into a single expression. The atmospheric turbulences were modeled following the Gamma-Gamma, Málaga, Double Generalized Gamma, and Double Weibull, while the RF channels basically follows, the correlated Rayleigh and Nakagami-m distributions.

Utilizing the unification of the optical channels, a simple asymmetric RF/FSO dual-hop was studied for decode-and-forward and amplify-and-forward relay schemes i.e. for both fixed gain relaying as well as variable gain relaying. Opprtunistic and partial relay selection were assumed to select the best relay for the asymmetric RF/FSO dual-hop cooperative systems. For all the above transmission systems under study, exact closed-form analytical expressions were derived for statistical characteristics such as the CDF, the PDF, the MGF, and the moments. These unified statistical characteristics were utilized to derive exact closed-form analytical expressions for the OP, the BER for various binary modulation schemes, and the ergodic capacity. It was satisfactorily demonstrated that the proposed hybrid RF/FSO transmission system performed highly better than the traditional RF path.

The unification of the optical channel components included both types of detection techniques i.e. heterodyne as well as intensity modulation/direct detection (IM/DD) and it also included the effect of pointing errors as well as negligible pointing errors. Specifically, the cumulative distribution function (CDF), the probability density function (PDF), the moment generating function (MGF), and the moments were derived. These lead to the derivation of the outage probability (OP), the higher-order amount of fading (AF), the average bit-error rate (BER) of binary modulation schemes, and the ergodic capacity.

A comprehensive performance analysis of the proposed systems was conducted over an aggregate model of hardware impairments and then special cases were considered mainly

SEL, TWTA, SSPA, and IQ imbalance. The impacts of these hardware imperfections were quantified and studied in depth on the reliability of the full RF dual-hop relaying systems as well as mixed RF/FSO cooperative systems. We conclude that the performance metrics of the proposed systems experience severe limitations caused by the hardware impairments and this impacts become more pronounced as the average SNR becomes large. Importantly, the capacities of the system are saturated by the HPA non-linearities and this limitation becomes more significant if we consider the joint impact of the HPA non-linearities and the IQ imbalance. The impacts of the hardware impairments have been also observed by the creation of irreducible floors affecting the outage and the error performance mainly at high SNR.

Finally, the asymmetric RF/FSO dual-hop transmission system was analyzed considering the co-channel interference in the RF channels. We introduced a mathematical model of the interferers in order to quantify their impacts on the system performance. We concluded the that system works much better for interference-free case. However, the outage performance deteriorates as the interferers' powers increase and hence, the coverage reliability of the proposed systems degrades.

8.2 Future Research Directions

The results presented on hybrid RF/FSO transmission systems have indeed further motivated to exploration and pursuit of the following possible venues for further research work with a practical application to the region and globally. The different possible tasks are:

8.2 Multiple Best Relay Selection Protocol in Mixed RF/FSO Cooperative Systems

The performance of such a hybrid RF/FSO may be improved manifolds. At present, the hybrid transmission system presented in this work is losing on capacity since it is taking only a single RF (lesser bandwidth (BW)) user's message and transmitting over a high BW FSO link. The system may be improved by selecting N-best users i.e. N can be set in such a way that the high BW FSO link can be utilized to the maximum. Hence, N-best users may be selected based on certain SNR threshold and multiplexed together to be transmitted over the high BW FSO link ultimately utilizing one of the main advantages of a FSO link. This must definitely improve the performance and utility of such a hybrid RF/FSO transmission system especially by utilizing the maximum possible capacity.

8.2 Mixed RF/FSO Cooperative Systems with Incremental Relaying

At present, the hybrid transmission system is losing a time slot each time the relay is sending the RF message over the FSO link, assuming that the destination receives the message correctly via the direct RF link. To overcome this issue, the relay can be made to transmit only in the case when the destination does not receives the transmitted message from the source as error-free. This will reduce the time loss that was caused due to unnecessary transmissions every time slot at the relay end, ultimately improving the performance of such a hybrid RF/FSO transmission system.

8.2 Hybrid RF/FSO Dual Hop Relaying Systems with Multiple Parallel Relays under Selective Relaying/Best Relay Selection

Considering a scenario wherein there are multiple parallel relays between the users and the BS and/or the internet backbone, there can be many possibilities of improving the performance of the system. Either all the relays may be utilized or just the best relay or may be the N-best relays by setting a certain threshold. Besides this, if there is also a presence of direct RF path(s) between the users and BS then there can be a possibility of applying the diversity techniques to further improve the performance. Hence, in this way many possibilities are open for study to improve the performance of such asymmetric transmission systems.

8.2 Massive MIMO, Indoor, and Outdoor mmWave Channels Modeling

- Modeling interference in heterogeneous networks using stochastic geometry.
- Modeling blockage effects in cellular networks using random shape theory.
- Analyzing coverage and rate in mmWave cellular networks.
- Analyzing body-blockage effects in mmWave networks.
- Comparing SINR and rate in sub-6 GHz and mmWave massive MIMO networks.
- Characterizing the channels geometrically rather than statistically using Ray Tracing Method.

- Applying adaptive beamforming techniques, hybrid precoding, and combining for power and bandwidth efficient uses.

References

[1] The Wolfram Functions Site. Accessed: 2016. [Online]. Available: http://functions.wolfram.com.

[2] A. Erdelyi, W. Magnus, F. Oberhettinger, and F. G. Tricomi. *Tables of Integral Transforms*, volume 1. ser Bateman manuscript Project, California Institute of Technology. McGraw-Hill Book Company, Inc., 1954.

[3] M. A. Al-Habash, L. C. Andrews, and R. L. Phillips. Mathematical model for the irradiance probability density function of a laser beam propagating through turbulent media. *Optical Engineering*, 40:1554–1562, August 2001.

[4] H. AlQuwaiee, I. S. Ansari, and M. S. Alouini. On the performance of free-space optical communication systems over double generalized gamma channel. *IEEE Journal on Selected Areas in Communications*, 33(9):1829–1840, Sept 2015.

[5] S. Anees and M. R. Bhatnagar. Performance evaluation of decode-and-forward dual-hop asymmetric radio frequency-free space optical communication system. *IET Optoelectronics*, 9(5):232–240, 2015.

[6] I. S. Ansari, F. Yilmaz, and M. S. Alouini. On the performance of hybrid RF and RF/FSO dual-hop transmission systems. In *2013 2nd International Workshop on Optical Wireless Communications (IWOW)*, pages 45–49, Oct 2013.

[7] I. S. Ansari, F. Yilmaz, and M. S. Alouini. Performance analysis of free-space optical links over Málaga ($\mathcal{M}$) turbulence channels with pointing errors. *IEEE Transactions on Wireless Communications*, 15(1):91–102, Jan 2016.

[8] A.P. Prudnikov, Yu.A. Brychkov and O.I. Marichev. *Integrals and Series, Volume 1, Elementary Functions*. Gordon and Breach Science Publishers, 1986.

[9] Shlomi Arnon, John Barry, George Karagiannidis, Robert Schober, and Murat Uysal. *Advanced Optical Wireless Communication Systems*. Cambridge University Press, New York, NY, USA, 1st edition, 2012.

[10] I. Avram, N. Aerts, H. Bruneel, and M. Moeneclaey. Quantize and forward cooperative communication: Channel parameter estimation. *IEEE Transactions on Wireless Communications*, 11(3):1167–1179, March 2012.

[11] E. Balti and M. Guizani. Impact of Non-Linear High Power Amplifiers on Cooperative Relaying Systems. *IEEE Transactions on Communications*, PP(99):1–1, 2017.

[12] E. Balti, M. Guizani, B. Hamdaoui, and B. Khalfi. Aggregate hardware impairments over mixed rf/fso relaying systems with outdated csi. *IEEE Transactions on Communications*, PP(99):1–1, 2017.

[13] E. Balti, M. Guizani, B. Hamdaoui, and B. Khalfi. Mixed rf/fso relaying systems with hardware impairments. In *GLOBECOM 2017 - 2017 IEEE Global Communications Conference*, pages 1–6, Dec 2017.

[14] E. Balti, M. Guizani, B. Hamdaoui, and Y. Maalej. Partial relay selection for hybrid RF/FSO systems with hardware impairments. In *2016 IEEE Global Communications Conference (GLOBECOM)*, pages 1–6, Dec 2016.

[15] Elyes Balti, Mohsen Guizani, and Bechir Hamdaoui. Hybrid rayleigh and Double-Weibull over impaired RF/FSO system with outdated CSI. In *IEEE ICC 2017 Mobile and Wireless Networking (ICC'17 MWN)*, pages 2093–2098, Paris, France, May 2017.

[16] E. Bjornson, M. Matthaiou, and M. Debbah. A new look at dual-hop relaying: Performance limits with hardware impairments. *IEEE Transactions on Communications*, 61(11):4512–4525, November 2013.

[17] Hanen Bouhadda, Hmaied Shaiek, Daniel Roviras, Rafik Zayani, Yahia Medjahdi, and Ridha Bouallegue. Theoretical analysis of BER performance of nonlinearly amplified FBMC/OQAM and OFDM signals. *EURASIP Journal on Advances in Signal Processing*, 2014(1):60, 2014.

[18] N. D. Chatzidiamantis, H. G. Sandalidis, G. K. Karagiannidis, S. A. Kotsopoulos, and M. Matthaiou. New results on turbulence modeling for free-space optical systems. In *Telecommunications (ICT), 2010 IEEE 17th International Conference on*, pages 487–492, April 2010.

[19] D. B. da Costa and S. Aissa. End-to-end performance of dual-hop semi-blind relaying systems with partial relay selection. *IEEE Transactions on Wireless Communications*, 8(8):4306–4315, August 2009.

[20] D. Dardari, V. Tralli, and A. Vaccari. A theoretical characterization of nonlinear distortion effects in OFDM systems. *IEEE Transactions on Communications*, 48(10):1755–1764, Oct 2000.

[21] G. T. Djordjevic, M. I. Petkovic, A. M. Cvetkovic, and G. K. Karagiannidis. Mixed RF/FSO relaying with outdated channel state information. *IEEE Journal on Selected Areas in Communications*, 33(9):1935–1948, Sept 2015.

[22] G. Farhadi and N. C. Beaulieu. On the ergodic capacity of wireless relaying systems over Rayleigh fading channels. *IEEE Transactions on Wireless Communications*, 7(11):4462–4467, November 2008.

[23] A. A. Farid and S. Hranilovic. Diversity gain and outage probability for mimo free-space optical links with misalignment. *IEEE Transactions on Communications*, 60(2):479–487, February 2012.

[24] Ahmed A. Farid and Steve Hranilovic. Outage capacity optimization for free-space optical links with pointing errors. *J. Lightwave Technol.*, 25(7):1702–1710, Jul 2007.

[25] W. Gappmair, S. Hranilovic, and E. Leitgeb. OOK performance for terrestrial FSO links in turbulent atmosphere with pointing errors modeled by Hoyt distributions. *IEEE Communications Letters*, 15(8):875–877, August 2011.

[26] Z. Ghassemlooy, W. Popoola, and S. Rajbhandari. *Optical Wireless Communications: System and Channel Modelling with MATLAB.* CRC Press, Inc., Boca Raton, FL, USA, 1st edition, 2012.

[27] I. S. Gradshteyn and I. M. Ryzhik. *Table of integrals, series, and products.* Elsevier/Academic Press, Amsterdam, seventh edition, 2007.

[28] H. R. Alhennawi and M. M. H. El Ayadi and M. H. Ismail and H. A. M. Mourad. Closed-Form Exact and Asymptotic Expressions for the Symbol Error Rate and Capacity of the H-Function Fading Channel. *IEEE Transactions on Vehicular Technology*, 65(4):1957–1974, April 2016.

[29] A. Host-Madsen and Junshan Zhang. Capacity bounds and power allocation for wireless relay channels. *IEEE Transactions on Information Theory*, 51(6):2020–2040, June 2005.

[30] C. Hoymann, W. Chen, J. Montojo, A. Golitschek, C. Koutsimanis, and X. Shen. Relaying operation in 3GPP LTE: Challenges and Solutions. *IEEE Communications Magazine*, 50(2):156–162, February 2012.

[31] William C. Jakes and Donald C. Cox, editors. *Microwave Mobile Communications*. Wiley-IEEE Press, 1994.

[32] Helena Jakuszenkow. On properties of the generalized gamma distribution. *Demonstratio Mathematica*, 7(1):13–22, 1974.

[33] A. Jurado-Navas, J. M. Garrido-Balsells, J. F. Paris, M. Castillo-VÃ¡zquez, and A. Puerta-Notario. Further insights on Málaga distribution for atmospheric optical communications. In *2012 International Workshop on Optical Wireless Communications (IWOW)*, pages 1–3, Oct 2012.

[34] M. A. Kashani, M. Uysal, and M. Kavehrad. A novel statistical channel model for turbulence-induced fading in free-space optical systems. *Journal of Lightwave Technology*, 33(11):2303–2312, June 2015.

[35] A. Kashyap and M. Shayman. Routing and traffic engineering in hybrid RF/FSO networks. In *IEEE International Conference on Communications*, volume 5, pages 3427–3433, May 2005.

[36] M. A. Khalighi and M. Uysal. Survey on Free Space Optical Communication: A Communication Theory Perspective. *IEEE Communications Surveys Tutorials*, 16(4):2231–2258, Fourthquarter 2014.

[37] S. K. Korotky. Price-points for components of multi-core fiber communication systems in backbone optical networks. *IEEE/OSA Journal of Optical Communications and Networking*, 4(5):426–435, May 2012.

[38] K. Kumar and D. K. Borah. Quantize and encode relaying through FSO and hybrid FSO/RF links. *IEEE Transactions on Vehicular Technology*, 64(6):2361–2374, June 2015.

[39] Larry C. Andrews and Ronald L. Phillips. *Laser Beam Propagation through Random Media, Second Edition*. SPIE Press Monograph Vol. PM152. SPIE Publications, 2nd edition, 2005.

[40] H. Lei, I. S. Ansari, G. Pan, B. Alomair, and M. S. Alouini. Secrecy capacity analysis over $\alpha - \mu$ fading channels. *IEEE Communications Letters*, 21(6):1445–1448, June 2017.

[41] J. Li, M. Matthaiou, and T. Svensson. I/Q imbalance in AF dual-hop relaying: Performance analysis in Nakagami-m fading. *IEEE Transactions on Communications*, 62(3):836–847, March 2014.

[42] Jian Li and J. Ilow. Adaptive volterra predistorters for compensation of non-linear effects with memory in ofdm transmitters. In *4th Annual Communication Networks and Services Research Conference (CNSR'06)*, pages 4 pp.–103, May 2006.

[43] N Hastings M Evans and B Peacock. Statistical Distributions, Third Edition. *Measurement Science and Technology*, 12(1):117, 2001.

[44] N. Maletić, M. Cabarkapa, and N. Neskovic. Performance of fixed-gain amplify-and-forward nonlinear relaying with hardware impairments. *International Journal of Communication Systems*, pages n/a–n/a, 2015.

[45] A. Mansour, R. Mesleh, and M. Abaza. New challenges in wireless and free space optical communications. *Optics and Lasers in Engineering*, 89:95 – 108, 2017. 3DIM-DS 2015: Optical Image Processing in the context of 3D Imaging, Metrology, and Data Security.

[46] M. Matthaiou, A. Papadogiannis, E. Bjornson, and M. Debbah. Two-way relaying under the presence of relay transceiver hardware impairments. *IEEE Communications Letters*, 17(6):1136–1139, June 2013.

[47] P. K. Mittal and K. C. Gupta. An integral involving generalized function of two variables. *Proceedings of the Indian Academy of Sciences - Section A*, 75(3):117–123, 1972.

[48] Murat Uysal, Carlo Capsoni, Zabih Ghassemlooy, Anthony Boucouvalas, Eszter Udvary. *Optical Wireless Communications: An Emerging Technology*. Signals and Communication Technology. Springer International Publishing, 1 edition, 2016.

[49] M. Niu, J. Cheng, and J. F. Holzman. Error rate performance comparison of coherent and subcarrier intensity modulated optical wireless communications. *IEEE/OSA Journal of Optical Communications and Networking*, 5(6):554–564, June 2013.

[50] Mingbo Niu, Julian Cheng, and Jonathan F. Holzman. Error rate performance comparison of coherent and subcarrier intensity modulated optical wireless communications. *J. Opt. Commun. Netw.*, 5(6):554–564, Jun 2013.

[51] M. I. Petkovic, A. M. Cvetkovic, G. T. Djordjevic, and G. K. Karagiannidis. Partial relay selection with outdated channel state estimation in mixed RF/FSO systems. *Journal of Lightwave Technology*, 33(13):2860–2867, July 2015.

[52] A.P. Prudnikov and Yu. A. Brychkov. *INTEGRAL AND SERIES, Volume 1.* Computing Center of the USSR Academy of Sciences, Moscow, 1990.

[53] A.P. Prudnikov and Yu. A. Brychkov. *INTEGRAL AND SERIES, Volume 3, More Special Functions.* Computing Center of the USSR Academy of Sciences, Moscow, 1990.

[54] J. Qi and S. Aissa. Analysis and compensation of power amplifier nonlinearity in mimo transmit diversity systems. *IEEE Transactions on Vehicular Technology*, 59(6):2921–2931, July 2010.

[55] J. Qi, S. Aissa, and M. S. Alouini. Analysis and compensation of I/Q imbalance in amplify-and-forward cooperative systems. In *2012 IEEE Wireless Communications and Networking Conference (WCNC)*, pages 215–220, April 2012.

[56] C. Rapp. Effects of hpa-nonlinearity on a 4-dpsk/ofdm-signal for a digital sound broadcasting system. *European Conference on Satellite Communications*, pages 179–184, Oct. 22-24 1991.

[57] A. Ribeiro, Xiaodong Cai, and G. B. Giannakis. Symbol error probabilities for general Cooperative links. *IEEE Transactions on Wireless Communications*, 4(3):1264–1273, May 2005.

[58] H. E. Rowe. Memoryless nonlinearities with gaussian inputs: Elementary results. *The Bell System Technical Journal*, 61(7):1519–1525, Sept 1982.

[59] M. Safari and M. Uysal. Relay-assisted Free-Space Optical Communication. *IEEE Transactions on Wireless Communications*, 7(12):5441–5449, December 2008.

[60] H. Samimi and M. Uysal. End-to-end performance of mixed RF/FSO transmission systems. *IEEE/OSA Journal of Optical Communications and Networking*, 5(11):1139–1144, Nov 2013.

[61] G. Santella and F. Mazzenga. A hybrid analytical-simulation procedure for performance evaluation in m-qam-ofdm schemes in presence of nonlinear distortions. *IEEE Transactions on Vehicular Technology*, 47(1):142–151, Feb 1998.

[62] Nikhil Sharma, Ankur Bansal, and Parul Garg. Relay selection in mixed RF/FSO system over generalized channel fading. *Transactions on Emerging Telecommunications Technologies*, 2016.

[63] E. Soleimani-Nasab and M. Uysal. Generalized performance analysis of mixed RF/FSO cooperative systems. *IEEE Transactions on Wireless Communications*, 15(1):714–727, Jan 2016.

[64] Abdelaziz Soulimani, Mustapha Benjillali, Hatim Chergui, and Daniel Benevides da Costa. Performance analysis of M-QAM multihop relaying over mmwave weibull fading channels. *CoRR*, abs/1610.08535, 2016.

[65] M. Soysa, University of Alberta. Department of Electrical, and Computer Engineering. *Performance of Dual Hop Relay Systems with Imperfect CSI*. University of Alberta, 2011.

[66] M. Soysa, H. A. Suraweera, C. Tellambura, and H. K. Garg. Partial and opportunistic relay selection with outdated channel estimates. *IEEE Transactions on Communications*, 60(3):840–850, March 2012.

[67] H. A. Suraweera, M. Soysa, C. Tellambura, and H. K. Garg. Performance analysis of partial relay selection with feedback delay. *IEEE Signal Processing Letters*, 17(6):531–534, June 2010.

[68] Jia Tang and Xi Zhang. Transmit selection diversity with maximal-ratio combining for multicarrier DS-CDMA wireless networks over Nakagami-m fading channels. *IEEE Journal on Selected Areas in Communications*, 24(1):104–112, Jan 2006.

[69] X. Tang, Z. Wang, Z. Xu, and Z. Ghassemlooy. Multihop Free-Space Optical Communications Over Turbulence Channels with Pointing Errors using Heterodyne Detection. *Journal of Lightwave Technology*, 32(15):2597–2604, Aug 2014.

[70] O. Tipmongkolsilp, S. Zaghloul, and A. Jukan. The Evolution of Cellular Backhaul Technologies: Current Issues and Future Trends. *IEEE Communications Surveys Tutorials*, 13(1):97–113, First 2011.

[71] M. Uysal, Jing Li, and Meng Yu. Error Rate Performance Analysis of Coded Free-Space Optical Links over Gamma-Gamma Atmospheric Turbulence Channels. *IEEE Transactions on Wireless Communications*, 5(6):1229–1233, June 2006.

[72] J. Vazifehdan and J. H. Weber. Symbol error rate of space-time coded multi-antenna wireless cooperative networks. In *VTC Spring 2008 - IEEE Vehicular Technology Conference*, pages 1453–1457, May 2008.

[73] Zhengdao Wang and G. B. Giannakis. A simple and general parameterization quantifying performance in fading channels. *IEEE Transactions on Communications*, 51(8):1389–1398, Aug 2003.

[74] O. Waqar, M. Ghogho, and D. McLernon. Tight bounds for ergodic capacity of dual-hop fixed-gain relay networks under Rayleigh fading. *IEEE Communications Letters*, 15(4):413–415, April 2011.

[75] F. Yang, J. Cheng, and T. A. Tsiftsis. Free-space optical communication with nonzero boresight pointing errors. *IEEE Transactions on Communications*, 62(2):713–725, February 2014.

[76] L. Yang, M. O. Hasna, and X. Gao. Performance of mixed RF/FSO with variable gain over generalized atmospheric turbulence channels. *IEEE Journal on Selected Areas in Communications*, 33(9):1913–1924, Sept 2015.

[77] Rafik Zayani, Ridha Bouallegue, and Daniel Roviras. Adaptive predistortions based on neural networks associated with levenberg-marquardt algorithm for satellite down links. *EURASIP J. Wirel. Commun. Netw.*, 2008:2:1–2:15, January 2008.

[78] E. Zedini, I. S. Ansari, and M. S. Alouini. Performance Analysis of Mixed Nakagami-m and Gamma-Gamma Dual-Hop FSO Transmission Systems. *IEEE Photonics Journal*, 7(1):1–20, Feb 2015.

[79] E. Zedini, H. Soury, and M. S. Alouini. On the performance analysis of dual-hop mixed FSO/RF systems. *IEEE Transactions on Wireless Communications*, 15(5):3679–3689, May 2016.

[80] Y. Zhao, R. Adve, and T. J. Lim. Symbol error rate of selection amplify-and-forward relay systems. *IEEE Communications Letters*, 10(11):757–759, November 2006.

[81] Yahong Rosa Zheng and Chengshan Xiao. Simulation models with correct statistical properties for Rayleigh fading channels. *IEEE Transactions on Communications*, 51(6):920–928, June 2003.

[82] C. Zhong, M. Matthaiou, G. K. Karagiannidis, and T. Ratnarajah. Generic ergodic capacity bounds for fixed-gain AF dual-hop relaying systems. *IEEE Transactions on Vehicular Technology*, 60(8):3814–3824, Oct 2011.

Appendix A: MATLAB Implementation of Meijer G-Function

```
function out = MeijerG( an, ap, bm, bq, z )
an_str = vec2str(an);
ap_str = vec2str(ap);
bm_str = vec2str(bm);
bq_str = vec2str(bq);
z_str = num2str(z, 32);
MeijerGmupad_str = ['float(meijerG(', an_str, ',', ap_str, ',', ...
    bm_str, ',', bq_str, ',' z_str, '))'];

out = double(evalin(symengine, MeijerGmupad_str));

return;
function an_str = vec2str(an)

if isempty(an)
    an_str = '[]';
else
    an_str = ['[', num2str(an(1), 32)];
    for i=2:length(an)
        an_str = [an_str, ', ', num2str(an(i), 32)];
    end;
    an_str = [an_str, ']'];
end;
return;
```

Appendix B: MATLAB Implementation of Bivariate Meijer G-Function

```
function out = Bivariate_Meijer_G(am1, ap1, bn1, bq1, cm2,cp2,
    dn2, dq2, em3, ep3, fn3, fq3, x, y)
%***** Integrand definition *****
F = @(s,t)(GammaProd(am1,s+t).* GammaProd(1 cm2,s).* GammaProd(
    dn2, s) .* GammaProd(1 em3,t).* GammaProd(fn3, t).* (x.^s) .*
     (y.^t)) ./(GammaProd(1 ap1, (s+t)).* GammaProd(bq1,s+t) .*
    GammaProd(cp2, s) .* GammaProd(1 dq2,s) .* GammaProd(ep3, t)
    .* GammaProd(1 fq3,t));
%***** Contour definition *****
Sups = min(dn2); Infs =  max(1 cm2); % cs
cs = (Sups + Infs)/2;% s between Sups and Infs
Supt = min(fn3); Inft = max([ am1 cs em3 1]);% t > am1 s,s=cs
ct = Supt    ((Supt    Inft)/10);% t between Supt and Inft
W = 10; % W
%***** Bivariate Meijer G *****
out = ( 1/(2*pi)^2)*quad2d(F,cs 1i*W,cs+1i*W,ct 1i*W,ct+1i*W,'
    AbsTol',10^5,'RelTol',10^5,'MaxFunEvals',2000,'Singular',
    true); %Increase MaxFunEvals for higher W
%***** GammaProd subfunction *****
function output = GammaProd(p,z)
[pp zz] = meshgrid(p,z);
if (isempty(p)) output = ones(size(z));
else output = reshape(prod(gammaZ(pp+zz),2),size(z));
end
end
% The gamma function here is the complex gamma, available in
% www.mathworks.com/matlabcentral/fileexchange/3572 gamma
end
```

Appendix C: MATLAB Implementation of Fox H-Function

```
function out = Fox_H_Univariate(an, An, ap, Ap,bm, Bm ,bq, Bq,z)
%% Integrand definition
F = @(s)(GammaProd(bm,Bm,s).* GammaProd(1 an, An,s).* z.^( s) )
    ./ (GammaProd(1 bq, Bq,s).* GammaProd(ap,Ap,s));
%% Contour preparation:
epsilon = 10^1.2;
Sups = min((1 an)./An); Infs = max( bm./Bm);
if(isempty(Sups) && isempty(Infs))
WPx=1;
elseif(isempty(Sups) && ~isempty(Infs))
WPx = Infs +epsilon;
elseif(~isempty(Sups) && isempty(Infs))
WPx = Sups  epsilon;
else
WPx = (Sups + Infs)/2;% s between Sups and Infs
end
%% integration:
infity = 10;
out = (1/(2i*pi))*integral(F,WPx 1 i*infity , WPx+1i*infity);
return
%% ***** GammaProd subfunction *****
function output = GammaProd(p,x,X)
[pp, XX] = meshgrid(p,X);
xx = meshgrid(x,X);
if (isempty(p))
output = ones(size(X));
else output = reshape(prod(double(gammaZ(pp+xx.*XX)),2),size(X))
    ;
end
end
end
```

Appendix D: MATLAB Implementation of Bivariate Fox H-Function

```
function out = Bivariate_Fox_H(an1,alphan1,An1,ap1,alphap1,Ap1,
    bq1,betaq1,Bq1,cn2,Cn2,cp2, Cp2,dm2, Dm2, dq2, Dq2, en3, En3,
    ep3, Ep3, fm3, Fm3, fq3, Fq3, x, y)
%note there is no bm since m=0
%***** Integrand definition *****
F=@(s,t)(GammaProd(1 an1,alphan1,s,An1,t).*GammaProd(dm2, Dm2, s
    ).* GammaProd(1 cn2,Cn2,s).* GammaProd(fm3, Fm3,t).*
    GammaProd(1 en3,En3,t).* (x.^s) .* (y.^t))./ (GammaProd(1 bq1
    ,betaq1,s,Bq1,t).* GammaProd(ap1, alphap1,s , Ap1,t).*
    GammaProd(1 dq2,Dq2,s).* GammaProd(cp2, Cp2,s).* GammaProd(1
    fq3,Fq3,t).* GammaProd(ep3, Ep3,t) );
%***** Contour definition *****
% cs
css = 0.1;
Sups = min(dm2./Dm2);
Infs = max((cn2 1)./Cn2);
if(isempty(Sups) && isempty(Infs))
cs=1;
elseif(isempty(Sups) && ~isempty(Infs))
cs = Infs +css;
elseif(~isempty(Sups) && isempty(Infs))
cs = Sups  css;
else
cs = (Sups + Infs)/2;% Sups< s <Infs
end
% ct
Supt = min(fm3./Fm3);
Inft = max([(( 1+an1 alphan1.*cs)./An1)
((en3 1)/En3)]);
if(isempty(Supt) && isempty(Inft))
ct=1;
```

```
25 elseif(isempty(Supt) && ~isempty(Inft))
26 ct = Inft +css;
27 elseif(~isempty(Supt) && isempty(Inft))
28 ct = Supt  css;
29 else
30 ct = (5*Supt + Inft)/6;% Supt< t <Inft
31 end
32 W = 10;
33 out = real(((1/pi/2i)^2)*quad2d(F,cs 1i*W,cs+1i*W,ct 1i*W,ct+1i*
       W,'Singular',true));
34 %***** GammaProd subfunction *****
35 function output = GammaProd(p,x,X,y,Y)
36 if(nargin==3)
37 [pp, XX] = meshgrid(p,X);
38 xx = meshgrid(x,X);
39 if (isempty(p))
40 output = ones(size(X));
41 else
42 output = reshape(prod(double(gammaZ(pp+xx.*XX)),2),size(X));
43 end
44 elseif(nargin==5)
45 [pp, XX] = meshgrid(p,X);
46 xx = meshgrid(x,X);
47 yy = meshgrid(y,X);
48 [pp, YY] = meshgrid(p,Y);
49 if (isempty(p))
50 output = ones(size(X));
51 else
52 output = reshape(prod(double(gammaZ(pp+xx.*XX+yy.*YY)),2),size(X
       ));
53 end
54 end
55 end
56 end
```

Appendix E: MATLAB Implementation of Complex Gamma Function

```
function [f] = gammaZ(z)
% GAMMA  Gamma function valid in the entire complex plane.
%        Accuracy is 15 significant digits along the real axis
%        and 13 significant digits elsewhere.
%        This routine uses a superb Lanczos series
%        approximation for the complex Gamma function.
%
%        z may be complex and of any size.
%        Also  n! = prod(1:n) = gamma(n+1)
%
%usage: [f] = gamma(z)
%
%tested on versions 6.0 and 5.3.1 under Sun Solaris 5.5.1
%
%References: C. Lanczos, SIAM JNA  1, 1964. pp. 86 96
%           Y. Luke, "The Special ... approximations", 1969 pp. 29 31
%           Y. Luke, "Algorithms ... functions", 1977
%           J. Spouge,  SIAM JNA 31, 1994. pp. 931 944
%           W. Press,  "Numerical Recipes"
%           S. Chang, "Computation of special functions", 1996
%           W. J. Cody "An Overview of Software Development for Special
%           Functions", 1975
%
%see also:  GAMMA GAMMALN GAMMAINC PSI
%see also:  mhelp GAMMA
%
%Paul Godfrey
%pgodfrey@intersil.com
%http://winnie.fit.edu/~gabdo/gamma.txt
```

```
%Sept 11, 2001

siz = size(z);
z=z(:);
zz=z;

f = 0.*z; % reserve space in advance

p=find(real(z)<0);
if ~isempty(p)
    z(p)=z(p);
end

% 15 sig. digits for 0<=real(z)<=171
% coeffs should sum to about g*g/2+23/24

g=607/128; % best results when 4<=g<=5

c = [  0.99999999999999709182;
      57.156235665862923517;
     -59.597960355475491248;
      14.136097974741747174;
      -0.49193138160976201978;
        .33994649984811888699e-4;
        .46523628927048575665e-4;
       -.98374475304879564677e-4;
        .15808870322491248884e-3;
       -.21026444172410488319e-3;
        .21743961811521264320e-3;
       -.16431810653676389022e-3;
        .84418223983852743293e-4;
       -.26190838401581408670e-4;
        .36899182659531622704e-5];

%Num Recipes used g=5 with 7 terms
```

```
65 %for a less effective approximation
66
67 z=z 1;
68 zh =z+0.5;
69 zgh=zh+g;
70 %trick for avoiding FP overflow above z=141
71 zp=zgh.^(zh*0.5);
72
73 ss=0.0;
74 for pp=size(c,1) 1: 1:1
75     ss=ss+c(pp+1)./(z+pp);
76 end
77
78 %sqrt(2Pi)
79 sq2pi=  2.50662827463100050241576528481l0;
80 f=(sq2pi*(c(1)+ss)).*((zp.*exp( zgh)).*zp);
81
82 f(z==0 | z==1) = 1.0;
83
84 %adjust for negative real parts
85 if ~isempty(p)
86     f(p)= pi./(zz(p).*f(p).*sin(pi*zz(p)));
87 end
88
89 %adjust for negative poles
90 p=find(round(zz)==zz & imag(zz)==0 & real(zz)<=0);
91 if ~isempty(p)
92     f(p)=Inf;
93 end
94
95 f=reshape(f,siz);
96
97 return
```

Appendix F: PYTHON Implementation of Multivariate Fox H-Function

```
from _future_ import division
import numpy as np
import scipy.special as special
import itertools


def detBoundaries(params, tol):
    '''Determine rectangular boundaries of integration region of Fox H
        function.'''
    boundary_range = np.arange(0, 50, 0.05)
    dims = len(params[0])
    boundaries = np.zeros(dims)
    for dim_l in range(dims):
        points = np.zeros((boundary_range.shape[0],dims))
        points[:, dim_l] = boundary_range
        abs_integrand = np.abs(compMultiFoxHIntegrand(points, params))
        index = np.max(np.nonzero(abs_integrand> tol*abs_integrand[0]))
        boundaries[dim_l] = boundary_range[index]
    return boundaries


def compMultiFoxHIntegrand(y, params):
    '''Compute complex integrand of Fox H Function at points given by rows of
        matrix y.'''
    z, mn, pq, c, d, a, b = params
    m, n = zip(*mn)
    p, q = zip(*pq)
    npoints, dims = y.shape
    s = lj*y
    lower = np.zeros(dims)
    upper = np.zeros(dims)
    for dim_l in range(dims):
        if b[dim_l]:
            bj, Bj = zip(*b[dim_l])
            bj = np.array(bj[:m[dim_l+1]])
            Bj = np.array(Bj[:m[dim_l+1]])
            lower[dim_l] =  np.min(bj/Bj)
```

```
36          else:
37              lower[dim_l] =  100
38          if a[dim_l]:
39              aj, Aj = zip(*a[dim_l])
40              aj = np.array(aj[:n[dim_l+1]])
41              Aj = np.array(Aj[:n[dim_l+1]])
42              upper[dim_l] = np.min((1 aj)/Aj)
43          else:
44              upper[dim_l] = 0
45      mindist = np.linalg.norm(upper lower)
46      sigs = 0.5*(upper+lower)
47      for j in range (n[0]):
48          num = l    c[j][0]    np.sum(c[j][l:] * lower)
49          cnorm = np.linalg.norm(c[j][l:])
50          newdist = np.abs(num) / cnorm
51          if newdist < mindist:
52              mindist = newdist
53              sigs = lower + 0.5*num*np.array(c[j][l:])/(cnorm*cnorm)
54      s += sigs
55      s1 = np.c_[np.ones((npoints, l)), s]
56      prod_gam_num = prod_gam_denom = 1+0j
57      for j in range(n[0]):
58          prod_gam_num *= special.gamma(1 np.dot(s1,c[j]))
59      for j in range(q[0]):
60          prod_gam_denom *= special.gamma(1 np.dot(s1,d[j]))
61      for j in range (n[0], p[0]):
62          prod_gam_denom *= special(np.dot(s1,c[j]))
63      for dim_l in range(dims):
64          for j in range(n[dim_l+1]):
65              prod_gam_num *= special.gamma(1    a[dim_l][j][0]    a[dim_l][j][1]*s
                    [:,dim_l])
66          for j in range(m[dim_l+1]):
67              prod_gam_num *= special.gamma(b[dim_l][j][0] + b[dim_l][j][1]*s[:,
                    dim_l])
68          for j in range (n[dim_l+1], p[dim_l+1]):
69              prod_gam_denom *= special.gamma(a[dim_l][j][0] + b[dim_l][j][1]*s
                    [:, dim_l])
70          for j in range(m[dim_l+1], q[dim_l+1]):
71              prod_gam_denom *= special.gamma(1 b[dim_l][j][0]    b[dim_l][j][1]*s
                    [:, dim_l])
72      zs = np.power(z,  s)
73      result = (prod_gam_num/prod_gam_denom)*np.prod(zs,axis=1)/(2*np.pi)**dims
```

```
74    return result
75
76  def compMultiFoxH(params, nsubdivisions, boundaryTol=0.0001):
77  ''' Estimate multivariate integral using rectangular quadrature.
78      Input: 'params': list containing z, mn, pq, c, d, a, b. 'nsubdivisions
            ': the number of divisions taken along each dimension.
79      'boundaryTol': tolerance used for determining the boundaries. Output: '
            result' the estimated value of the Fox H function... '''
80
81      boundaries = detboundaries(params, boundaryTol)
82      dim = boundaries.shape[0]
83      signs = list(itertools.product([1, 1], repeat=dim))
84      code = list(itertools.pproduct(range(int(nsubdivisions/2)),repeat=dim))
85      quad = 0
86      res = np.zeros((0))
87      for sign in signs
88          points = np.array(sign)*(np.array(code)+0.5)*boundaries*2/
                nsubdivisions
89          res = np.r_[res,np.real(compMultiFoxHIntegrand(points,params))]
90          quad += np.sum(compMultiFoxHIntegrand(points, params))
91      volume = np.prod(2*boundaries/nsubdivisions)
92      result = quad*volume
93      return result
```

Appendix G: IEEE Formal Reuse Licence

Thesis / Dissertation Reuse

The IEEE does not require individuals working on a thesis to obtain a formal reuse license, however, you may print out this statement to be used as a permission grant:

Requirements to be followed when using any portion (e.g., figure, graph, table, or textual material) of an IEEE copyrighted paper in a thesis:

1) In the case of textual material (e.g., using short quotes or referring to the work within these papers) users must give full credit to the original source (author, paper, publication) followed by the IEEE copyright line © 2011 IEEE.
2) In the case of illustrations or tabular material, we require that the copyright line © [Year of original publication] IEEE appear prominently with each reprinted figure and/or table.
3) If a substantial portion of the original paper is to be used, and if you are not the senior author, also obtain the senior author's approval.

Requirements to be followed when using an entire IEEE copyrighted paper in a thesis:

1) The following IEEE copyright/ credit notice should be placed prominently in the references: © [year of original publication] IEEE. Reprinted, with permission, from [author names, paper title, IEEE publication title, and month/year of publication]
2) Only the accepted version of an IEEE copyrighted paper can be used when posting the paper or your thesis on-line.
3) In placing the thesis on the author's university website, please display the following message in a prominent place on the website: In reference to IEEE copyrighted material which is used with permission in this thesis, the IEEE does not endorse any of [university/educational entity's name goes here]'s products or services. Internal or personal use of this material is permitted. If interested in reprinting/republishing IEEE copyrighted material for advertising or promotional purposes or for creating new collective works for resale or redistribution, please go to http://www.ieee.org/publications_standards/publications/rights/rights_link.html to learn how to obtain a License from RightsLink.

If applicable, University Microfilms and/or ProQuest Library, or the Archives of Canada may supply single copies of the dissertation.